To the Graduate Council:

I am submitting herewith a dissertation written by Habte Giorgis Churnet entitled "The Relationships between Dolomitization and Sphalerite Mineralization in the Lower Ordovician Upper Knox Carbonate Rocks of the Copper Ridge District, East Tennessee." I recommend that it be accepted in partial fulfillment of the requirements for the degree of Doctor of Philosophy, with a major in Geology.

Kula C. Misra

K. C. Misra, Major Professor

We have read this dissertation and recommend its acceptance:

Kenneth R. Walker

Otto C. Kopp

Lawrence A. Taylor

John E. Bloor

Norman Woodward Jr.

Accepted for the Council:

L Evans Porter

Vice Chancellor
Graduate Studies and Research

Thesis
79b
.C387
cop. 2

THE RELATIONSHIPS BETWEEN DOLOMITIZATION AND SPHALERITE MINERALIZATION IN THE LOWER ORDOVICIAN UPPER KNOX CARBONATE ROCKS OF THE COPPER RIDGE DISTRICT, EAST TENNESSEE

A Dissertation

Presented for the

Doctor of Philosophy

Degree

The University of Tennessee, Knoxville

Habte Giorgis Churnet

December 1979

1406091

ACKNOWLEDGMENTS

My sincere gratitude is extended to Dr. K. C. Misra who served as a major advisor and whose suggestions, criticisms and encouragement greatly improved this research. It is also a pleasure to extend my gratitude to other members of the dissertation committee, Dr. K. R. Walker, Mr. H. Wedow, Jr., Dr. L. A. Taylor, Dr. O. C. Kopp, and Dr. J. E. Bloor, for their advice during the research period as well as the suggestions and improvements they offered in the presentation of this manuscript. My thanks and appreciation are also extended to Dr. D. Walia and Mr. Geoffrey Gleason of the Oak Ridge Associated Universities for their help in obtaining trace element analysis using the neutron activation facility.

The writer has benefitted from discussions with Mr. Gary E. Smith while employed by the Anaconda Company during the summer of 1978.

The writer expresses his appreciation to Mr. R. Morris and Mr. H. Mantooth of the New Jersey Company for the opportunity offered to him and his colleagues to collect some samples from the Idol mine.

The writer extends his thanks to fellow graduate students at The University of Tennessee at Knoxville, particularly to Mr. D. Lown and P. Geraci, for their encouragement and assistance.

The writer was sponsored and supported by AFGRAD to perform his graduate study, including this research.

ABSTRACT

The relationships of dolomitization to sphalerite mineralization were investigated in the Lower Ordovician Upper Knox carbonate rocks, of the Copper Ridge District, East Tennessee. Part of the Upper Knox Group consists of the Kingsport and Mascot formations, which consist of three easily recognizable lithofacies: limestone, fine-grained dolostones (Fd) and coarser than fine-grained dolostones (CFd).

Textural and trace element data suggest that the neomorphism of the limestones and the formation of the CFd occurred in the presence of fresh water. Theoretical considerations involving mixing of fresh and marine water show that dolomitization is feasible for mixtures between 10-40 wt. % of marine water, and neomorphism of limestone between 40-60 wt. % marine water. The presence of high-Mg calcite inclusions in the CFd indicates that the dolomitization occurred quite early. Presence of ghost fossils, crystal zoning, poikilotopic textures, as well as lack of mudcracks suggest that the CFd formed from dolomitization of subtidal to intertidal limestones. This imples that the preserved limestones and the CFd are probably facies equivalents. In contrast, both the absence of some features and the presence of others suggest that the Fd are of the type that form in Holocene peritidal environments. These criteria include presence of mudcracks, birdseyes, planar to wavy cryptalgal laminae, indirect evidence of the former presence of gypsum, rarity of fauna, and the fine-grained nature of the constituent dolomite crystals. Low Na and Sr concentrations in

the Fd suggest that their formation also involved presence of fresh water.

A fence diagram, based on sections measured during this study in conjunction with those reported by Harris (1969), shows that most of the Mascot represents a broad, tidal flat environment, adjacent to the Kingsport shallow marine environment. The Kingsport was dotted with islands. These islands served as catchment areas of fresh water which has the potential to cause brecciation as well as dolomitization depending on the amount of marine water mixed with it. The fence diagram also shows that ore-grade mineralization is related to facies boundaries that resulted from the record of islands and adjacent shallow marine environments.

Textural relationships between sphalerite and various types of dolomite crystals indicate that the mineralization is later than the formation of the dolostones. However, textural evidences could be misleading since fluctuations in the amount of introduced reduced sulfur to an ore solution could result in equilibrium or disequilibrium boundary relationships. That introduction of reduced sulfur was the mechanism of precipitation of sphalerite is suggested by equilibrium boundary relationships between sphalerite and some vug-fill dolomite crystals. Nonetheless, some limestone beds in close proximity to abundantly mineralized breccia bodies are not dolomitized, but farther away, the same beds are dolomitized implying that ore-forming solutions did not form dolostones. However, in some bedded-ore occurrences sphalerite and dolomite crystals of the CFd variety are intimately

associated, implying that mineraliation and dolomitization were coeval. The association of sphalerite with CFd in bedded-ore deposits, the need for sufficient sulfur to produce ore-grade mineralization, and the relationship of ore-grade mineralization to facies boundaries is used to speculate that the mineralization was probably earlier than the post-Knox unconformity.

TABLE OF CONTENTS

CHAPTER		PAGE
I.	GENERAL INTRODUCTION	1
II.	FRESH WATER DILUTION OF MARINE WATER AS A MECHANISM OF DOLOMITIZATION	6
	Introduction	6
	Previous Work	13
	Procedure and Results	15
	Discussion	23
	Conclusion	25
III.	TRACE ELEMENT CONTENTS OF THE UPPER KNOX ROCKS AND GENETIC IMPLICATIONS	27
	Introduction	27
	Methods of Investigation	28
	Results	29
	Discussion of Results	37
	Interpretation of Trace Element Data	43
	Conclusion	54
IV.	IMPLICATIONS OF SEDIMENTARY AND DIAGENETIC FEATURES OF THE LOWER ORDOVICIAN UPPER KNOX GROUP CARBONATE ROCKS, COPPER RIDGE DISTRICT, EAST TENNESSEE	55
	Introduction	55
	Methods of Investigation	60
	Measured Sections	61
	Carbonate Petrology	68
	Sedimentary and Diagenetic Setting	104
	Summary and Conclusions	117
V.	SPHALERITE MINERALIZATION IN THE COPPER RIDGE DISTRICT	118
	Introduction	118
	Ore Textures and Characteristics of Sulfides and Dolomite	120
	Field Occurrences of Sphalerite	133
	Comparison of Mineralized and Barren Sections	137
	Discussion on the Genesis of Sphalerite Deposits	141
	Conclusions	147
VI.	SUMMARY AND CONCLUSIONS	148

BIBLIOGRAPHY 154

APPENDIXES 170

A. ASSUMPTIONS AND PROCEDURE USED TO DETERMINE THE EFFECT OF DILUTION OF MARINE WATER BY FRESH WATER 171

B. ESTIMATION OF ERROR OF Mn AMOUNT USING THE ELECTRON MICROPROBE MAC (400-S) 190

C. A GRAPHICAL METHOD OF REPRESENTING LUMINESCENT PATTERNS IN DOLOMITE CRYSTALS 194

D. CONCENTRATIONS OF TRACE ELEMENTS (ppm) IN CARBONATE MINERALS AT THE FLAT GAP MINE FROM WEST (1974) 197

E. STAINING TECHNIQUES 200

F. COLUMNAR SECTIONS OF THE UPPER KNOX, COPPER RIDGE DISTRICT 202

G. PETROGRAPHIC DESCRIPTIONS OF CARBONATES 204

VITA 237

LIST OF TABLES

TABLE		PAGE
2-1.	Dolomitization Models	9
2-2.	Dissolved Ionic Species in Fresh and Marine Water	16
2-3.	Concentrations of Ionic Species (ppm) for Different Weight Percent of Marine Water in the Mixture	17
2-4.	Percentage Distribution of Ionic Species that Remain Uncomplexed, for Different Weight Percent of Marine Water in the Mixture	19
2-5.	Apparent and Effective Activities (a) and Corresponding Degrees of Saturation (IAP/keq.) of Carbonates for Different Weight Percent of Marine Water in the Mixture	21
3-1.	Composition (wt. %) of Dolomite Crystals Obtained by Electron Microprobe Analyses	32
3-2.	Neutron Activation Analyses of Trace Element Concentrations (ppm) in the Upper Knox Rocks	36
3-3.	Approximate Partition Coefficients of Trace Elements in Calcite, Magnesite, and Dolomite at 25°C	39
3-4.	Correlation Matrices of Trace Elements in Carbonate Minerals of Limestones and Dolostones from the Flat Gap Mine, Copper Ridge District	47
4-1.	Generalized Section of the Lower Paleozoic, East Tennessee Zinc Districts (Adapted from Hill, 1971a)	58
4-2.	Grain Size Classification of Dolostones	70
4-3.	Comparison of Fine-Grained and Coarser than Fine-Grained Dolostones	72
4-4.	Composition (wt. %) of Carbonates Obtained by Electron Microprobe Analysis	74
A-1.	Molalities $x10^5$ of Dissolved Ionic Species for Different Weight Percent Marine Water in the Mixture	174

TABLE PAGE

A-2. Ionic Strengths (I) and mZ^2x10^5 of Solutions for Different Weight Percent Marine Water in the Mixture . . . 175

A-3. Calculated Parameters for the Extended Debye-Hückel Equation: $\text{Log } \gamma_i = -\frac{W}{X} + Y$, where $W=AZ^2\sqrt{I}$, $X=1+a^\circ_i B\sqrt{I}$ and $Y=bI$ 177

A-4. Calculated Values of $\gamma_i x10^5$ and $a_i\ 10^5$ in Mixtures for Different Weight Percent of Marine Water in the Mixture (γ_i is Calculated Using Parameters Listed in Appendix A, and $a_i=\gamma_i\ m_i$. Values of m_i are Taken from Table A-1) . . . 178

A-5. Comparison of Activity Coefficients for Marine Water (I=0.7) 179

A-6. Percentage Distribution of Cationic Species in Complexes for Different Weight Percent of Marine Water in the Mixture 186

A-7. Percentage Distribution of Anionic Species in Complexes for Different Weight Percent of Marine Water in the Mixture 187

A-8. Equilibrium Reactions and Constants 188

D-1. Concentration of Trace Elements (ppm) in Carbonate Minerals at the Flat Gap Mine from West (1974) 198

G-1. Petrographic Description of Carbonates from River Ridge 205

G-2. Petrographic Description of Carbonates from Joe Mill-Rucker Branch Creeks 226

G-3. Petrographic Description of Carbonate Rocks from Shiloh 232

G-4. Petrographic Description of Carbonates from Lee Valley 234

LIST OF FIGURES

FIGURE		PAGE
2-1.	Effect of Dilution on Ionic Species	20
2-2.	Saturation Curves of Carbonates	22
3-1.	Summary of the Zonal Luminescent Patterns of Dolomite Crystals Belonging to the Coarser than Fine-Grained Dolostones	30
3-2.	Electron Microprobe Traverse Across a Zoned Dolomite Crystal. Numbers at the Top Correspond to Analysis Spots on a Traverse from Rim through Center to Rim of a Crystal	33
3-3.	Electron Microprobe Traverse Across a Zoned Dolomite Crystal. The Figure Shows that the Distribution of Fe in Dolomite Tends to Increase towards the Rims of the Dolomite	35
3-4.	Schematic Diagram Illustrating that Different Zonal Patterns Can be Observed in Different Cuts of a Zoned Dolomite	52
4-1.	Location of Upper Knox Carbonate Rocks Used in This Study	56
4-2.	Photomicrograph of Oosparite (Sample RR-49A)	75
4-3.	Photomicrograph of a Slightly Dolomitized Limestone (Sample RR-49C_2)	76
4-4.	Wavy Laminae at Joe Mill Creek-Rucker Branch Section	82
4-5.	Polygonal Mudcracks	83
4-6.	Nodular Vug Fills at Joe Mill Creek-Rucker Branch Creek Section	85
4-7.	Nodular and Lensoid Features with Geopetal Sediment Fill at Joe Mill-Rucker Branch Section	86
4-8.	Photomicrograph of an Oolitic Chert (Sample RR-44A)	93
4-9.	Photomicrograph of Zoned Dolomite (Sample RR-59B)	96

FIGURE PAGE

4-10. Photomicrograph of Partially Dolomitized Biopelsparitic Packstone (Sample RR-60C) 100

4-11. Photomicrograph of Partially Dolomitized Biopelsparitic Packstone (Sample RR-72) 100

4-12. Photomicrograph of Partially Dolomitized Intrapelsparitic Grainstone (Sample RR-68A) 101

4-13. Photomicrograph of a Slightly Dolomitized Biointrapelsparitic Grainstone (Sample RR-70C) 102

4-14. Photomicrograph of a Slightly Dolomitized Limestone (Sample RR-68C) 102

4-15. Columnar Section of the Upper Knox in the Copper Ridge District 106

4-16. Columnar Section of Part of the Upper Knox in the Copper Ridge District 108

4-17. Fence Diagram of the Lower Mascot and Kingsport Formations in the Copper Ridge District 109

5-1. Photomicrograph (Plane-Polarized Reflected Light) Showing Sphalerite (Sph) Replacing Pyrite (Py) 122

5-2. Photomicrograph (Plane-Polarized Reflected Light) of a Zoned Pyrite (Sample Idol-51) 122

5-3. Photomicrograph (Plane-Polarized Reflected Light) Showing Pyrite (Py) and Marasite (Ms) Relationships (Sample Idol-51) 123

5-4. Photomicrograph (Plane-Polarized Reflected Light) Showing Iron Sulfides (Py) Occurring Near the Boundary of Fine-Grained Dolomite Fragment (Fd) and Vug-Fill Dolomite (V_S) (Sample Tandy Dalton-1) 123

5-5. Photomicrograph (Plane-Polarized Reflected Light) Showing that Iron Sulfide (Py) Formed after Brecciation of Vug-Fill Dolomite (Sph) (Sample Idol-11) 124

5-6. Photomicrograph (Plane-Polarized Reflected Light) Showing Pyrite (Py) Occurring in Fractures of Sphalerite (Sph) (Sample Shiloh-52) 124

FIGURE PAGE

5-7. Photomicrograph (Plane-Polarized Reflected Light) Showing Iron Sulfides (Py) Engulfed by Sphalerite (Sph) (Sample Idol-19) 125

5-8. Photomicrograph (Plane-Polarized Reflected Light) Showing Sphalerite Crystals (Sph) Occurring in Alternate Laminae of Internal Sediments (Sample Idol-1) 128

5-9. Photomicrograph (Plane-Polarized Reflected Light) Showing Sphalerite (Sph) Replacing Vug-Fill Dolomite (Vf) (Sample Joe Mill-60) 128

5-10. Photomicrograph (Plane-Polarized Reflected Light) Showing Dolomite (Vf) Replacing Sphalerite (Sph) (Sample Joe Mill-50) 130

5-11. Photomicrograph (Plane-Polarized Reflected Light) Showing Sharp Boundaries between Sphalerite (Sph) and Vug-Fill Dolomite (Vf) (Sample Idol-51) 130

5-12. Photomicrograph (Plane-Polarized Reflected Light) Showing Sharp and Replacive Boundary Relationships between Sphalerite (Sph) and Vug-Fill Dolomite (Vf) Rhomb (Sample Joe Mill-50) 131

C-1. Graphical Representation of a Dolomite Rhomb with Darker Core and Brighter Rim 195

C-2. Graphical Representation of a Dolomite Rhomb with Brighter Core and Darker Rim 195

C-3. Negative Photomicrograph of a Partially Dolomitized Limestone (Sample RR-49D1) 196

F-1. Columnar Sections of the Upper Knox, Copper Ridge District 203

CHAPTER I

GENERAL INTRODUCTION

Part of the Lower Ordovician Upper Knox carbonate rocks comprise the Kingsport and the Mascot formations. The Kingsport consists of interbedded limestones and dolostones; whereas the overlying Mascot consists chiefly of dolostones and is truncated by the Post-Knox unconformity. In the Valley and Ridge Province of East Tennessee the sediments occur in NE-trending thrust blocks. Among these linear trends the Copper Ridge and the Mascot-Jefferson City districts are locals of sphalerite mineralization (Maher, 1971). The mineralization of ore grade is associated with brecciated horizons straddling the Kingsport-Mascot contact and as such is stratabound (Hill, 1971; Hoagland, 1971, 1977).

Prior to 1960, sphalerite mineralization in East Tennessee was considered to be related to the Appalachian (Upper Paleozoic) tectonism. Even recently, Ridge (1968, 1972) entertained such an idea. However, since Kendall (1960) showed that the layering of internal sediments between breccia fragments is parallel to the bedding in the country rocks, many geologists (Wedow and Marie, 1965; Crawford and Hoagland, 1968; Hill, 1969; Harris, 1971; Hoagland, 1971, 1977) believe that the brecciation which helped to localize mineralization occurred prior to Appalachian tectonism. In particular, the Post-Knox unconformity with its sinkholes and postulated interconnected ancient aquifer system at greater depths (about 250-700 feet beneath the Post-Knox unconformity) is believed to

have been a contributing factor in the brecciation. In the opinion of many geologists, the brecciation is thought to arise from dissolution of limestones and the foundering of overlying dolostones. In proximity to ore zones dolostones are reported to be thicker whereas limestones are thinner (Wedow and Marie, 1965; Harris, 1969). According to Wedow and Marie (1965) this is due to solution thinning of the limestones accompanied by dilatational thickening of the dolostones. An alternative explanation for this phenomenon is made apparent by the construction of a fence diagram discussed in Chapter IV of this dissertation.

There is an abundance of dolomite in the environ of ore deposits (Crawford and Hoagland, 1968; Hill, 1969, 1971). Even in those cases where the ore horizon is laterally traceable to limestones, such as the U-bed of the Kingsport Formation, most of the breccia fragments, the breccia matrix, as well as a thin selvage of the wall rock proximal to the orebody, may consist of dolomites and dolostones (Kendall, 1960; Crawford and Hoagland, 1968). The origin of the dolomites and the dolostones that constitute breccia fragments and matrix, and one of the major lithologies of the country rock, have been a subject of different interpretations. These interpretations include: (1) dolomitization by ground water which was transported through an interconnected paleoaquifer system carrying excess Mg made available from erosion of the Mascot dolostones during the formation of the Post-Knox unconformity (Harris, 1971), (2) dolomitization during sedimentation by incipient subtidal processes (Harris, 1973), and (3) dolomitization by mineralizing fluids giving rise to particularly the coarser-grained dolostones and the cement of the fine-grained dolostones (West, 1974).

A careful study shows that there were several exposure surfaces prior to the Post-Knox erosional event. Further, the dolostones were formed quite early, so that dolomitization related to the Post-Knox unconformity (Harris, 1971) does not appear plausible. The incipient subtidal dolomitization process proposed by Harris (1973) is largely based on the presumed stromatolitic features (SH-C and SH-V) preserved in cherts, for example at the River Ridge section (Harris, 1969). A careful examination does not show an abundance of these features. Moreover, there are numerous lines of evidence to suggest that the bulk of the dolostones were formed in areas above the subtidal environment. The chemical analysis data obtained by West (1974), which he used to suggest that the coarser-grained dolostones formed from ore-forming solutions, can actually be used to suggest that these dolostones formed from a mixture of fresh and marine water (Chapter III). An intimate association of vug-fill dolomite crystals and sphalerite are reported by many workers (e.g., Hill, 1969; Hoagland, 1976), and this suggests that some of the vug-fill dolomites and sphalerite are cogenetic (Chapter V). But, it must be cautioned that much as vug-fill calcites do not form limestones, so too vug-fill dolomites do not form dolostones.

In order to understand the relationships between dolomitization and sphalerite mineralization, textural relationships between sphalerite and various types of dolomite crystals, as well as a study of the lithologies and characterization of the dolomite types in mineralized and unmineralized sections in a particular locality, namely the Copper Ridge district, was the approach chosen for this dissertation. Data from

this study are used to suggest that the dolomitization processes could be different from those proposed by previous workers. At least the coarser than fine-grained dolostones (with dolomite grains exceeding 0.062 mm) are interpreted to be a product of marine and fresh water mixing.

There are several dolomitization models in the literature (e.g., seepage refluxion, solution cannibalization). Pertinent aspects of the various models are reviewed in brief, so that the mixing model herein proposed to explain the generation of at least some of the Upper Knox dolostones in the Copper Ridge district could be viewed in proper perspective. Chapter II deals with this aspect of the research. A discussion on the effect of dilution is emphasized by considering a theoretical mixing model involving mixing of river water with marine water. Such a theoretical treatment shows the range of mixtures of solutions in which calcite and aragonite are undersaturated and dolomite oversaturated, so that dissolution of precursor limestones and replacement by dolomite become feasible.

An approach to interpreting trace element data is discussed in Chapter III. Using this approach, trace element data obtained during this study as well as those of West (1974) give an idea of the type of solutions from which dolostones formed.

Detailed petrographic study coupled with chemical data are used to characterize the carbonate minerals, in particular, dolomites (Chapter IV), leading to a better understanding of the lithologies. Sections measured at various localities within the Copper Ridge district allow the

construction of a fence diagram that shows the spatial and temporal relationships of the lithologies. From such a construction it is apparent that there were several exposure surfaces that could probably trap fresh water lenses. Such fresh water lenses have the potential of creating permeability as well as promoting dolomitization, depending on the proportion of mixing of fresh and marine water.

The environment of deposition of the host rocks give a better understanding of the setting of the host carbonates for mineralization and is further discussed in Chapter V. The relationship of vug-fill dolomites associated with sphalerites are perhaps the best clues available for understanding the mechanisms of precipitation of sphalerite.

CHAPTER II

FRESH WATER DILUTION OF MARINE WATER AS A MECHANISM OF DOLOMITIZATION

I. INTRODUCTION

The formation of dolostones is a controversial issue. Part of the problem is that the exact conditions of the formation of dolomite in sedimentary environments have not been experimentally verified (e.g., Katz and Mathews, 1977). Based on thermodynamic considerations, it can be shown that marine water in equilibrium with dolomite is oversaturated with respect to dolomite. But, marine water in equilibrium with calcite is undersaturated with respect to dolomite (Saas, 1965). Although there are some dolomites that are purported to have formed from marine water (e.g., Friedman and Sanders, 1967; Behrens and Land, 1972), there is no convincing evidence for the precipitation of dolomite from such a solution (Berner, 1971). Based on conceptual models involving epeiric seas, it has been suggested that dolomite forms by direct precipitation from hypersaline waters (Shaw, 1964; Irwin, 1965). The hypersaline waters were thought to have developed from lack of agitation by tidal activity and from evapoconcentration (Irwin, 1965). But, Klein and Ryer (1978) have suggested that ancient epeiric seas would have been dominated by tidal activity because widest shelves in modern epeiric seas are characterized by greatest tidal current velocities and tidal ranges. Also, Textoris (1969) has suggested that even higher tidal activity

would have prevailed before the Early Paleozoic, if the moon was closer to the Earth in those times. Nonetheless, some studies of dolomites observed in Holocene intertidal to supratidal flats (e.g., Persian Gulf, Illing et al., 1965; Bush, 1973; Bahama Banks, Shinn et al., 1965; Southern Bonaire, Deffeyes et al., 1965) have led to the interpretation that dolostones are formed by penecontemporaneous (very early diagenetic replacement) dolomitization of carbonate sediments from hypersaline water, characterized by high Mg^{++}/Ca^{++} ratios. By analogy to these modern peritidal environments and on the basis of characteristics of the dolostones, observed in specific sedimentologic settings, several models of dolomitization have been proposed (see reviews by Fairbridge, 1957; Ingerson, 1962; Friedman and Sanders, 1967; Lovering, 1969; Zenger, 1972a; and Bathurst, 1975). The premise most common to all these models is that an Mg^{++}/Ca^{++} ratio higher than that of normal water is required to dolomitize precursor lime muds or limestones. Accordingly, one of the key requirements for dolomitization is often considered to be finding a means of raising the Mg^{++}/Ca^{++} ratios of solutions. This is thought to be achieved in a variety of ways, which may be grouped into two categories: by abstraction of Ca^{++} from solutions, or by adding Mg^{++} to solutions. Abstraction of Ca^{++} from solutions may be achieved by formation of $CaCO_3$ compounds and of gypsum (Shinn et al., 1965; Illing et al., 1965; Deffeyes et al., 1965; Bush, 1973). The Mg^{++} content of solutions may be increased: from decay of algal material (Gebelein and Hoffman, 1973); presence of clays affording ionic exchange between layered lattices (Kahle, 1965); dissolution of high Mg-calcite (Goodell and Garman, 1969);

leaching from preexisting Mg-bearing sediments (Freeman, 1971; Hanshaw et al., 1971; Harris, 1971); leaching from proximal igneous rocks (Hewett, 1928; Ilich, 1974).

The Mg^{++}/Ca^{++} mole ratio in ideal dolomite is 1:1, but in protodolomites that form in Holocene environments, it is less than unity. This implies that a higher Mg^{++}/Ca^{++} ratio is not necessary for dolomitization, although it may help to speed up reactions that lead to the formation of dolomite as suggested by Land (1967). Nonetheless, for extensive dolomitization sufficient amounts of both Mg^{++} and Ca^{++} are necessary. In recent years, it has been suggested that this could also be attained by pressure solution (Logan and Semeniux, 1976; Wanless, 1979), or by dilution of saline solutions (Badiozamani, 1973; Land, 1973; Folk and Siedlecka, 1972; Gebelein, 1977).

In this chapter, a review of dolomitization models is given in the form of a table (Table 2-1). Also, in order to emphasize the effect of dilution of marine water, a theoretical mixing model is discussed. The effect of dilution, taken in isolation, is to reduce the ionic strength of solutions, and to release ions from their complexes. Saturation curves of the major carbonate minerals for mixed solutions show that dolomite remains supersaturated for mixtures up to 90 wt. % fresh water, whereas aragonite and calcite are undersaturated in mixtures greater than 60 wt. % fresh water. Thus, mixing creates a condition where precursor lime muds and limestones could be dolomitized by dissolution and replacement.

Table 2-1. Dolomitization models

Dolomitization Model	Proposed Mechanisms of Dolomitization	Characteristics in Dolomites	Examples Cited	Remarks
Primary	Precipitation from normal marine water.	Sr = 650 ppm; enriched in ^{18}O; no replacement features	Holocene dolomites, Baffin Bay, Texas, Behrens and Land (1972).	*According to Saas (1965) marine water in equilibrium with calcite is undersaturated with respect to dolomite. *Baffin Bay, Texas, was also used as an example of a schizohaline environment by Folk and Sidelecka (1974).
	Precipitation from hypersaline epeiric seas that are not agitated by tidal activity. High Mg/Ca caused by formation of Ca-minerals, coupled with evapoconcentration.		Conceptual model, Shaw (1964), Irwin (1965). Mississippian system in parts of North and South Dakota, Irwin (1965).	Variations of this model have been used, e.g., Laporte 1971) for the Paleozoic central Appalachian Shelf; Harris (1973) for the Upper Cambrian-Lower Ordovician of Tennessee and Virginia. But, Harris's (1973) interpretation is not supported by the study of Upper Knox, Copper Ridge district, East Tennessee (e.g., Churnet and Misra, 1978, 1979). *Modern epeiric seas with widest shelves are characterized by the greatest tidal current velocities and tidal ranges, which suggest that ancient shallow seas were dominated by tides (Klein and Ryer, 1978). Also, tidal activity would have been pronounced before the Early Paleozoic, if the moon was closer to the Earth in those times (Textoris, 1969).
Capillary Concentration	Interstitial water in supratidal environments move upward by surface tension, and evaporate. Environment is replenished by marine water seeping laterally through sediments and/or by occasional flooding. Reduction of Ca^{++} in solution by formation of Ca-minerals coupled with evaporation causes high Mg/Ca ratios.	Fine grain-sizes, 3 μm, mudcracks, algally laminated sediments. Dolomitization is penecontemporaneous to lime mud deposition.	Holocene dolomites, Andros Islands, Bahamas, Shinn et al. (1965). Holocene dolomites, Persian Gulf Sabkha, Illing et al. (1965).	*Field measurements of salinities by Gebelein (1977, 1979) indicated chlorinities less than that of marine water. He interpreted that the dolomites formed from dilution by fresh water. (On the questions of high Mg/Ca ratios see Zenger, 1972a, 1972b).
Evaporative Pumping	Almost same as above but instead of upward motion due to surface tension, it is predominantly reduction in pressure in pore spaces	Apparently same as above.	Apparently all peritidal environments. Experimental studies, Hsü and Sigenthaler (1969).	

Table 2-1. (Continued)

Dolomitization Model	Proposed Mechanisms of Dolomitization	Characteristics in Dolomites	Examples Cited	Remarks
Evaporative Pumping Continued	that creates a vertically upward directed hydraulic gradient, causing marine water to seep laterally through sediments to a supratidal environment.		Field measurements in Abu Dhabi Sabkha by Hsü and Schneider (1973).	
Seepage Refluction	Marine water seeps laterally through sediments and/or occasionally floods a supratidal and lagoon environment. Evapoconcentration and reduction of Ca^{++} from formation of Ca-minerals results in denser brines of high Mg/Ca ratio. Refluxtion of the denser brines back to the ocean through sediments dolomitizes them.	Fine-grained and coarser-grained	Permian Basin, West Texas, Adams and Rhodes (1960); Holocene, South Bonaire (fine-grained, 5 μm); Plio-Pleistocene North Bonaire (coarser-grained 40-80 μm), Deffeyes et al. (1965).	*The Holocene occurrence of South Bonaire was more interesting because it would have served as a modern analog. But, drilling the bottom of the Pekelemear Lake and the adjacent sediment rubble showed the presence of a volcanic tuff underlain by sediments with normal marine pore waters (Lucia, 1968; Murray, 1969). Thus, this is a conceptual model. Also, motion of water in evaporative environments is toward the land to replace loss by evaporation (Hsü and Siegenthaler, 1969; Hsü and Schneider, 1973). *Formation of the Plio-Pleistocene of N. Bonaire involved fresh water as indicated by low Na-contents (350 ppm) and $\delta^{18}O$ values ranging from +1.97 to 4.1 (Seibly, 1979).
Algal Derivation	Organically complexed Mg^{++} between algal sheaths gets released during decomposition of the algal sheaths.	Cryptalgal laminae	Gebelein and Hoffman (1973)	Experimentally determined that sheath material of Schizotrux calcicola produced high Mg/Ca ratios, and produced high-Mg calcites. Reported that a 2-mm algal mat layer could produce 1-mm dolomite layer. Dolomitization is late diagenetic.
Solution Cannibalization	Dissolution of high-Mg calcite resulting in increased Mg/Ca ratio of solutions.	??	Andros Islands, Goodell and Garman (1969).	Four sequences of dolostones capped by limestones were recorded from drill cores up to 14,585 feet below surface. Reconstruction showed that the limestone horizons are coeval with regional unconformities, suggesting that the limestones marked disconformities. Dissolution of a part of the limestones caused dolomitization. *Hanshaw et al. (1971) suggested that such a process would not give enough magnesium to cause extensive dolomitization.

Table 2-1. (Continued)

Dolomitization Model	Proposed Mechanisms of Dolomitization	Characteristics in Dolomites	Examples Cited	Remarks
Hydrothermal Ground Waters	The Mg/Ca ratio in ground water is sufficient to cause dolomitization if the temperature of the solution is raised sufficiently.	??	No specific examples, Lovering (1969).	Experimentally-determined boundary lines, separating stability fields of calcite and dolomite at high temperatures, were extrapolated to low temperature. For a given concentration, the boundary is a straight line with a positive slope, for a temperature versus Ca/Mg molar ratio semi-log plot. Dolomite field is on the high temperature side. It was found that modern supratidal solutions plot in the dolomite field (Lovering, 1969). *According to Land (1967) Mg/Ca ratio of a solution determine speed of reaction. *Since solubility of calcite decreases rapidly with increase in temperature (Holland, 1967) it seems unlikely that extensive dolomitization can occur, unless Mg^{++} is supplied from an extraneous source.
Ore-Forming Solution	Wall rock reaction.	Coarse-grained dolostones.	East Tennessee, Hill (1969).	*In the vicinity of abundantly mineralized breccia bodies proximal to these breccias some limestone beds are not dolomitized, whereas farther away they are (see Chapter V).
Mixing of Fresh and Saline Water	High alkalinity (derived from dissolution of carbonate and organic decomposition) meteroric waters mixing with low alkalinity, high-ionic-strength sea waters.	Fine-grained (1 μm).	Holocene, Southwest Andros Island Bahamas, Gebelein (1977).	Field measurements from 100 wells in Southwest Andros showed that, ridges up to 2m above meantide level act as input areas of rain water for development of fresh water lenses within tidal flat sediments. Below the ridges chlorinities are less than 2,500 ppm all year around and active dissolution takes place. In mixing zone lenses (2,500 and 15,000 ppm Cl^-) high-Mg calcite and protodolomite form. Of the older Holocene sediments, areas highly flashed by fresh water have highest protodolomite concentration. Above information was confirmed in West Andros Island, but rare protodolomite was observed in hypersaline parts also (Gebelein, 1979).
	Fluctuating hypersaline to fresh water.	Both indicators of hypersalinity and fresh water. Siedlecka (	Late Paleozoic, Bear Island, Folk and Siedlecka (1974).	Indicators of hypersalinity are fine-grained crystals, length-slow chalcedony and sulfates; and of fresh water are limpid dolomite, and poikilotopic sparry calcite. Zoned dolomite and euhedral quartz observed but not diagnostic. This type was called schizohaline environment, apparently to distinguish it from the Dorag type of Badiozamani (1973).

Table 2-1. (Continued)

Dolomitization Model	Proposed Mechanisms of Dolomitization	Characteristics in Dolomites	Examples Cited	Remarks
Mixing of Fresh and Saline Water (Continued)	High CO_2 pressure of meteoric water being reduced due to mixing with marine water induces precipitation. Reduction of ionic strength may favor nucleation and growth (see also remarks).	Low Na content, low Sr/Ca ratio, and depletion in ^{13}C.	Pleistoce Hope Gate reef, north Jamaica, Land (1973).	Similar characteristics were observed from the Middle Ordovician, Mifflin Member dolostones of Wisconsin by Badiozamani (1973). Using a theoretical mixing model he demonstrated that dolomitization is feasible for mixtures between 5% and 30% marine water in mixture. Because for this range, the mixture is undersaturated with respect to calcite than the fresh water end-member whereas it is supersaturated with respect to dolomite.
Pressure, Solution as a Result of Dynamic Metamorphism	Mg^{++} made available from dissolution of precusor limestone at solution fronts.	All types of dolostones in significant amounts, and all textures observed in them.	Canning Basin, Western Australia, Logan and Semeniux (1976).	Authors argue that only small scale dolomitization is observed in modern environments, and that their mode of formation may not explain the larger-scale dolomitization of ancient times. *Playford and Lawry (1966); Playford and Cockbain (1976) have interpreted the same lithologies as reef complexes. *Based on fossil-size reduction, Logan and Semeniux estimate 80% dissolution. But, 4% dissolution would be estimated if reduction estimates of "Stylolite type" cleavages of Alvarez et al. (1978) were to be used.
Pressure Solution	Mg^{++} made available from dissolution of precusor limestones at solution fronts.	Fine-grained, coarse-grained dolostones, zoned dolomites.	Paleozoic, Arizona, Western Maryland, Southeast Kansas, Wanless (1979).	Response of limestone to overburden or tectonic pressure depends on the nature and structural resistance of limestone. Clean limestone that has no structural resistance develops nonseam solution (pervasive solution thinning). Dolomite growth is always observed associated with nonseam solution (Wanless, 1979).

*Observations that do not support the proposed model of dolomitization.

II. PREVIOUS WORK

Mixing of solutions as a viable means of dolomitization was proposed by several workers; for example, Hanshaw et al. (1971), Katz (1971), Land (1972, 1973), Badiozamani (1973), Folk and Siedlecka (1974), Folk and Land (1975), Mazzulo and Friedman (1977), and Churnet and Misra (1978). From a qualitative mass balance regarding the porosities of the dolomitized Hope Gate and undolomitized Falmouth reefs of north Jamaica, and the amount of Mg^{++} necessary for the observed diagenetic change, Land (1973) proposed that dolomitization occurred due to mixing of marine and meteoric water in a phreatic mixing zone. A quantitative approach involving mixing of solutions is a complicated problem. In addition to the uncertainty of the equilibrium constants of carbonates (Garrels and Christ, 1965), the complication arises because of the numerous variables involved, such as the composition of end member solutions, the solubility of salts in the presence of other salts that may or may not have common ions, the exact composition of the salts that are in equilibrium with the solution, and the temperature as well as the partial pressure of carbon dioxide at the time of mixing. However, it is possible in model mixing of solutions with certain simplifying assumptions.

Based on solubility data, Runnels (1969) emphasized the possibility that mixing of solutions could cause supersaturation or undersaturation of a constituent depending on whether or not the end member solutions were respectively undersaturated or supersaturated to begin with. In Runnels' approach, one first determines the solubility curve of a rock-forming mineral, then to estimate the effect of mixing of solutions

which have an ion in common with the rock-forming mineral, it is considered sufficient to join by a straight line the points on the solubility space that represent the solution compositions to be mixed. If a part of the solubility curve truncated by the straight line join is convex upward then mixing of the solutions would cause undersaturation of the rock-forming mineral. On the other hand, if the truncated part of the solubility curve is convex downwards, then mixing of solutions would cause supersaturation with respect to the rock-forming mineral. Based on considerations of saturation indexes, Plummer (1975) argued that due to changes in ionic strength with corresponding changes in activities of ions, the saturation degrees of mixtures would be different from those which would be predicted from a linear combination of solubilities of the end member solutions shown by Runnels (1969).

The effect of dilution considered in isolation would be to lower the degree of saturation of mixtures of solutions whose ionic strengths are close to the dilute end member of the starting solutions. The importance of this principle to carbonate diagenesis including dolomitization cannot be overemphasized, because as a consequence of dilution, carbonates (aragonite, calcite, and dolomite) which have different degrees of saturation become undersaturated for different mixing proportions in the mixtures. In application of this principle, Badiozamani (1973) used ground water from one of the wells of the Yucatan Peninsula and marine water as end member solutions and showed that the mixed solutions are undersaturated with respect to calcite for higher proportions of sea water content, whereas they are supersaturated

with respect to dolomite for lower proportions of sea water content. Plummer (1975) considered mixing four ground water solutions from Yucatan Peninsula and central Florida with marine water and saline ground water. He showed that in some cases the mixtures, including those of Yucatan ground water solutions, could be supersaturated with respect to calcite for all proportions of sea water content. This demonstrated that mixing ground water with solutions of higher ionic strength is not an isolated case of dilution but also depends on the amount of Ca^{++} in the ground water as well as the P_{CO_2}. The isolated effect of dilution may be demonstrated by mixing fresh surface water with marine water. The procedures and results of such an investigation are discussed below.

III. PROCEDURE AND RESULTS

A detailed treatment of the procedure and the assumptions used is given in Appendix A. Only the essential features of the procedure and results are discussed below.

Concentrations of dissolved ionic species of fresh and marine water were selected from the literature (Table 2-2). For general applicability of the results, the mean composition of river waters of the world (Livingston, 1963) is used to obtain the concentrations of dissolved ionic species in fresh water. The composition selected for marine water is that given by Davis (1977). Concentrations of dissolved ionic species in mixtures of marine and fresh waters are computed for different proportions of mixing (by weight) of the two (Table 2-3).

Table 2-2. Dissolved ionic species in fresh and marine water

Dissolved Ionic Species	Concentration in ppm	
	Fresh Water[x]	Marine Water[xx]
$C\ell^-$	7.8	19353.0
$SO_4^=$	11.2	2709.0
HCO_3^-	58.4	142.0
$CO^=_3$	*	*
Na^+	6.3	10762.0
Mg^{++}	4.1	1293.0
Ca^{++}	15.0	411.0
K^+	2.3	399.0
Br^-	@	67.3
$H_3BO_3^o$	@	4.4
Sr^{++}	@	7.9
F^-	@	1.3
NO_3^-	1.0	@
Fe^{++}	0.67	@
SiO_2^o	13.1	@

[x]Mean composition of river waters of the world (Livingston 1963, p. 41).

[xx]Major constituents of marine water (Davis 1977, p. 172).

*These concentrations can be obtained from P_{CO_2} and pH values, see Appendix A.

[@]Present only as minor constituents (e.g., Fe^{++} in marine water is 0.01 ppm - Mason, 1966). Concentrations of these are assumed to be zero for calculation subsequent to determining ionic strength of solutions.

Table 2-3. Concentrations of ionic species (ppm) for different weight percent of marine water in the mixture

Dissolved Ionic Species	0%	5%	10%	15%	20%	30%	40%	50%	60%	70%	80%	90%	100%
$C\ell^-$	7.8	975.1	1942.3	2909.6	3876.8	5811.5	7745.9	9680.4	11614.4	13549.4	15484.0	17418.5	19353.0
$SO_4^=$	11.2	146.1	281.0	415.9	550.8	820.5	1090.3	1360.1	1629.9	1899.7	2169.4	2439.2	2709.0
HCO_3^-	58.4	62.6	66.8	70.9	75.1	83.5	91.8	100.2	108.6	116.9	125.3	133.6	142.0
$CO_3^=$	0.16	0.8	1.6	2.4	3.2	4.8	6.4	8.0	9.6	11.2	12.8	14.4	16.0
Na^+	6.3	544.1	1081.9	1619.7	2157.4	3233.0	4308.6	5384.2	6459.7	7535.2	8610.9	9686.4	10762.0
Mg^{++}	4.1	68.7	133.0	197.5	261.6	390.8	519.7	648.6	777.4	906.3	1035.2	1164.1	1293.0
Ca^{++}	15.0	34.9	54.6	74.5	94.2	133.8	173.4	213.0	252.6	292.2	331.8	371.4	411.0
K^+	2.3	22.2	42.0	61.9	81.6	121.3	161.0	200.7	240.3	280.0	319.7	359.3	399.0
Br^-	0	3.4	6.7	10.1	13.5	20.2	26.9	33.7	40.4	47.1	53.8	60.6	67.3
H_3BO_3	0	0.2	0.4	0.7	0.7	1.3	1.8	2.2	2.6	3.1	3.5	4.0	4.4
Sr^{++}	0	0.4	0.8	1.2	1.6	2.4	3.2	4.0	4.7	5.5	6.3	7.1	7.9
F^-	0	0.1	0.1	0.2	0.3	0.4	0.5	0.7	0.8	0.9	1.0	1.2	1.3
NO_3^-	1.0	1.0	0.9	0.9	0.8	0.7	0.6	0.5	0.4	0.3	0.2	0.1	0
Fe^{++}	0.67	0.6	0.6	0.6	0.5	0.5	0.4	0.3	0.3	0.2	0.1	0.1	0
SiO_2	13.1	12.4	11.8	11.1	10.5	9.2	7.9	6.6	5.2	3.9	2.6	1.3	0

For a fixed proportion of fresh and marine water, the mixture is a single solution. Garrels and Thompson (1962) have developed a model for determining the amount of ions that occur as inorganic complexes in a single solution. The method involves deriving mass balance and mass action equations for various carbonate species, and gives 17 equations with 17 unknowns. In order to determine the percentage of ions that exist in complexes, these 17 equations can be solved simultaneously, or as discussed in Appendix A, they could be determined by a short-cut method recommended by Garrels and Thompson (1962). The latter procedure is also discussed by Berner (1971) and was adopted in this study.

After determining the percentage of ions that are tied as complexes, the percentage distributions of ionic species that remain as free ions was calculated (Table 2-4). The effect of dilution on the amount of complexing is illustrated by a plot of the percentage of ionic species tied in complexes versus wt. % marine water in mixtures (Fig. 2-1). Two sets of ionic activity products (IAP) for carbonate minerals, namely aragonite, calcite and dolomite,—a set of apparent IAP's without considering the effects of complex ion formation, and another set (effective IAP's) after considering the effects of complex ion formation were calculated. These give two sets of values for degrees of saturation (IAP/Keq.; where Keq. is the equilibrium constant calculated from the free energy of formation of a mineral at 25° C., and 1 atm.). The results are given in Table 2-5. A plot of degrees of saturation of the three carbonate minerals versus wt. % marine water in mixtures is shown in Fig. 2-2.

Table 2-4. Percentage distribution of ionic species that remain uncomplexed, for different weight percent of marine water in the mixture.

Ionic Species	0%	5%	10%	15%	20%	30%	40%	50%	60%	70%	80%	90%	100%
Mg^{++}	97.1	92.9	41.0	90.8	90.3	89.7	89.7	89.3	89.0	88.8	88.6	88.5	88.2
Ca^{++}	96.4	92.8	91.8	91.4	91.2	90.9	90.7	90.6	90.5	90.5	90.5	90.5	90.5
Na^{+}	99.9	99.4	99.1	98.9	98.8	98.5	98.4	98.3	98.2	98.1	98.0	97.9	97.8
K^{+}	100	99.5	99.3	99.2	99.1	98.9	98.8	98.7	98.6	98.6	98.5	98.5	98.4
$SO_4^{=}$	92.96	75.0	67.8	63.2	60.0	55.1	51.7	49.0	46.6	44.7	43.1	41.6	40.1
$CO_3^{=}$	60.2	28.4	22.7	19.6	17.7	15.5	13.9	12.7	11.8	11.2	10.5	10.0	9.7
HCO_3^{-}	99.1	95.9	93.6	91.6	89.7	86.4	83.6	81.0	78.7	76.5	74.4	72.5	70.7

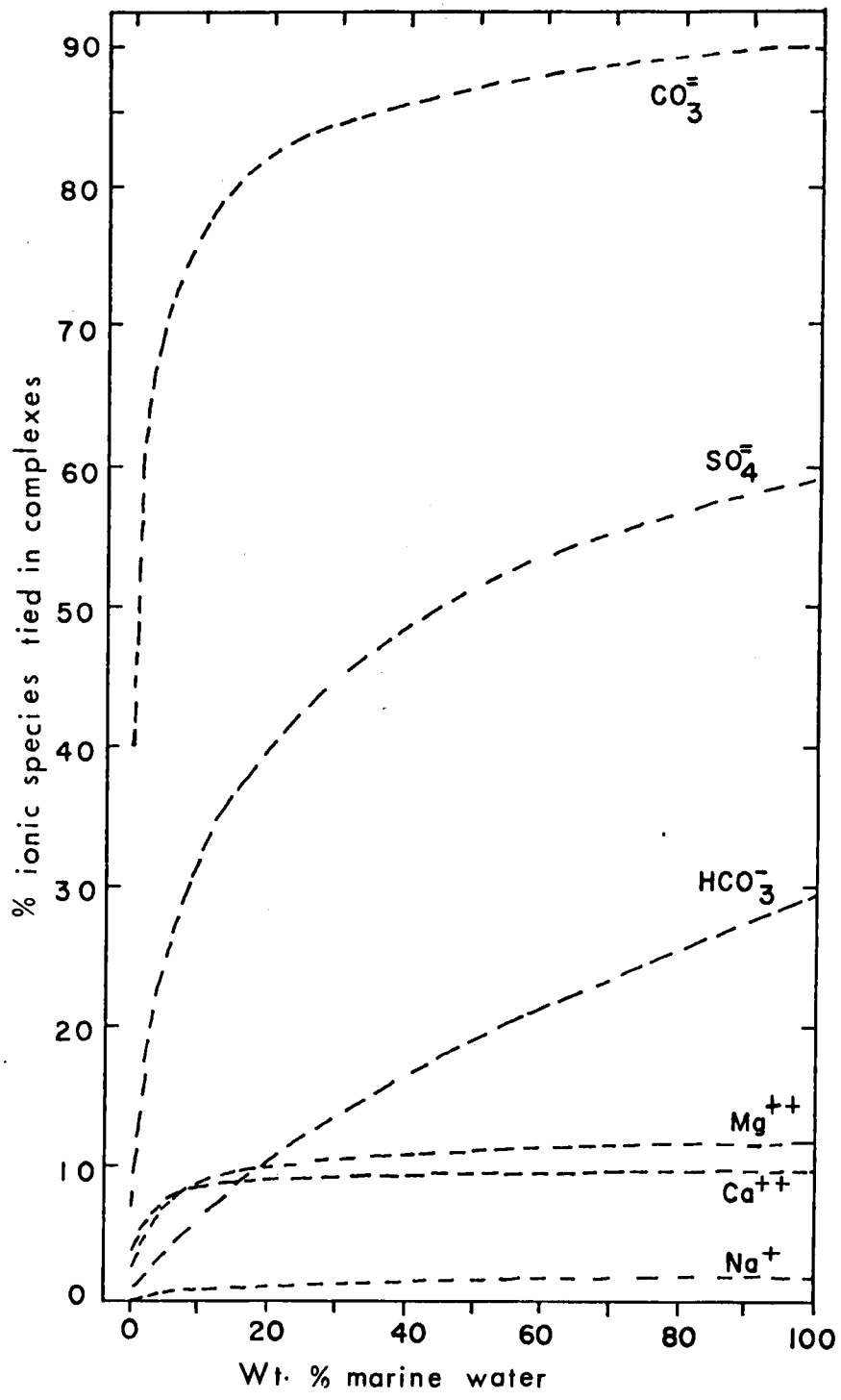

Figure 2-1. Effect of dilution on ionic species.

Table 2-5. Apparent and effective activities (a) and corresponding degrees of saturation (IAP/keq.) of carbonates for different weight percent of marine water in the mixture

Activities and Degrees of Saturation	0%	5%	10%	15%	20%	30%	40%	50%	60%	70%	80%	90%	100%
Apparent values													
$^{a}CO_3^{=}\times10^{6}$	2.2	6.7	12	14	16	22	28	31	35	40	42	46	50
$^{a}Ca^{++}\times10^{5}$	30	46	60	74	86	110	132	152	172	192	211	230	249
$^{a}Mg^{++}\times10^{5}$	14	156	263	360	449	618	716	930	1080	1228	1374	1520	1665
Dolomite	0.020	3.22	22.7	52.2	98.9	329	803	1360	2270	3770	5110	7400	1040
Calcite	0.153	0.716	1.67	2.42	3.21	5.63	8.60	10.95	14.00	17.86	20.60	24.65	29.07
Aragonite	0.103	0.481	1.126	1.63	2.16	3.78	5.78	7.36	9.41	12.00	13.84	16.56	19.53
Effective values													
$^{a}CO_3^{=}\times10^{7}$	13	19	27	27	28	34	39	39	41	44	44	46	49
$^{a}Ca^{++}\times10^{6}$	289	427	551	676	784	1000	1197	1377	1557	1738	1910	2082	2253
$^{a}Mg^{++}\times10^{6}$	136	1449	2409	3269	4054	5543	6930	8277	9590	10880	12160	13452	14685
Dolomite	0.007	0.223	0.967	1.61	2.48	6.41	12.6	17.3	25.1	36.6	44.9	59.2	79.4
Calcite	0.087	0.189	0.346	0.426	0.512	0.791	1.09	1.25	1.48	1.78	1.95	2.23	2.56
Aragonite	0.059	0.128	0.223	0.285	0.343	0.531	0.729	0.840	1.00	1.19	1.31	1.50	1.72

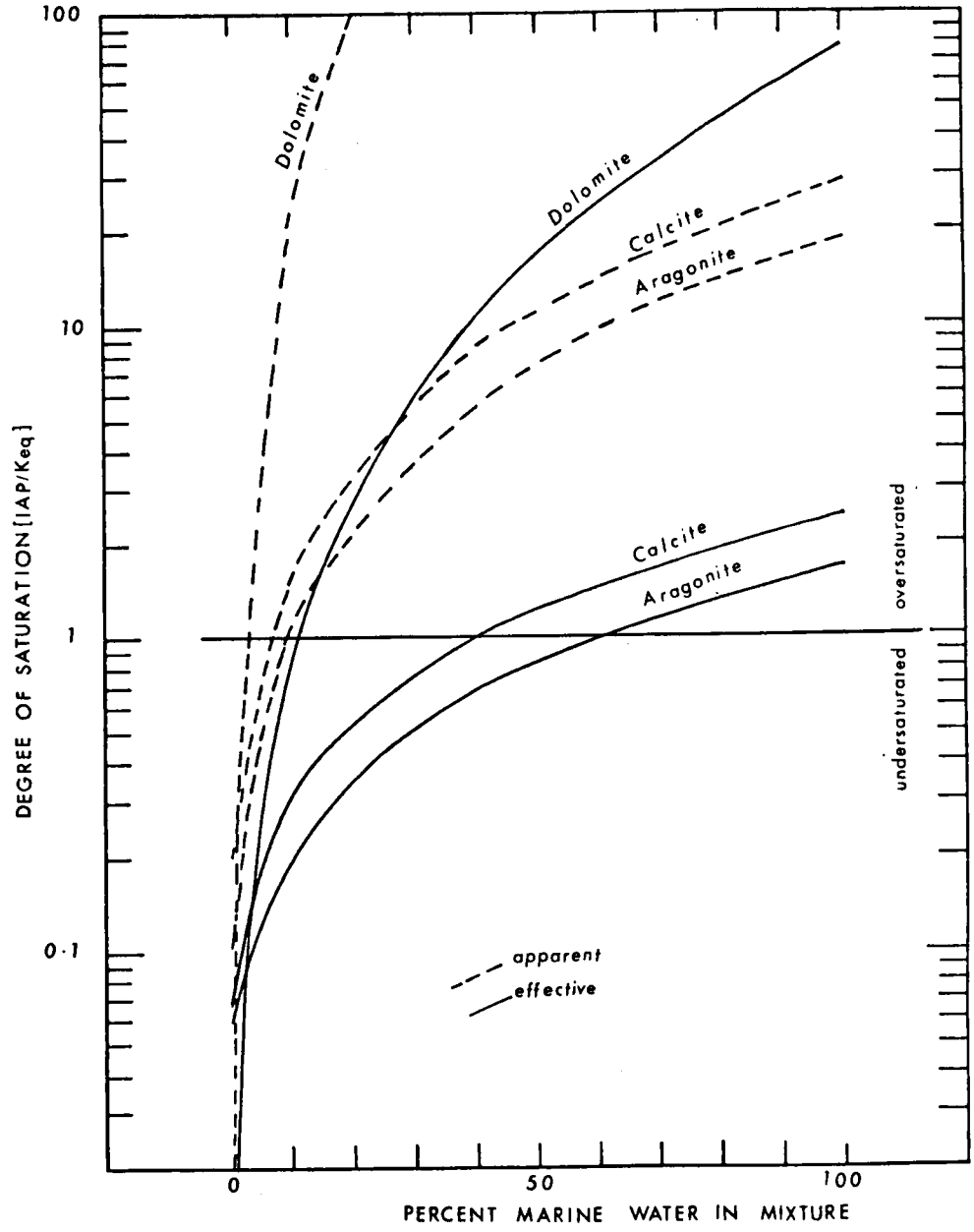

Figure 2-2. Saturation curves of carbonates.

IV. DISCUSSION

Figure 2-1 shows a decrease in the degree of complexing with increased dilution of marine water. Such a decrease in the degree of complexing is greater at higher values of dilution in marine water (e.g., 5% marine, 95% fresh). The figure also shows that the percentages of anions released by dilution are more than that of cations.

In Table 2-5, two IAP values are given. Here it can be seen that the effective IAP, which is calculated, after considering effects of formation of complex ions, is lower than the apparent IAP calculated without consideration of complexing. The effective IAP is the solubility product of the relevant carbonate, because it is obtained using ions that are not tied up as ionic complexes.

Assuming that no ionic complexes exist, it is possible to obtain apparent degrees of saturation whose values decrease due to a decrease of ionic strength as a consequence of dilution (Fig. 2-2). However, on account of the reduction in the availability of free ions due to formation of dissolved complexed ions in the solutions, the degree of saturation of carbonates is reduced for all mixtures of marine and fresh water. Such a decrease in the saturation degree of dolomite is relatively less than that of calcite for mixtures with higher proportions of fresh water. This is because dilution released the carbonate ion (mostly from $MgCO_3^o$) about 90% of which existed as dissolved complexed ions under marine conditions, to less than 40% under fresh water. Figure 2-2 (using the curves for the effective degrees of

saturation) shows for which proportions of the mixture carbonates are undersaturated. Thus:

Aragonite is undersaturated for < 60 wt % marine water in the mixture,

Calcite is undersaturated for < 40 wt % marine water in the mixture,

Dolomite is undersaturated for < 10 wt % marine water in the mixture.

It is interesting to note that the saturation curves for the three carbonates in question were considered in isolation although they are shown superposed in one diagram (Fig. 2-2). Supposing we consider a very localized environment over which fresh and marine water are allowed to mix and supposing 10% of $CO_3^=$ (for 99 wt % marine water in the mixture) were about to be engaged to form aragonite, because aragonite may form spontaneously (Goldsmith, 1953; Fyfe and Bischoff, 1965), then the solution may not be saturated with respect to calcite and dolomite, as the remaining $CO_3^=$, i.e., 90% is tied up in complexes. Such a concept makes one wonder if marine water in equilibrium with aragonite, particularly over a microenvironment around aragonite, may be considered to be oversaturated with respect to calcite and dolomite (see also Saas, 1965). On the other hand, dilution by fresh water, as shown previously, releases ions from their complexes as well as reduces the ionic strength of solutions and thereby promotes the replacement of aragonite, dolomitization being preferred for 10-40 wt % marine water in the mixture. At this stage, it might be worthwhile to speculate further.

Perhaps the rate of change of dilution of saline waters might give rise to different grain sizes of dolomites. It might well be that dilution by fresh water of hypersaline solutions, such as by rare but short-lived showers and surface runoff characteristic of an arid climite, might, over a short period, cause release of ions and induce dolomitization giving rise to fine-grained dolomites; whereas, in a phreatic mixing zone longer periods of mixing at a fresh and marine water mixing front might result in dolomites with coarser grain sizes.

It should also be pointed out that the curves (Fig. 2-2) are indicative of a general situation of mixing and may also apply to carbonate cementation in clastic sediments. In particular cases though, they may not apply, for as Land (1973) noted, some fresh water rivers are oversaturated with respect to calcite, whereas others are not. Also, in areas where gypsum may be present, dissolution of gypsum by fresh water could result in increasing the calcite saturation of the fresh water end member several fold, so that, for lower proportions of marine water in the mixtures, calcitization of dolomite may prevail.

V. CONCLUSION

Some of the main points from the review of the dolomitization models are as follows:

1. The seepage refluxion model, involving downward movement of brines, has no demonstrated modern analog. Laboratory measurements indicate that motion of saline water in an evaporative supratidal environment is directed upward to replace loss by evaporation.

2. For extensive dolomitization, ample Mg^{++} should be available. But the mechanisms that favor the formation of dolomite are increase in Mg/Ca ratio, decrease in P_{CO_2}, increase in pH, increase in temperature and dilution of solutions. These mechanisms could act singly or in combination in order to cause dolomitization.

A theoretical investigation of the isolated effect of dilution shows that aragonite and calcite are undersaturated, and dolomite oversaturated for 10 to 40 wt % marine water in mixtures of fresh and marine waters. Thus, dolomitization (by dissolution and replacement) is feasible for this range of mixtures.

CHAPTER III

TRACE ELEMENT CONTENTS OF THE UPPER KNOX ROCKS AND GENETIC IMPLICATIONS

I. INTRODUCTION

The Upper Knox carbonate rocks studied in the Copper Ridge district, East Tennessee, consist of dolostones and limestones. The dolostones fall into two distinct groups: fine-grained dolostones consisting of < 0.062 millimeter-sized dolomite crystals, and coarser than fine-grained dolostones consisting of dolomite crystals generally greater than 0.1 mm in diameter. Justification for this grouping as well as interpretation of the field relations and petrographic characteristics of these carbonate rocks is discussed in Chapter IV. The present chapter deals with an assessment of the conditions of carbonate precipitation using the trace element contents in these rocks. This assessment is critically dependent on the availability of partition coefficients of trace elements between carbonate minerals and the parent solutions. As it is difficult to precipitate dolomite in the laboratory under low temperature conditions, experimentally determined partition coefficients of trace elements between dolomite and solution are not available. Even for calcite, experimentally determined partition coefficients of most trace elements are not available. However, approximate values of partition coefficients can be estimated. Although the absolute magnitudes of these estimates are higher than would be found from experimental

determinations, the ordering of the partition coefficients appear reliable. Both experimentally determined partition coefficients and the ordering of trace elements based on approximate partition coefficients provide constraints for the evaluation of the conditions under which the carbonate rocks formed.

II. METHODS OF INVESTIGATION

A Nuclide Corporation Luminoscope, Model ELM-2A, was used to study luminescent patterns in carbonate minerals. The intensity of the luminescent colors is not only a function of the characteristics of the crystal [i.e., presence of impurities and/or lattice defects (Nickel, 1978)], but it is also a function of the operating conditions (Ebers, 1976; Ebers and Kopp, 1979). Therefore, all the samples were studied under constant operating conditions as follows: a beam diameter of about 2 cm; a current of 0.6 mA; a voltage of 12 KV; and an exposure time for photographic films (Kodak Ektachrom: Tungston, ASA 160, 3200 K) of 1 to 2 minutes.

An automated three-channel MAC 400-S electron microprobe analyzer was used to analyze for Fe, Mn, Ca, Mg in dolomite and calcite. The operating conditions were as follows: a voltage of 15 KV; a specimen current $\approx$ 0.4 μA; and a beam diameter $\approx$ 5μ. Data were obtained for Kα lines using LiF (for Mn, Fe), PET (for Ca), and RAP (for Mg) analyzing crystals. Matrix corrections were made by using the ABFAN computer program (Boyd et al., 1969). The precision of the analytical results are estimated to be ± 2% each for Ca and Mg, ± 6% for Fe, and for Mn:

± 75% to ± 30% for concentrations ranging from 0.04 to 0.1 wt. % Mn, and ± 30% to ± 15% for concentrations ranging from 0.1 to 0.2 wt. % Mn (see Appendix B for estimation of error in Mn analysis).

Neutron activation analysis was conducted at the Oak Ridge Associated Universities. Accurately weighed powdered samples (in the range of 2 gm) were put in polyethylene containers. A high intensity neutron emitter with the following specifications was used as source: 28 mg ^{252}Cf, April 1976; Half life = 2.65 years; decay, 3% Fission, 97% alpha; neutron emission rate, 2.34×10^{6} n/sec-mg; thermal flux = 1.5×10^{8} cm^{-2} sec^{-1}. A Li-drifted Ge crystal was used as detector. Data were obtained by the absolute determination method for Kα lines (Lyon, 1964). Corrections for dead time and instrumental drift were made by the automation of the system. Precision of analytical results are estimated to be ± 0.5-1.2% for Mn; ± 0.7-1.6% for K; ± 1-5% for Na; ± 4-10% for Sr; and ± 3-9% for Al.

III. RESULTS

Zoning in Dolomite Crystals

When studied with a plane-polarized transmitted light petrographic microscope dolomite crystals of the coarser than fine-grained dolostones usually display a zoning pattern of cloudy centers and clearer rims. Some of these cloudy centers appear to be ghost peloids. Irrespective of the above type of zoning, as many as eight growth zones were observed in these dolomite crystals (Fig. 3-1), when studied with a luminoscope. Dolomite crystals belonging to fine-grained dolostones do not display such growth zones.

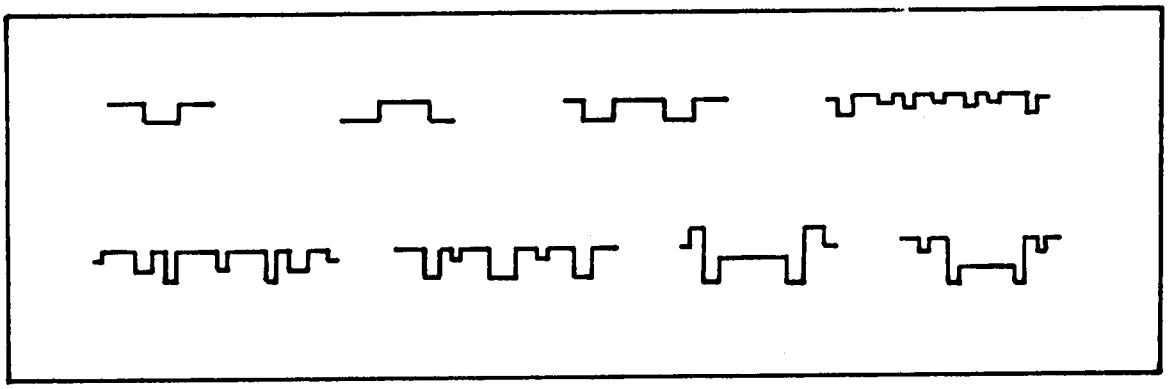

Figure 3-1. Summary of the zonal luminescent patterns of dolomite crystals belonging to the coarser than fine-grained dolostones. Relative intensities of the luminescence zones are shown on vertical axes, and the corresponding widths are displayed on horizontal axes. On the vertical axes, brighter luminescent zones are shown on higher levels than the adjacent darker zones. Both the intensities and widths of luminescent growth zones were visually assessed from the luminescent patterns of specimens studied using a luminoscope. For details of such a method of representation, see Appendix C.

Luminescent patterns in calcite have been correlated with variations in Fe/Mn ratios (Long and Agrell, 1965; Feazel, 1978). Dolomites associated with sphalerite mineralization in East Tennessee were observed by Ebers (1976) to luminesce shades of red, but he made no quantitative analysis of the compositional variations. The luminescence patterns of fracture-fill dolomites from the Mascot-Jefferson City district studied by Cobb (1974) were interpreted to be due to variations in the Fe and Mn contents, higher Fe and Fe/Mn ratios corresponding to darker zones, and indications of higher Mn contents corresponding to brighter zones. However, the Mn concentrations were very low and the analytical uncertainty for Mn was estimated by Cobb (1974) to be ± 75%.

The Mn contents of the coarser than fine-grained dolomites analyzed in the present study were also very low (Table 3-1, part A) and in some cases below the detectability limit of Mn (which is about 0.04 st. %). This problem was circumvented by analyzing vug-fill dolomite crystals which, in general, show similar luminescent zones of various shades of red but sometimes have higher concentrations of Mn (e.g., Table 3-1, part C). To avoid the uncertainty in locating the boundaries between dark and bright zones, electron microprobe analyses were performed on preselected crystals of vug-fill dolomite that luminesced either uniformly dark red or uniformly bright red. Compositional data so obtained, a representative set of which is included in Table 3-1, suggest that brighter luminescent zones are characterized by higher Mn/Fe ratios.

The coarser than fine-grained dolomites show distinct compositional zoning (Table 3-1, part A; Fig. 3-2). Electron microprobe analyses on

Table 3-1. Composition (wt. %) of dolomite crystals obtained by electron microprobe analyses

A. Coarser than fine-grained dolomite (Analyses were performed at approximately equidistant points on a traverse across a zoned dolomite crystal; Sample SS-4)

Traverse Point	Mn	Fe	Ca	Mg	Total
1	*	0.30	19.46	10.67	30.45
2	0.05	0.50	25.11	10.30	35.96
3	*	0.12	24.00	10.54	34.66
4	*	0.27	22.00	10.39	32.69
5	*	0.04	27.91	9.13	37.11
6	0.08	0.07	32.39	4.61	37.14
7	0.05	0.28	23.42	10.73	34.48
8	*	0.18	26.56	7.92	34.65
9	0.18	0.15	26.22	8.94	35.49
10	*	0.18	21.82	12.01	34.01
11	*	0.49	22.66	10.86	34.01
12	0.18	0.52	25.59	9.68	35.97
13	0.11	0.46	21.72	12.03	34.32

B. Dark red luminescent vug-fill dolomite (Sample S-13)

Analysis Point	Mn	Fe	Ca	Mg	Total
1	0.04	0.98	22.02	12.21	35.26
2	0.05	0.99	21.96	12.39	35.39
3	0.08	0.90	22.11	12.67	35.76
4	0.05	0.94	21.97	12.49	35.49
5	0.06	0.87	21.73	12.38	35.05
6	0.05	0.86	21.47	12.19	34.57
7	0.05	.078	21.87	12.28	34.98
8	*	0.91	21.41	12.40	34.74
9	*	0.91	21.75	12.37	35.03
10	0.08	0.92	21.34	12.44	34.78
11	0.04	0.90	21.10	12.44	34.19
12	0.04	0.82	21.97	12.57	35.41
13	0.05	0.93	21.82	12.16	34.96
14	0.10	0.91	21.82	11.97	34.79
Average		0.90	21.75	12.33	35.03

C. Bright red luminescent vug-fill dolomite (Sample RR-83)

Analysis Point	Mn	Fe	Ca	Mg	Total
1	0.10	0.41	22.37	12.81	35.68
2	0.10	0.41	21.87	13.08	35.40
3	0.19	0.56	21.61	12.77	35.14
4	0.13	0.35	21.38	12.77	34.62
5	0.07	0.50	21.65	12.83	35.05
6	0.10	0.45	22.08	13.19	35.81
7	0.13	0.46	22.01	12.94	35.54
8	0.24	0.89	21.57	12.51	35.20
9	0.10	0.37	22.46	13.03	35.95
Average	0.13	0.48	21.86	12.88	35.38

*Values less than 0.04 wt. %.

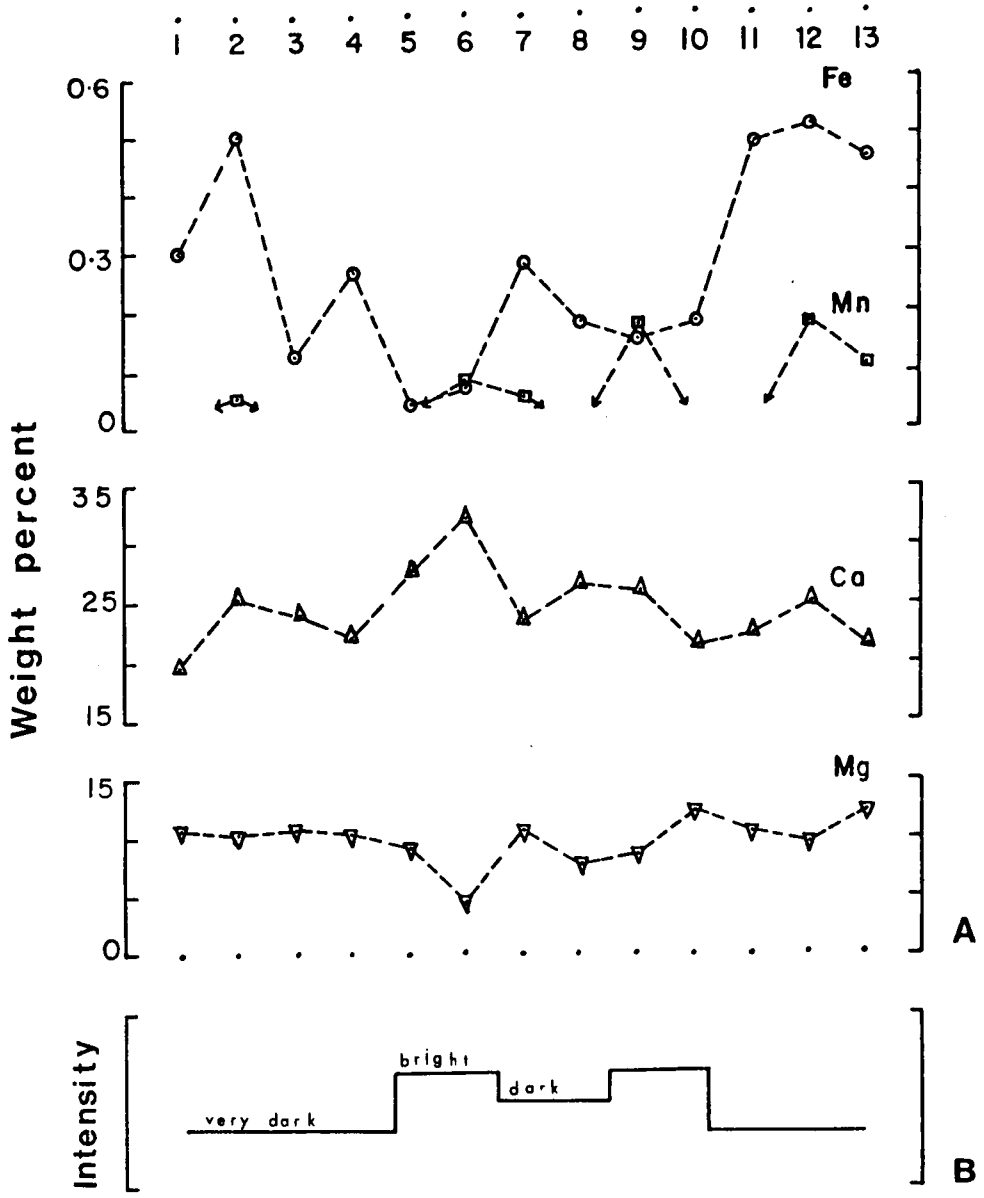

Figure 3-2. Electron microprobe traverse across a zoned dolomite crystal. Numbers at the top correspond to analysis spots on a traverse from rim through center to rim of a crystal. Corresponding compositional data are given in Table 3-1A. The relative intensities and the approximate locations of luminescent zonal boundaries are shown at the bottom of the figure (B).

such dolomite crystals indicate a general increase in Fe from the core to the rim of individual crystals. Qualitative information on the distribution of Fe in these dolomites, obtained by staining with acidified potassium ferricyanide solution, corroborate the quantitative data obtained from the selected dolomite crystals. Most of the coarser than fine-grained dolomites (CFd) in the Copper Ridge district stain deep blue at the edges suggesting an increase in Fe toward the rims (e.g., Evamy, 1963). Due to large errors in the low Mn concentrations of CFd it is not possible to judge if Mn varies systematically with Fe. As shown in Fig. 3-3, the variation of Fe in a crystal does not necessarily correspond to the variation of the Ca/Mg ratio.

Trace Elements in Bulk Samples

Whole rock, neutron activation analyses of selected samples from the Copper Ridge district are given in Table 3-2. Analyses were performed on six samples for each of the three major lithologies in the district (limestone, fine-grained dolostone, and coarser than fine-grained dolostone) and three samples of greenish shaly material that occurs interbedded with the carbonate rocks. The samples were collected from the unmineralized River Ridge section and from the mineralized sections at Shiloh and Joe Mill zinc prospects and Idol mine (see Chapter IV for details). These data indicate that the lithologies in mineralized and barren localities may not be distinguished by their Na, K, Mn, Sr, and Al contents.

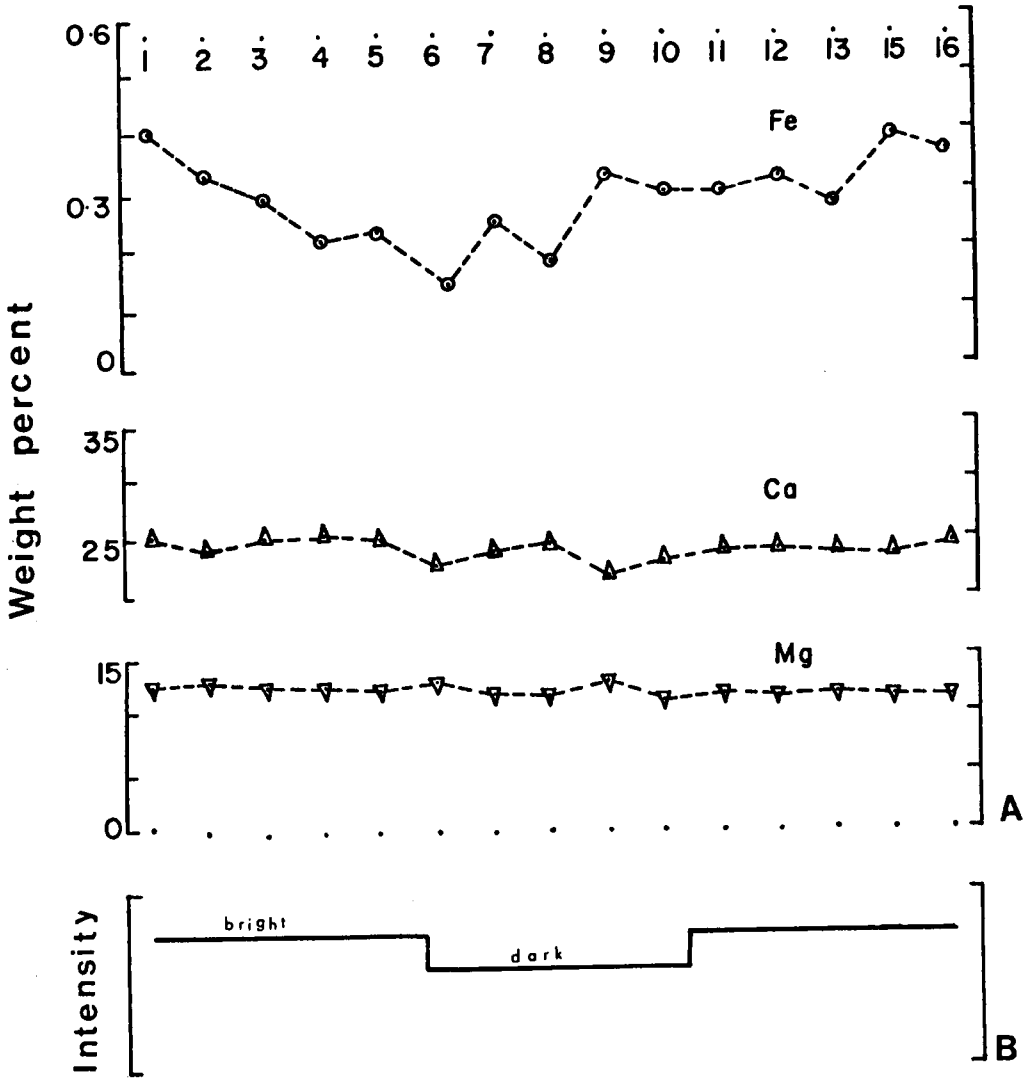

Figure 3-3. Electron microprobe traverse across a zoned dolomite crystal. The figure shows that the distribution of Fe in dolomite tends to increase towards the rims of the dolomite. This increase is not dependent on the variation of the Ca/Mg ratio. The relative intensities and the approximate location of the luminescent zonal boundaries are shown at the bottom of the figure (B).

Table 3-2. Neutron activation analyses of trace element concentrations (ppm) in the Upper Knox rocks

Sample	Na	K	Mn	Sr	Al
		A. Limestone			
RR-60D	155 ± 3	16710 ± 2	49 ± .9	200 ± 10	@
RR-49B$_1$	70 ± 2	4441 ± 2	33 ± .6	281 ± 4	4164 ± 3
J-24	75 ± 4	4497 ± 4	66 ± .7	188 ± 10	3701 ± 7
J-26D	92 ± 4	5097 ± 5	135 ± .5	229 ± 11	4781 ± 3
SS-11	57 ± 5	3704 ± 4	103 ± .7	214 ± 11	@
SS-7	42 ± 5	803 ± 13	53 ± .9	273 ± 7	@
		B. Coarser than fine-grained dolostone			
RR-82A	242 ± 2	696 ± 16	118 ± .6	@	@
RR-79F	256 ± 1	3440 ± 3	927 ± .5	@	3772 ± 4
J-17	362 ± 1	2743 ± 4	209 ± .7	@	2491 ± 4
J-22	363 ± 2	@	121 ± .5	@	9961 ± 3
J-20	365 ± 2	6964 ± 3	102 ± .5	@	7346 ± 6
SS-15	327 ± 4	17235 ± 4	825 ± .6	@	17208 ± 5
		C. Fine-grained dolostone			
RR-42	48 ± 5	899 ± 10	38 ± .8	226 ± .6	@
RR-94	196 ± 1	3226 ± 2	76 ± .5	67 ± 19	3167 ± 4
J-8	204 ± 2	3876 ± 5	211 ± 1	@	3178 ± 4
J-15A	201 ± 2	11080 ± 2	99 ± .6	@	@
S-10	209 ± 3	7869 ± 4	241 ± 1	@	6956 ± 7
SS-1	200 ± 2	3766 ± 5	@	@	@
		D. Greenish shaly material			
RR-87	545 ± 2	84811 ± .8	66 ± .7	@	97019 ± 3
RR-89	581 ± 1	88151 ± .7	92 ± .6	@	97603 ± 9
Idol Stop 1519	720 ± 4	@	79 ± 1	@	104739 ± 3

@ - Not detected

RR - Samples from the unmineralized River Ridge Section.

J - Samples from the mineralized Joe Mill-Rucker Branch Section.

S and SS - Samples from the mineralized Shiloh Section.

IV. DISCUSSION OF RESULTS

Theoretical Considerations

For a particular set of environmental conditions, carbonate phases which precipitate from a given solution incorporate trace elements according to the partition coefficients of these trace elements between the carbonate phases and the solution. There are three important aspects to the partition coefficients of trace elements: (1) the magnitude of the partition coefficients, (2) the ordering of the partition coefficients, and (3) whether the partition coefficients are greater or less than unity.

The partition coefficients K_T^{MX} of a trace element (T) between a crystallizing major phase (MX) and its supersaturated aqueous solution (L) with which the solid major phase (S) is in equilibrium can be expressed by the Berthelot-Nernst Homogeneous Distribution Law as:

$$K_T^{MX} = \left(\frac{m_T}{m_M}\right)_S \Big/ \left(\frac{m_T}{m_M}\right)_L$$

where m is molal concentration; X denotes anion, and M denotes cation of a major element.

Under certain simplifying assumptions, Crocket and Winchester (1966) showed that the partition coefficient of a trace element is approximately equal to the ratio of the solubility product (K_{sp}) of the pure major phase (MX) to that of the pure trace element phase (TX); i.e.,

$$K_T^{MX} = \frac{\left(K_{sp}\right)_{MX}}{\left(K_{sp}\right)_{TX}} .$$

Derivation of this approximate relation involves the following assumptions: the temperature and pressure are kept constant, other ions and organisms have no effect on the partitioning, and the solution is ideal. Approximate values of $K_T^{calcite}$ estimated by Crocket and Winchester (1966) are given in Table 3-3.

Some partition coefficients have been determined experimentally. At 25°C, these values are: $K_{Zn^{++}}^{calcite} + 5.7 \pm 0.03$ (Crocket and Winchester, 1966); $K_{Sr^{++}}^{calcite} = 0.14$ (Kinsman and Holland, 1969; Kinsman, 1969); $K_{Sr^{++}}^{aragonite} = 1.14$ (Kinsman and Holland, 1969). For similar temperatures, Pingitori (1978) considered $K_{Mg^{++}}^{calcite} = 0.02$, and $K_{Mn^{++}}^{calcite} = 15$ to be reasonable estimates. Evidently, the $K_T^{calcite}$ values obtained by the approximation discussed above are higher than those obtained experimentally. This is largely because of the assumption that the solution is ideal. However, it is important to note that the ordering of the partition coefficients for calcite obtained from the above data, $Mn^{++} > Zn^{++} > Sr^{++} > Mg^{++}$, is also apparent from the approximate values given in Table 3-3. In absence of experimental data, it appears reasonable to assume that the ordering of the partition coefficients for calcite as given in Table 3-3 is valid.

Approximate values of partition coefficients for magnesite calculated from solubility products show similar ordering as for calcite.

Table 3-3. Approximate partition coefficients of trace elements in calcite, magnesite, and dolomite at 25°C

Carbonate Phase	*Crystal Class	*Divalent Cationic Radius Å	*Log K_{sp}	*$K_T^{calcite}$	$K_T^{magnesite}$	$K_T^{dolomite}$
$NiCO_3$	O	0.69	-6.88	0.035	0.60	0.35
$MgCO_3$	H	0.66	-8.04	0.50	M	M
$CaCO_3$	H	0.99	-8.34	M	2.00	M
$BaCO_3$	O	1.43	-8.78	2.8	5.50	1.4
$SrCO_3$	O	1.16	-9.15	6.5	12.88	3.3
$CuCO_3$		0.72	-9.61	18	37.15	18.6
$ZnCO_3$	H	0.71	-9.82	30	60.25	30.1
$FeCO_3$	H	0.74	-10.66	210	416.87	208.4
$CdCO_3$	H	0.97	-11.29	890	1,778.87	445.0
$MnCO_3$	H	0.80	-11.57	1,700	3,388.44	1,694.2
$PbCO_3$	O	1.24	-12.95	41,000	81,283.05	20,500

*Adopted from Crocket and Winchester (1966).

H is hexagonal, ditrigonal scalenohedral, space group 3 2/m. O is orthorhombic, dipyramidal space group 2/m 2/m 2/m.

M = major element.

$K_T^{magnesite}$ calculated in the present study using the approximation method of Crocket and Winchester (1966).

Calculation of $K_T^{dolomite}$ is explained in the text.

Ordering of Partition Coefficients for Dolomite

Using the solubility products of dolomite and other carbonate compounds, the ordering of partition coefficients of trace elements in dolomite can be assessed, and it is the same as for calcite. Nonetheless, considering that trace elements proxy for Ca^{++} in the $CaCO_3$ layer and for Mg^{++} in the $MgCO_3$ layer of dolomite (e.g., Berry and Mason, 1968), approximate partition coefficients for dolomite may be obtained from partition coefficients for magnesite and calcite. The latter approach may be more valuable because partition coefficients for calcite and magnesite can be experimentally determined. However, experimentally determined partition coefficients for calcite and magnesite are available only for a few trace elements. Thus, the ordering of partition coefficients for dolomite may be estimated using the approximate partition coefficients for magnesite and calcite.

Although it appears that the partition coefficients of trace elements, for example Fe^{++} and Mn^{++}, in $MgCO_3$ will be similar to that of dolomite, it is reasonable to expect the Fe^{++}/Mg^{++} and Mn^{++}/Mg^{++} ratios in magnesite would be twice that in a coexisting dolomite (where only half of the layers in the crystal consist of $MgCO_3$). Similar arguments were made for Sr^{++}/Ca^{++} ratios in calcite being twice that in coexisting dolomite (Badiozamani, 1973; Land, 1973).

Approximate values of $K_T^{dolomite}$ are estimated to be half of either $K_T^{calcite}$ or $K_T^{magnesite}$ depending on the closeness of the ionic radii of divalent trace element cations of Ca^{++} or Mg^{++}, respectively. These values are given in Table 3-3. It should be emphasized that although

the estimated magnitudes of the partition coefficients are only approximations, their ordering appears to be the same as for calcite.

One Solution Model

The ordering of partition coefficients can be used to assess whether a particular distribution pattern of trace elements in carbonate minerals is compatible with their formation from one or more solutions. For the purpose of illustration of principles, the simplest case where only one solution is involved is discussed below.

(1) Closed system of limited volume

During precipitation of crystals from a closed system of limited volume, the uptake of trace elements with $K_T^{MX} > 1$ will be greater at the centers than at the rims. This is because at low temperatures no change in composition of crystals can occur after precipitation, whereas the solution is progressively depleted in its trace/major element content by a logarithmic distribution relationship (Crocket and Winchester, 1966). Also, the distribution of trace elements will be expected to reflect the ordering of their partition coefficients. Thus, in contrast to trace elements with lower K_T^{MX}, those with higher K_T^{MX} would be more concentrated at the cores of crystals than at the rims. The partition coefficients of Zn and Mn in calcite were used to illustrate such relationships (Pingitori, 1978). For the same conditions, the distribution of trace elements with $K_T^{MX} < 1$ should show an increase towards the rims of crystals (for example, Sr^{++} in calcite), because the solution will be progressively enriched in the trace/major element ratio (Kinsman, 1969).

(2) Open system of limited volume

For an open system a large number of possibilities may be envisaged. Some of these were discussed in detail by Kinsman (1969) and Pingitori (1978) for calcites. One aspect of the anticipated behavior of trace elements is summarized below.

A solution undersaturated with respect to minerals that surround pore spaces is allowed to pass through pore spaces of sediments. Dissolution of adjoining minerals supplies elements to the solution. It is assumed that the transportation of the solution through the sediments is slow enough so that replacement (by dissolution and precipitation) can occur. In the initial stages of the growth of a crystal, trace elements with $K_T^{MX} < 1$ will be incorporated in the replacing mineral to a smaller extent and the solution will be enriched in these trace elements. If the solution now moves to another site, and its previous position is occupied by a fresh solution, the continued growth of the crystal will record a lower trace/major element ratio than the precursor mineral. In contrast, trace elements with $K_T^{MX} < 1$ will be incorporated in a replacing mineral to a greater extent whereas the solution becomes depleted in these trace elements.

Depending on the system flow (e.g., repeated combinations of slow and fast flow of pore solution), it appears that a diagenetic mineral can be enriched in certain trace elements (those with $K_T^{MX} > 1$) and depleted in others (those with $K_T^{MX} < 1$) compared to the precursor minerals. Pingitori (1978) considered that the upper limit of incorporation of trace elements in a replacing crystal by "autoenrichment"

would be K_T^{MX} times the trace/major element mole ratio in the replaced crystal.

V. INTERPRETATION OF TRACE ELEMENT DATA

Sodium

In the three major lithologies the Na contents are: 82 ± 40 ppm in limestones, 319 ± 56 ppm in coarser than fine-grained dolostones, and 176 ± 63 ppm in fine-grained dolostones. Such small amounts of Na were interpreted by Land (1973, p. 86) as suggesting that the carbonates did not form from normal marine solution. One of the examples Land (1973) used to propose that some ancient dolostones were not formed from normal marine solution, was the whole rock analytical data of Weber (1964). Weber's (1964, p. 1825) data for Na are: 391 ± 563 ppm (average of 141 samples) for fine-grained dolostones, and 251 ± 122 ppm (average of 96 samples) for coarser grained dolostones. The Na contents of the Copper Ridge dolostones, which clearly are within the range given by Weber (1964), suggest that the Copper Ridge dolostones formed from a more dilute solution than either normal marine or hypersaline solutions. The Na content of incompletely dolomitized limestones analyzed by Weber is 2250 ± 3090 ppm (average of 24 samples), on the average higher than those in Copper Ridge District. This suggests that the Copper Ridge limestones were probably neomorphosed in environments where the solution was not entirely marine.

Manganese

Using the data (Mason, 1966, p. 195) for distribution of elements in marine water, the mole ratio $\frac{Mn^{++}}{Ca^{++}} = \frac{.002}{400} \times \frac{40.08}{54.94} = 3.65 \times 10^{-6}$. Assuming that the partition coefficient of Mn in calcite is constant and using the value of 15 (which was considered to be a reasonable value by Pingitori, 1978), a crystal of calcite that forms from marine water should have a $\frac{Mn^{++}}{Ca^{++}}$ mole ratio of 5.47×10^{-5}. This corresponds to about 30 ppm Mn in calcite. The Copper Ridge limestones have a higher Mn content (73 ± 38 ppm as obtained during this study, and 301 ± 179, as obtained by West, 1974). This does not necessarily mean that the limestones formed from solutions with higher content of Mn than normal marine water. The higher Mn contents of the Copper Ridge dolostones could be due to autoenrichment as suggested by Pingitori (1978) to explain the higher Mn content of the Pleistocene limestones of Barbados (27 ppm) compared to the Mn content of the aragonitic limestone precursor (17.6 ppm). Other possible explanations include substitution of Mn from the associated shaly material (79 ± 13 ppm Mn), uncertainty in the value of the partition coefficient used for Mn^{++}, and incorrectness of the assumption that the partition coefficient of Mn^{++} is a constant.

Even less is known about the partition coefficient of Mn^{++} in dolomite. However, Mn^{++} contents of the Copper Ridge dolostones are similar to those given by Weber, 1964 (245 ± 454 ppm, from 140 samples of fine-grained dolostones; 237 ± 325 ppm, from 95 samples of coarser grained dolostones). The purpose of this comparison is to indicate that high values of Mn in dolostones are not unusual, and do not necessarily require

enrichment by solutions associated with sphalerite mineralizing fluids as suggested by West (1974). More discussion on the problem of Mn distribution is given later.

Strontium

If $K_{Sr^{++}}^{calcite}$ is 0.14 as determined by Kinsman and Holland (1969), the Sr content of limestones in the Copper Ridge District (av. 231 ± 38 ppm) is lower than would be expected had they formed directly from marine water. Actually, in modern environments, the types of $CaCO_3$ compounds that form directly from marine water are high-Mg calcite with Sr contents of 1000 to 5000 ppm and aragonite with an average Sr content of about 9800 ppm (Kinsman, 1969). Thus, the low content of Sr in the Copper Ridge district limestones indicates that they probably were not neomorphosed under marine water. This agrees with data obtained from the Flat Gap Mine by West (1974, Appendix C).

Averages calculated from the data of West (1974) show that the abundance of Sr in calcites of limestones is 188 ± 42 ppm (from 14 samples), in dolomites of coarser grained dolostones is 52 ± 43 ppm (from 43 samples), and in dolomites of fine-grained dolostones is 37 ± 20 ppm (from 4 samples). Thus the Sr/Ca ratio in the coarser dolomites (0.00024) is about half of that in the calcites (0.00047), suggesting that the limestones and the coarser grained dolostones formed from similar solutions. The Sr contents of the dolomites in both the fine-grained and the coarser grained dolostones are much lower than would be anticipated had they formed directly from marine water,

since dolomites which are purported to be direct precipitates from marine water have higher (> 600 ppm) amounts of Sr (Beherns and Land, 1972).

The partition coefficients of trace elements is also dependent on temperature. Experimentally determined $K_{Sr^{++}}^{calcite}$ at 100°C = 0.08 (Kinsman, 1969; Kinsman and Holland, 1969). Katz et al. (1972) experimentally determined that during the transformation of aragonite to calcite in the presence of an aqueous solution, the value of $K_{Sr^{++}}^{calcite}$ is actually lower than the one given by previous workers. They found that $K_{Sr^{++}}^{calcite}$ = 0.055 and 0.058 at 40 and 94°C, respectively. Whether one chooses the value given by previous workers or by Katz et al. (1972), the Sr contents of the River Ridge carbonates would be explained by change in temperature only if they formed at temperatures higher than 100°C. Such temperatures are not attained in normal sedimentary environments or during most stages of diagenesis.

Ordering of Trace Elements and Correlation Matrices

The trace elements, except for Mn, and trace/major element ratios discussed above suggest that the diagenetic solution, in the presence of which the limestones were neomorphosed and the coarser than fine-grained dolostones formed, was not a marine solution. More insight about the diagenetic environment may be gained from an evaluation of how the trace elements correlate with each other. To this end, the distribution of trace elements in carbonate minerals from the Flat Gap mine, obtained by West (1974), were used to produce correlation matrices (Table 3-4). These correlation matrices give Pearson correlation

Table 3-4. Correlation matrices* of trace elements in carbonate minerals of limestones and dolostones from the Flat Gap Mine, Copper Ridge district

	Cd	Zn	Fe	Mn	
		A. Limestones			
Zn	0.73				R
	0.005				SL
Fe	-0.07	-0.01			R
	0.855	0.968			SL
Mn	0.46	0.73	0.03		R
	0.112	0.003	0.937		SL
Sr	0.38	0.04	-0.13	-0.34	R
	0.206	0.894	0.726	0.240	SL
		B. Dolostones			
Zn	0.63				R
	0.000				SL
Fe	.05	0.07			R
	0.772	0.670			SL
Mn	0.38	0.37	0.60		R
	0.013	0.015	0.00		SL
Sr	0.37	0.28	0.21	0.18	R
	0.014	0.076	0.169	0.244	SL

*Correlation coefficients determined from data of West (1974, Appendix D) using SAS routine PROC CORR, Barr et al. (1975). R is the Pearson Correlation coefficient and SL is the significance level of probability. The number of samples used for correlation are 13 for the limestones and 44 for the dolostones.

coefficients (R) along with the significance levels (SL), and were obtained using the SAS routine PROC CORR (Barr et al., 1976) on an IBM 370/148 computer. The correlations obtained for both limestones and dolostones appear to be compatible with the mixing of two solutions—one (solution A) containing Sr, Cd, and Zn with another (solution B) containing Fe, and the amount (in the mixture) of solution B progressively increasing through time. The reasons for this interpretation are as follows.

The partition coefficients of trace elements in calcite and dolomite are assumed to be constant. Assuming that the ordering of the partition coefficients discussed earlier is valid, $K^{MX}_{Cd^{++}} > K^{MX}_{Zn^{++}} > 1$, and $K^{MX}_{Sr^{++}} < 1$, where MX refers to calcite or dolomite. If solution A was of finite volume and carbonates crystallized from it, in a closed system, the amount of Cd and Zn incorporated in the minerals will be expected to decrease through time, whereas the Sr will be expected to show an increase. This will be indicated by correlation matrices that show positive correlations between Cd and Zn suggestive of simultaneous decrement, and a poor or negative correlation between Sr on one hand and Cd and Zn on the other.

If a solution deficient in Cd, Zn, and Sr is mixed with solution A, carbonates that crystallize from the mixture would be expected to show a decrease in all of these trace elements through time. If the solution that is allowed to mix with solution A contains Fe (solution B) and its amount in the mixture progressively increases through time, carbonates that form from such a mixed solution should, through time, show an

increase in Fe and a decrease in the other trace elements. Elements introduced into the mixture from dissolution of precursor carbonates will have the effect of changing the magnitude of trace/major element ratio. But they may not change the trend of the distribution of trace elements incorporated in the minerals, if a continuous dissolution and reprecipitation process is envisaged. Fluctuations in the proportion of the mixtures of solution, as well as the amount, type and rate of dissolution of precursor carbonates will result in complicating the correlations of trace elements. Nonetheless, the proposed mixing model appears to best explain the correlation matrices given in Table 3-4, and the compositional variations obtained by electron microprobe analysis (Fig. 3-2, p. 33).

Correlation of trace elements such as Mn and Fe from recent carbonate sediments formed in fresh, brackish and marine waters showed that the trace elements were indicative of the environments of deposition of the sediments (Friedman, 1969). The fresh water sediments had higher trace elements in contrast to those of marine water. The correlation matrices presented in Table 3-4 indicate that Sr, Fe, Zn, and Cd patterns are interpretable on the assumption that their partition coefficients are constant. If this assumption is correct, the correlations of trace elements suggest that the calcites and dolomites in the Copper Ridge district were produced by mixing of two solutions. One solution (A) is considered to have had Sr, Cd and Zn, and probably was marine water. In contrast, the other solution (B) is considered to have had Fe and was probably fresh water.

Problem of Mn

The case of Mn is problematic. For instance, Table 3-4 shows that at 0.003 significance level Mn is positively correlated to Zn and at 0.112 significance level it is positively correlated to Cd. Such correlations may suggest that Mn has the same source as Zn and Cd. But, at 0.240 significance level Mn is negatively correlated to Sr which would not be compatible if Sr, Mn, Zn and Cd had the same source and were allowed to mix with another solution of lower ionic strength. Also, Mn, does not correlate with Fe (in limestones) suggesting that probably it did not have the same source as Fe.

Such unsystematic relationship of Mn to other elements is not unique to the Lower Ordovician carbonate rocks in the Copper Ridge district. Weber (1964) has noted it, and the correlation matrices for the Pleistocene corals of Barbados, produced by Pingitori (1978, p. 809), show it. Such observations lead the author to suspect that the partition coefficient of Mn^{++} is probably not constant.

The reason for the possible inconstancy of the partition coefficient of Mn^{++} is not clear. According to Itchikuni (1973) the partition of Sr^{++} between calcite and solution is increased by the presence of Mn^{++}. This is thought to be so, because structural distortions of calcite due to replacement of Ca^{++} by ions of smaller radii, such as Mn^{++}, will be compensated if Sr^{++} is also incorporated. However, the correlation matrices in Table 3-4, part A, and those given by Pingitori (1978) show negative correlations between Sr and Mn. Probably, the explanation may lie with site occluding mechanisms, or the

rate of diffusion of Mn^{++} being slower than the rate of growth of crystals for certain increments of crystal layers. Such mechanisms are discussed by Kinsman and Holland (1969). For example, for temperatures less than 100°C, they determined experimentally that $K_{Sr^{++}}^{aragonite}$ was independent of the rate of precipitation of aragonite, whereas $K_{Mg^{++}}^{calcite}$ was dependent on the rate of precipitation of calcite. Study of the variation of cathodoluminescence intensities in crystals helps to understand the partitioning of Mn.

Cathodoluminescence and the Mn Problem

When studied with a cathodoluminoscope the growth zones of a crystal (e.g., dolomite) are displayed as several luminescent bands of variable widths and intensities. Although the observed display of luminescent bands could depend on the way in which a sample is cut for investigation (Fig. 3-4), their mode of occurrence in a crystal is a record of the geochemical environment in which the crystal grew. Luminescence in minerals is thought to arise from the presence of activator elements such as Mn, whereas reduction in the intensity of luminescence is from quencher elements such as Fe (e.g., Nickel, 1978). As noted earlier bright luminescent zones in dolomite correspond to a higher Mn/Fe ratio, and dark zones to a lower ratio. But why does the Mn/Fe ratio vary during the growth of a single crystal?

Oglesby (1976) proposed that the incorporation of Mn^{++} and Fe^{++} in carbonate phases depends on the Eh-pH conditions of the environment. However, the applicability of Oglesby's (1976) model is limited by the

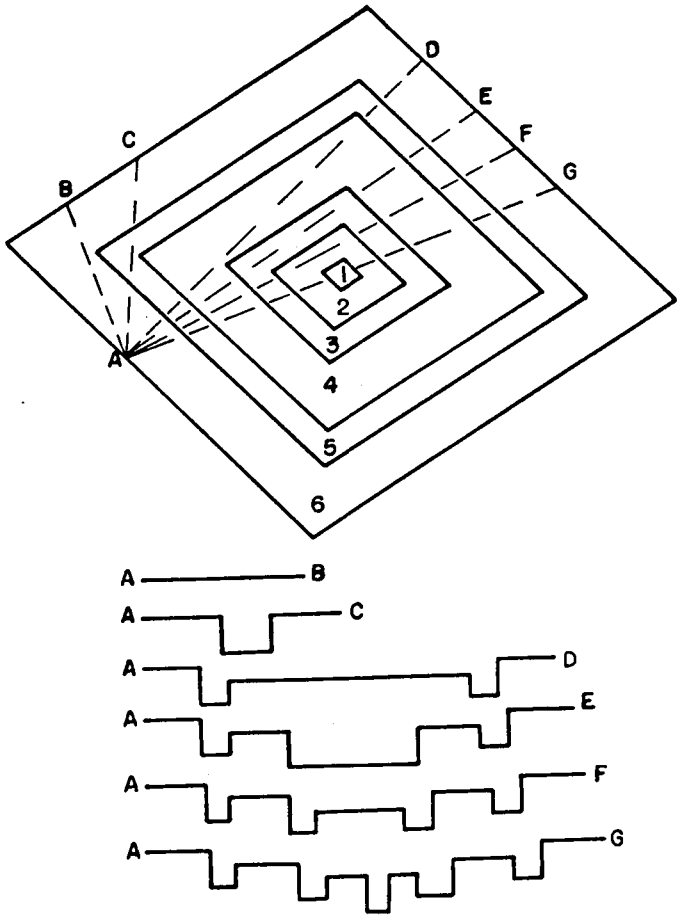

Figure 3-4. Schematic diagram illustrating that different zonal patterns can be observed in different cuts of a zoned dolomite. The top diagram shows a zoned dolomite. Zones 1, 3, 5 are darker zones with darkness increasing towards core. Zones 2, 4, 6 are brighter zones with brightness increasing towards rim. The zonal patterns obtained from different cuts are shown in the bottom diagram. Cut A-B shows only zone 6; cut A-C shows zones 5 and 6; and so on.

assumption that the distribution of Mn^{++} and Fe^{++} in the carbonate phases is governed by the stability of pyrrolusite and goethite.

The evaluation of trace element data other than Mn, as discussed above, leads to the conclusion that the coarser than fine-grained dolostones formed from a mixed solution of fresh and marine water. Mixing of such solutions could result in changes in the pH values of mixtures (Gebelein, 1977, 1979) and contribute to the variation in the amounts of Mn^{++} and Fe^{++} incorporated in carbonate phases. Moreover, the growth rates of crystals may have played a more important role, particularly in the distribution of Mn. In a mixing environment, dolomitization is feasible for a mixture with 10 to 40 wt. % marine water (see Chapter II). Within this range the diluted portion has lower Mg/Ca ratio. It has been suggested by Land (1967) that higher Mg/Ca ratios in a solution lead to faster growth rate of dolomites. Fluctuations of the water table in a diagenetic environment could provide conditions of varying Mg/Ca ratios. As a dolomite crystal grows (by dissolution and replacement) the growth rate of different crystal layers could vary depending on the fluctuation of the water table. If the diffusion of Mn^{++} is sluggish, presumably due to complex ion formation, crystal layers that grew at relatively faster rates may be depleted in Mn. The above explanation suggests that zoned dolomite crystals are indicative of a mixing diagenetic environment.

VI. CONCLUSION

The Lower Ordovician, Upper Knox carbonate rocks in the Copper Ridge district have low Na and Sr contents indicating that they formed in the presence of fresh water. In the case of the coarser than fine-grained dolostones and limestones this is corroborated by the correlation matrices of Fe, Zn, Cd, and Sr. The Sr/Ca ratio in the coarser than fine-grained dolostones is half that of the limestones suggesting that these lithologies formed from similar solutions. Dolomite crystals in the coarser than fine-grained dolostones show several luminescent growth zones. It is suggested that these growth zones record fluctuations of the water table in diagenetic environments.

CHAPTER IV

IMPLICATIONS OF SEDIMENTARY AND DIAGENETIC FEATURES OF THE LOWER ORDOVICIAN UPPER KNOX GROUP CARBONATE ROCKS, COPPER RIDGE DISTRICT, EAST TENNESSEE

I. INTRODUCTION

Study Area

The Upper part of the Lower Ordovician Upper Knox Group carbonate rocks, according to the recent redefinition of Harris (1969), comprise the Mascot and the Kingsport Formations. The Mascot Formation consists of fine-grained (< 0.062 mm) dolostones, with a few beds of coarser than fine-grained (dolomite grain size exceeding 0.062, but not occurring as vug-fill) dolostones. In contrast, the underlying Kingsport Formation consists of coarser than fine-grained dolostones interbedded with limestones and few fine-grained dolostones. In East Tennessee, the Upper Knox occurs in the Valley and Ridge province, and the productive zinc districts of East Tennessee are restricted to these units.

The Copper Ridge zinc district spans a distance of 104 kilometers (Hill, 1971) along a NE trending linear belt. A 32-kilometer portion of the district was chosen for this study. Upper Knox carbonate sections were measured at River Ridge, Joe Mill Creek-Rucker Branch, and Shiloh. Other samples were taken from exposures at Lee Valley, Tandy Dalton prospect and Idol mine (Fig. 4-1). Field examination coupled with investigations conducted in the laboratory have enabled

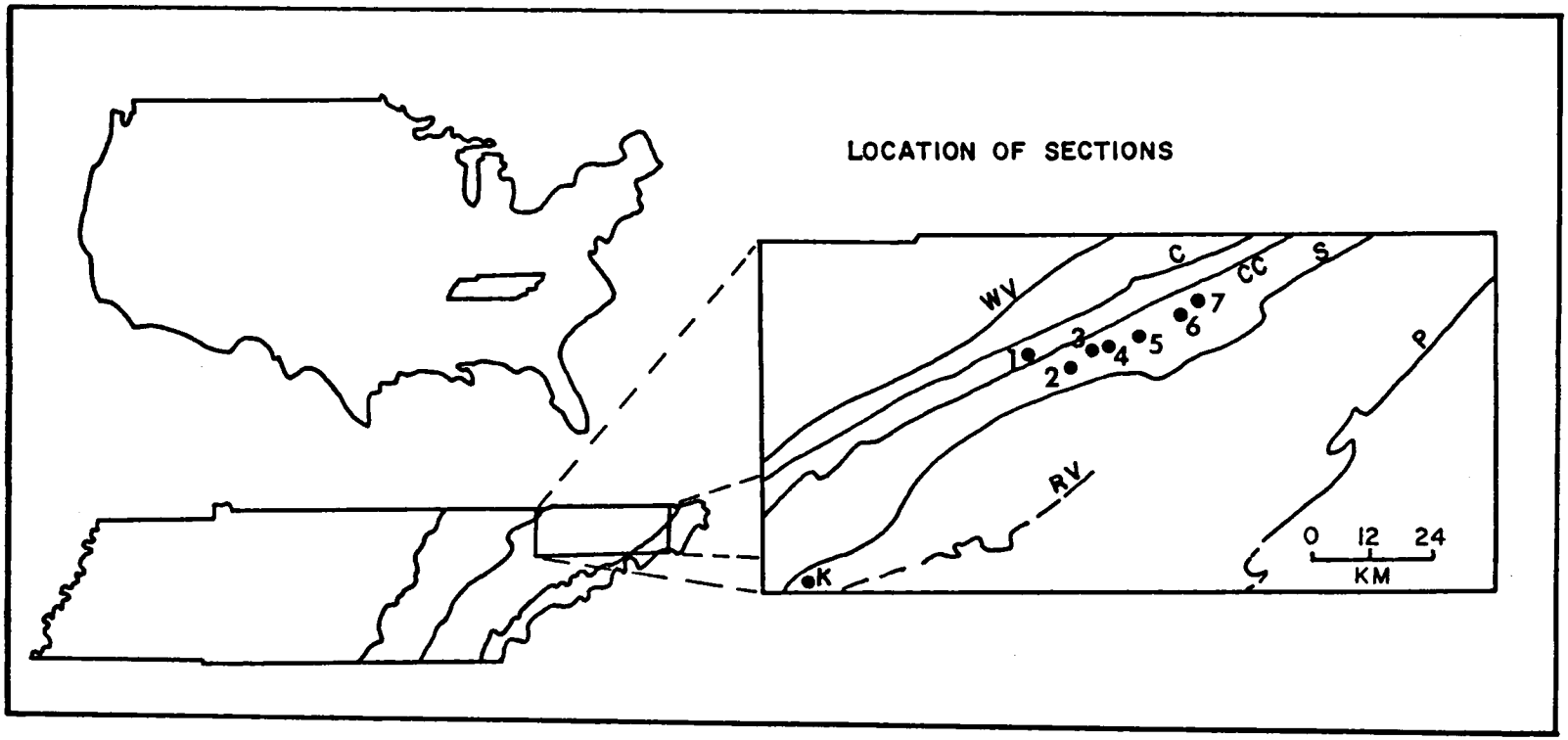

Figure 4-1. Location of Upper Knox carbonate rocks used in this study.

Source: Harris, 1969, and Geologic Map of East Tennessee by Swingle et al., 1966.

Note: 1. River Ridge; 2. Thorn Hill; 3. Idol mine and Joe Mill Creek-Rucker Branch; 4. Tandy Dalton prospect; 5. Flat Gap mine (Treadway); 6. Lee Valley; 7. Shiloh prospect; K. Knoxville. Faults: WV. Wallen Valley; C. Clinchport; CC. Copper Creek; S. Saltville; P. Pulaski; RV. Rocky Valley.

the author to characterize the lithologies and to suggest the paleoenvironments of their formation.

Geologic Setting and Previous Work

The Valley and Ridge physiographic province belongs to the Appalachian physiographic division. It is bounded in the east by the Blue Ridge Mountains, and in the west by the Appalachian (also called Cumberland or Allegheny) Plateaus. Tectonic activities during the Paleozoic resulted in thin-skinned, NE-trending, allochthonous sedimentary blocks in the Valley and Ridge province. The thrusting involved an estimated crustal shortening of about 55% (Roeder and Witherspoon, 1978). A number of ore bodies occur along NE-trending lineaments (Figure 1 of Maher, 1971). The Copper Ridge zinc district is one of these elongate districts.

The stratigraphy of the Lower Paleozoic is summarized in Table 4-1. Published stratigraphic sections containing the upper part of the Knox Group in the Copper Ridge district include: the Thorn Hill section (Hall and Amick, 1934), the Lee Valley section (Rodgers and Kent, 1948), and the River Ridge section (Harris, 1969). Harris (1969) has summarized the state of the stratigraphic nomenclature of the Upper Knox both in the Copper Ridge district and the Mascot-Jefferson City district about 30 miles to the southwest and has proposed a redefinition of the stratigraphy. He suggested that the Kingsport include the Longview and part of the previous Kingsport Formation, so that the redefined Kingsport Formation would be identified by the occurrence of coarser than fine-grained dolostones interbedded with limestones and few fine-grained

Table 4-1. Generalized section of the Lower Paleozoic, East Tennessee zinc districts (adapted from Hill, 1971a)

Age		Name	Thickness Meters	Character of Rock
Middle Ordovician (Chazyan)		Holston, Lenoir and Mosheim Ls. (Chickamauga)	400 ±	Pink (Holston), Dark-gray (Lenoir), and dove-gray birds-eye (Mosheim) limestones.
		unconformity		unconformity
Lower Ordovician	Knox Group	Mascot Formation	75 - 203	Light- and dark-gray dolostone in Copper Ridge. Moderately cherty. Interbedded limestone abundant in Jefferson City area. Main ore zones in lower fifth of formation.
		Kingsport Formation	45 - 105	Dark- to light-gray, fine-grained dolostone and dove to brown limestone. Upper third mostly limestone. Chert and arenaceous zones numerous. Limestone locally altered to coarser dolostone. Main ore zones in upper third of formation.
		Chepultepec Formation	180 - 225	Mostly dolostone in Copper Ridge. Light- and dark-gray dolostone and limestone in Jefferson City area. Cherty. Sandstone beds at base.
Upper Cambrian		Copper Ridge Formation	315 ± 360 ±	Dark, sugary, and light-gray, fine-grained cherty dolostone. Some limestone in Jefferson City area.
	Consauga Group	Maynardville Ls.	75 ±	Light-blue to dark-gray laminated limestone and dolostone.
		Nolichucky Sh.	135 ±	Dark-gray, greenish and yellow shales and thin limestones.
		Maryville Ls.	150 ±	Massive blue to black limestones, mostly ribboned with dolostone.
Middle Cambrian		Rogersville Sh.	75 ±	Light-green shale.
		Rutledge Ls.	105 ±	Massive blue to black limestone, mostly ribboned with dolostone.
		Pumpkin Val. Sh.	90 ±	Greenish to purplish shale with thin siltstone beds.
Lower Cambrian		Rome Sh.	360 ±	Varicolored shale, mostly maroon, siltstone, sandstone; some dolostone and limestone layers.
		Shady Dol.	300 ±	White to blue-gray dolostone. Limestone present locally in lower part. (Shady not present in Copper Ridge or Mascot-Jefferson City areas.)

dolostones. Thus, the Kingsport would be distinct from the thick sequences of fine-grained dolostones of the underlying Chepultepec and the overlying Mascot Formations.

Two consistent features of zinc mileralization in East Tennessee are dolomitization and brecciation. In the opinion of many geologists (Wedow and Marie, 1965; Crawford and Hoagland, 1968; Hill, 1969, 1971; and Lawrence, 1971) brecciation resulted from dissolution of limestones and the foundering of overlying dolostones. Water that collected in topographic depressions during the Post-Knox subaerial exposure and seeped down through an aquifer system was thought to cause the dissolution of the limestones. Further brecciation was caused by action of mineralizing fluids (Hill et al., 1971).

The dolomites in East Tennessee fall into three distinct groups; fine-grained (< 0.062 mm), coarser than fine-grained (> 0.062, but excluding vug-fills), and vug-fill (pinkish or white and generally coarse-grained). Petrographic study suggested that the vug-fill dolomites associated with mileralization belong to different stages of emplacement (Snyder, 1975). The origin of dolostones is controversial. For instance, trace element distribution studies (West, 1974) showed that the concentration of Sr was an order of magnitude higher in limestones than in dolostones. In contrast, Cd, Zn, Fe, and Mg concentrations were lower in the limestones than in the dolostones. Based on these data, West (1974) proposed that the coarser-grained dolostones resulted from dolomitization by mineralizing solutions. Further, he speculated that invasion by mineralizing solutions of the

more porous fine-grained dolostones and the lack of permeability in the limestones might explain the dissimilarity of the trace element abundances between the two lithologies.

Harris (1971, 1973) has different interpretations about the origin of the dolostones. Reconstruction of the Tertiary limestones of eastern United States that contain interconnected aquifer systems (Legrand and Stringfield, 1971) was thought to be similar to a reconstruction of the Lower Ordovician Knox of East Tennessee (Harris, 1971). Considering also that Hanshaw et al. (1971) have suggested the feasibility of dolomitization by groundwater, Harris (1971) proposed that during the Post-Knox erosional period an undulating surface was developed so that erosion of the Mascot dolostone uplands supplied abundant Mg^{++} to ground waters that emanated from sinkholes in the lowlands. Such magnesium-charged ground water traversed deeper aquifer systems and caused dolomitization (Harris, 1971). In a later paper Harris (1973) emphasized the occurrence of chert nodules many of which he thought were replaced algal stromatolitic heads. He used this evidence for the subtidal formation of carbonates including the dolostones.

II. METHODS OF INVESTIGATION

A graduated stick, and 100-foot tape were used for measuring outcrop sections. The features observed in the field were recorded. Samples collected from the field were slabbed and 213 were thin-sectioned. Thin-sections were stained with acidified solutions of

Alizarine Red-S and potassium ferricyanide (Lindholm and Finkleman, 1972; see Appendix E for detail) and studied under transmitted-light microscope. Polished sections (37) were prepared for reflected-light petrographic work and for electron microprobe analysis. Most of the samples were also studied using cathodoluminescence. Powdered samples were prepared from 21 selected specimens for neutron activation analysis. The operating conditions for the Luminoscope, electron microprobe and neutron activation analyses as used during this study are described in Chapter III.

III. MEASURED SECTIONS

Portions of three exposures of the Upper Knox carbonates at Copper Ridge district were measured. The measured sections include the exposures at River Ridge, the Shiloh prospect; and the Joe Mill Creek-Rucker Branch (Fig. 4-1, p. 56). The River Ridge section is in the Clinchport fault block, whereas the others are on the adjacent Copper Creek fault block. At present the Upper Knox carbonates on these adjacent fault blocks are separated by a distance of about 6.1 km. Their location prior to the shortening by thrusting can be assessed by a palinspastic reconstruction method used by Roeder and Witherspoon (1978). In essence, this method first determines the base of deformation (from exposure thickness, bore hole, seismic and aeromagnetic data), then thrust fault planes are drawn steeper into space and gentler down depth until they asymptotically touch the base of deformation or are truncated by an upper fault plane. From such a reconstruction, using

Profile 5 of Roeder et al. (1978) the palinspastic distance between the Upper Knox carbonates on these adjacent fault blocks of the Copper Ridge district is estimated to be 13.5 km.

River Ridge Section

At River Ridge, the Upper Knox is exposed on a road cut about 5.4 km north of the Thornhill village, along U.S. Highway 25E. The top 7 meters of the Mascot Formation are not exposed on the road cut; rather, they are round the corner on a gently sloping hill. The post-Knox unconformity is not well exposed, but is present as a cherty horizon of fine-grained dolostones below the Middle Ordovician biodismicrite. The boundary where a sequence of fine-grained dolostones (Mascot) are underlain by a sequence chiefly of coarser than fine-grained dolostones (Kingsport) marks the Mascot-Kingsport contact. This contact is 159 meters below the post-Knox unconformity. The Kingsport-Chepultepec contact corresponds to that boundary where a sequence chiefly of coarser than fine-grained dolostones (Kingsport) is underlain by a sequence of fine-grained dolostones (Chepultepec). This contact is 260 meters below the post-Knox unconformity.

Harris (1969) published a description of this section, and most of his unit designations are still painted on the exposure. The same unit designations are used in this report. I consider the field description of Harris (1969) as very useful, except that many of the stromatolitic features described by Harris (1969) were not apparent to me. A columnar section of the 260 meters-thick outcrop of the Kingsport and Mascot formations of the River Ridge is given in Appendix F, and for cross

reference the unit designations of Harris are indicated on it. Thin-sections were prepared for 153 specimens from this exposure and detailed petrographic descriptions are included in Appendix G. Also many thin-sections were studied using a cathodoluminoscope.

On the whole the upper Knox at River Ridge section consists of beds and stylobeds (in the sense of Logan and Semenuix, 1976) mostly of dolostones with a few interbedded limestones in the Kingsport. The beds range in thickness from less than 10 cm to more than 1 meter. On the average the beds strike N 66° E and dip 27° SE. The features observed in the outcrop at River Ridge are itemized below, and the interpretations are discussed later.

(1) Cryptalgal laminae. The fine-grained dolostones, irrespective of the formations in which they occur (Chepultepec, Kingsport, or Mascot) are marked by the presence of wavy to planar cryptalgal laminae. Rarely some wavy laminae are discernible in the coarser than fine-grained dolostones, particularly near the base of the Kingsport.

(2) Reddish coloration. Reddish streaks occur mostly in fine-grained dolostones, as laminae parallel to bedding, although some of them are at oblique angles to bedding, throughout the exposure in the River Ridge. Some of the beds of the Mascot are reddish colored. Reddish coloration of the fine-grained dolostones of the Mascot becomes prominent, though not present in every bed, from 205 meters above the base of the Kingsport up to the post-Knox unconformity.

(3) Mudcracks. Mudcracks are not abundant, however a conspicuous mudcrack occurs at top of a fine-grained dolostone, unit 135, below a

greenish shaly bed parting. The mudcracks are filled by fine-grained dolomite crystals.

(4) Birdseyes. Some birdseyes were observed in some of the fine-grained dolostones, as well as in some of the limestones.

(5) Current indicators. An intraformational conglomerate consisting of fine-grained dolostone and chert fragments in a matrix of fine-grained dolomite crystals and quartz occurs near the base of the Mascot, unit 98. This conglomeratic unit is marked by uneven bottom and sharp top. A ripple laminated sandstone (30.0 cm thick, unit 100) occurs 5.4 meters above the conglomeratic unit.

(6) Burrows. Burrow features, in the field, were indicated by the mottled appearance of some of the coarser than fine-grained dolostones. In the field, burrows were not discernible in the limestones.

(7) Silica. Silica occurs as chalcedony, chert and quartz. Chert occurs in both fine-grained and coarser than fine-grained dolostones, sometimes as matrix between dolomite crystals. Numerous chert nodules and layers occur both at bed partings and inside of beds. Some of the cherts preserve oolitic textures and a few of the others appear to replace stromatolitic features. But many of the SH-V and SH-C stromatolitic features in cherts described by Harris (1969) do not appear to be either vertically or laterally linked hemispheroidal stromatolites. Instead, in vertical section, many of the cherts occur as doubly convex, lensoidal nodules.

Quartz grains occur in various beds, mostly in the fine-grained dolostones. The quartz occurs as two distinct grain-sizes. Often,

subrounded, finer (about 0.04 mm) quartz grains are associated with cryptalgal laminites. The more rounded and coarser (about 0.5 mm) quartz grains do not show such a relationship.

Length-slow chalcedony occurs in nodular vugs mostly as an outer lining to the central vug-fill dolomite crystals. This relationship appears to be restricted to fine-grained dolostones. Nodular vuggy features are abundant in the coarser than fine-grained dolostones, but they are filled by vug-fill dolomite without a chalcedonic lining.

(8) Breccia. Minor brecciation is observed in several beds. Conspicuous brecciated horizons occur at units 76 and 83.

(9) Faults. At 28 meters from the base of the Kingsport a minor thrust fault cuts the section and has an attitude of N 60°E, 32°SE. At 217 meters from the base of the Kingsport a normal fault striking N 65°E and dipping at 50°NW has a displacement of about 2 meters. Higher up at 227 meters from the base of the Kingsport, another fault strikes at N 35°E and dips at 56°NW, but it is not associated with a vertical displacement. Based on weakly developed slickensides it appears to have a right lateral displacement. Here the fault gouge is marked by reddish argillaceous material.

Joe Mill Creek-Rucker Branch Section

A side road leading to the Idol mine and the Joe Mill Creek-Rucker Branch section intersects the Clinch Valley road (a straight continuation of U.S. Highway 131) 1.6 km northeast of the Thorn Hill village. The Joe Mill Creek-Rucker Branch section is about 1.3 km northwest from the Clinch Valley road. The Upper Knox is exposed along Joe Mill Creek and

Rucker Branch, as well as on the side of a dirt road. A portion of the Upper Knox was tape-mapped along the dirt road that runs parallel to Rucker Branch, and along Joe Mill Creek below its confluence with Rucker Branch. A columnar section constructed from this map is included (Appendix F). Petrographic descriptions of thin-sections studied from this section are included (Appendix G). The thin-sections were also studied using cathodoluminescence.

On the average, the rocks have an attitude of N 60°E, 37°SE. The Kingsport-Mascot contact, according to Harris (1969) is 201 meters below the post-Knox uncomformity and corresponds to the top part of the limestone in the exposure, i.e., in the center of an old zinc prospect in this section. A few oncolites were observed in the limestone.

The lithologies in this section are similar to those at River Ridge section. However, several horizons in this section are brecciated, and in the Mascot Formation the breccia zones are underlain and overlain by unbrecciated beds. Some of the fractures are infilled by sphalerite. It is to be noted that nodular vugs (probably earlier sites of gypsum) do not contain sphalerite. Mineralization is restricted to secondary fractures. Mineralization was observed up to 131 meters above the Kingsport-Mascot contact on the road side adjacent to the Rucker Branch.

Shiloh Section

The Shiloh zinc prospect is located along a dirt road, 0.5 km from the Shiloh Methodist Church, itself located on a side of the Clinch Valley road near the Clinch High School. Except at the prospect, the

exposure along the dirt road is poor. However, the Upper Knox, although partially covered, is also exposed along Bird Creek, adjacent to the Shiloh prospect. A portion of the Upper Knox, 142 meters thick, was tape-mapped along this creek, and a columnar section constructed from it (Appendix F). Petrographic descriptions of microslides studied from this exposure are included (Appendix G).

On the average the beds strike N 68°E and dip 55°SE. Even though the exposure is incomplete, the approximate position of the Kingsport-Mascot contact can be judged on the basis that a sequence of fine-grained dolostones is underlain by a sequence of coarser than fine-grained dolostones interbedded with fine-grained dolostones and limestones. Based on this judgment the top part of the prospect is about 13 meters below the Kingsport-Mascot contact. The Shiloh prospect is reported to be 195 meters from the Post-Knox unconformity (Secrist, 1924). Thus, the Kingsport-Mascot in this section is about 182 meters below the unconformity.

The observed lithologies are similar to those at River Ridge section, except that near the top of the Kingsport a thicker unit of limestone is exposed here. The top-most exposed limestone consists of interlaminated biointrapelsparite and micrite, and is laterally traceable into the sphalerite bearing prospect. The limestone is further characherized by criss-crossing stylolites marked by insoluble greenish shaly material.

Miscellaneous Samples

Lee Valley section. This section is located alongside Highway 66 about 0.64 km north of the intersection of Highway 66 with Clinch Valley road. A measured section of the sedimentary rocks was published by Rodgers and Kent (1948). The beds here have an average attitude of N 60°E, 46°SE. The Upper Knox section here was not remeasured. But samples, taken from units 208 to 309 of Rodgers and Kent which were reported to correspond to mineralized horizons, were studied. This portion of the Lee Valley section consists of negligibly to partially dolomitized limestones with a few interbedded coarser than fine-grained dolostones. Petrographic descriptions of microslides prepared from these intervals are included in Appendix G.

Other localities. Samples were collected from Tandy Dalton prospect and Idol mine. Samples collected from these localities consist of brecciated fragments with sphalerite occurring as matrix fill. The petrographic character of these samples is better understood by use of the Luminoscope and reflected-light petrographic microscope. The descriptions are further discussed in Chapter V.

IV. CARBONATE PETROLOGY

In the stratigraphic record of the Upper Knox in the Copper Ridge district dolostones form the major lithology and limestones are relatively rate. The dolostones may be subdivided into different types based on the grain size of the constituent dolomite crystals. Such a

classification is used for interpretation of their environments of formation.

According to the field description of dolostones at the River Ridge section given by Harris (1969), dolostones with dolomite crystals mostly 0.05 mm in their longer dimensions but generally less than 0.1 mm are described as finely to very finely crystalline, e.g., unit 42 (Appendix G). But, the medium- and coarse-grained dolostone described by Harris (1969) do not fall into distinct grain size ranges. For example, unit 41 was described by Harris as finely to medium crystalline. Study of three thin-sections from this unit shows that the grain sizes, in the bulk of the material, vary from 0.5 to 0.8 mm, with some porphyrotopes (e.g., Friedman, 1965) reaching up to 2.0 mm. Only some pockets of 0.07 to 0.2 mm-sized dolomites occur adjacent to stylolites. On the other hand, units 66 and 82 were described by Harris (1969) as coarsely crystalline. Study of three thin-sections from these units show the average grain size to be $\leq$ 0.8 mm. Thus, although some units appear coarser grained than others, a distinction between coarser grained dolostones in the field may not be accurate.

An inspection of the grain size distribution of dolomites given in Appendix G suggests many possible grain size groupings of dolomites, with some gradation between the groups—for example, $<$ 0.1 mm, fine-grained; 0.1 to 0.8 mm, medium-grained; $>$ 0.8 mm coarse-grained (Churnet and Misra, 1978). Folk (1965) classified the grain sizes of carbonate minerals as given in Table 4-2. Although Folk's (1965) classification was not suggested specifically for dolomites, it may be

Table 4-2. Grain size classification of dolostones

A		B
< 0.016 mm	very finely crystalline	fine-grained (FD)
0.016-0.062 mm	finely crystalline	
0.062-0.25 mm	medium crystalline	coarser than fine-grained (CFd)
0.25-1.0 mm	coarsely crystalline	
< 1.0 mm	very coarsely crystalline	

Note: A - Grain size classification of carbonates after Folk (1965).

B - Grain size groups of dolomites used in this report.

useful to adopt his classification in this report because of its precedence and broad reference to carbonates. The grain sizes of dolomites in all the microslides described in this study are included in Appendix G. Except for one thin-section (J-13, Appendix G) very finely crystalline dolostones were not observed. Dolostones composed of crystals in the grain size group 0.02 to 0.07 mm have generally similar textural characteristics (Table 4-3). Dolostones composed of crystals whose grain sizes are, for example, 0.2 to 0.8 mm, have textural characteristics different from the finer grained dolostones (Table 4-3). Thus, it appears to be advantageous to subdivide the dolostones from the Copper Ridge district into two categories:

1. Fine-grained dolostones [composed of dolomites belonging to the finely crystalline and the very finely crystalline groups of Folk (1965)], and
2. Coarser than fine-grained dolostones consisting of dolomites belonging to the medium, coarse, and very coarsely crystalline groups of Folk (1965)].

The terminology coarser than fine-grained dolostone (dolomite) is awkward. However it encompasses a range of grain size, and is more precise than the terminology medium grained dolostones previously suggested by Churnet and Misra (1978). In the exposition that follows, the Upper Knox lithologies will be discussed under the headings of limestones, fine-grained dolostones, and coarser than fine-grained dolostones.

Table 4-3. Comparison of fine-grained and coarser than fine-grained dolostones

Criteria	Fine-Grained Dolostones (Fd)	Coarser than Fine-Grained Dolostones (CFd)
Grain size	Mostly 0.02 to 0.05 mm	Mostly 0.1 to 0.8 mm
Zoning	Predominantly unzoned	Mostly zoned, often several concentric luminescent zones detected. Generally Fe content increases from core to rim of a crystal
Relict features	Wavy to planar cryptalgal laminae	Often no laminae detected
	Mudcracks	No mudcracks observed; however, predolomitization fractures are observed
	No ghost fauna	Sometimes fossil fauna ghost features observed
Fabric	Xenotopic	Often hypidiotopic
	Generally no inclusions	Poikilotopic; high Mg-calcite inclusions in partially dolomitized limestones; also, sometimes block, calcite in sharp contact with dolomite cement
	Generally uniform grain size	Porphyrotopic
Vug-fill	Sometimes, an outer lining of chalcedony followed by dolomite	Dolomite
Ca/Mg ratio	Nearly stoichiometric	Higher than in ideal ordered dolomite
Na^{+} and Sr^{++} contents	Lower than expected if of marine origin	Lower than expected if of marine origin; Sr^{++}/Ca^{++} ratio equal to half that determined from limestones.

Limestones

Using the classification schemes of Folk (1959) and Dunham (1962), the limestones consist of interlaminated biointrapelsparitic grainstones/packstones and biomicritic wackestones, with some grapestones and rarely ooids. In decreasing order of abundance the recognized fauna includes trilobites, gastropods, ostracods, brachiopods, pelmatozoans, and sponges. Most of the allochems have micritic envelopes caused by microboring organisms such as algae and fungi (e.g., Perkins and Halsey, 1971). Planar algal-laminae are discernible in some micro-slides, for example RR-71D (Appendix G). Birdseyes (Shinn, 1968) are observed in some beds. Intra-allochem cements are neomorphosed to microspar. Interallochem cements are drusy and granular (e.g., Barthurst, 1958) to blocky (e.g., Dunham, 1969a).

Generally microspar and some of the granular interallochem cement luminesce with brassy yellow color. Electron microprobe analysis of some of the interallochem granular cement shows a Ca/Mg wt. % ratio of $\frac{40.8}{0.15}$ (Table 4-4) with negligible amounts of Fe and Mn.

The presence of winnowed sediments with marine fauna suggests that the limestones were deposited in a shallow marine environment at or adjacent to that zone where oceanic waves impinged on the sediment-water interface (intertidal to shallow subtidal). No shallow marine fibrous or elongate cements (Bricker, 1971; Bathurst, 1975) were observed except for the radial fabrics in ooids (Fig. 4-2). Instead, intra-allochem cements, and matrix have been neomorphosed to microspar, and inter-allochem cements are drusy and granular to blocky (Fig. 4-3) low

Table 4-4. Composition (wt. %) of carbonates obtained by Electron Microprobe Analysis

	Mn	Fe	Ca	Mg	Total Cation
A. Interallochem, granular calcite cement (Sample RR72)					
	*	*	39.61	0.30	39.91
	*	*	41.15	0.16	41.31
	0.05	*	38.80	0.12	38.98
	*	0.04	39.79	0.18	40.01
	*	*	37.05	0.12	37.19
	0.04	*	39.09	0.11	39.24
Average			39.25	0.16	39.41
B. Fine-grained dolomite (Sample RR45)					
	0.04	0.08	21.28	12.97	34.37
	*	0.11	21.10	12.91	34.12
	*	0.08	20.77	12.91	33.79
	*	0.09	21.21	12.91	34.22
	*	0.07	21.29	13.02	34.39
	*	0.06	20.97	12.93	33.96
Average		0.08	21.10	12.94	34.14

*Values less than 0.04 wt. %.

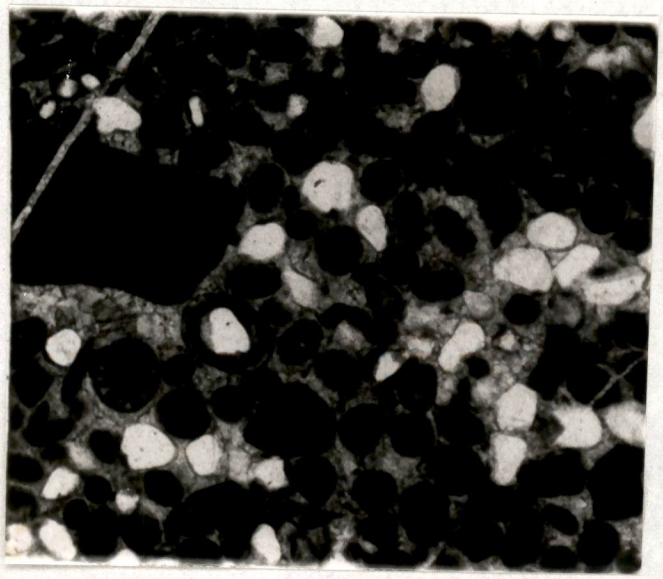

1 mm

Figure 4-2. Photomicrograph of oosparite (Sample RR-49A). Radial fabrics in ooids is observed. The cement between the ooids is granular calcite cement.

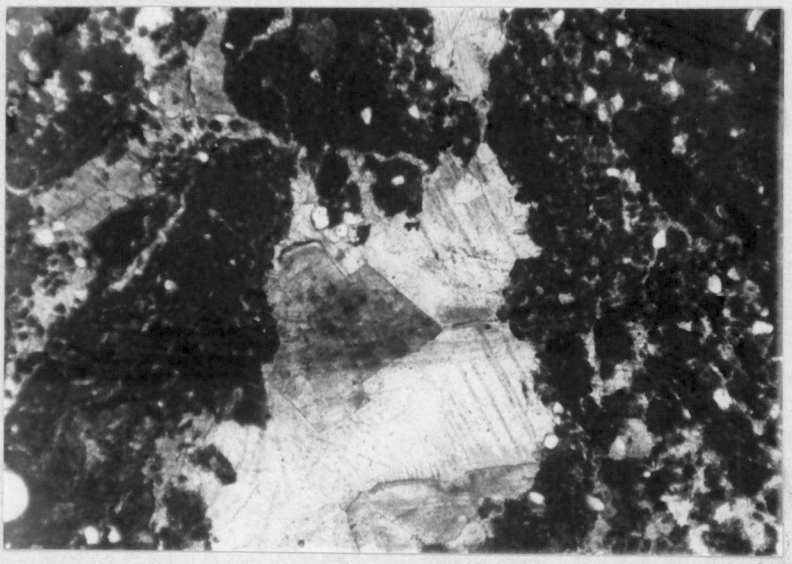

1 mm

Figure 4-3. Photomicrograph of a slightly dolomitized limestone (Sample RR-49C_2). In the center of picture is blocky calcite (white) cement in sharp contact with dolomite (cloudier).

Mg-calcites. Some of the interallochem cements are in sharp contact with dolomite, and in some cases poikilotopic with dolomite inclusions.

The allochems of the winnowed sediments (intraclasts, fossil fragments, ooids) suggest that the limestones formed in shallow marine environments. The clear blocky calcite cements are indicative of a phreatic environment of formation (Bricker, 1971; Land, 1973; Meyers, 1974). The dolomite inclusions in some of the calcite cements are diagnostic of mixing zone environment (Folk and Siedlecka, 1974). Such dolomite inclusions in calcite could have formed from a later alteration of high-Mg calcite inclusions as suggested by Meyers and Lohmann (1978). Alternatively, they could have formed contemporaneously from solutions that are saturated with respect to both calcite and dolomite. For instance, the sharp contacts between dolomite and calcite in inter-allochem pore spaces (e.g., Fig. 4-3) are suggestive of equilibrium conditions. Similar sharp boundaries, but involving different phases, namely sphalerite and calcite, were used to suggest equilibrium conditions (Anderson, 1975; Kyle, 1976). At any rate, even the granular interallochem cements could be indicative of the stabilization of the limestones under the influence of fresh water, as suggested from experimental studies by Badiozamani et al. (1977). Moreover, as discussed in the section on geochemistry, the low Na content, low Sr/Ca ratio as well as the interpretation of the correlations of trace elements are compatible with the stabilization of the limestones in the presence of fresh water.

Regeneration of primary limestone textures, and fabrics (ooids and peloids) is one of the classic dedolomite characteristics (Alberstadt and Reesman, 1978). This makes it difficult to distinguish between limestones that are negligibly dolomitized and dedolomites. Some of the microslides studied by the author appear to indicate evidence of dedolomitization. A probable example of dedolomitization is observed in an old prospect at the Joe Mill Creek-Rucker Branch section. Here, very slightly to partially dolomitized limestones are laterally traceable into dolostone (CFd) over a short distance. The dolomite crystals in the limestone adjacent to the dolostone are highly corroded. Dolomitic selvages occur around some fossil fragments (J-26A, Appendix G). Interestingly enough, primary allochems such as fossils and peloids are preserved despite the possibility that the rock was dolomitized and then dedolomitized. Another microslide (J-26C) from the same bed but about 1-1/2 meters away from the dolostone limestone contact has only very few corroded dolomite crystals. If this part of the limestone is also a product of dedolomitization, then it becomes a difficult matter to distinguish between dedolomite from limestone that perhaps was not dolomitized completely to begin with. On the other hand, it is difficult to perceive that between two samples taken 1-1/2 meters apart from each other and from the same bed, one would be a product of dedolomitization, but the other an original limestone. A possible explanation could be to call on differing and very localized geochemical environments. Some dolomite crystals in the partially dolomitized limestones at Shiloh prospect show evidence of calcitization. This is

also observed in some of the limestones at the unmineralized River Ridge section.

In these partially dolomitized limestones many of the dolomite crystals maintain sharp contacts with interallochem calcite cement (Fig. 4-3, p. 76). However, the same dolomite crystal that has a sharp contact with interallochem calcite cement is poikilotopic with calcite inclusions, and may have a serrated edge on its part that grows into the adjacent micritic material. Some of the poikilotopic crystals, particularly when entirely on micritic material have corroded and sometimes rounded edges. It appears reasonable to suggest that the sharp contact between interallochem cement and dolomite is an evidence of equilibrium coprecipitation. Similar mutual sharp boundary between sphalerite anc calcite were used to suggest equilibrium relationships by Kyle (1976). On the other hand, the continued growth of dolomite beyond interallochem pore spaces (Folk, 1965; Berner, 1971) could conceivably result in serrated edges if the growth was not completed.

As suggested earlier, the limestones were probably neomorphosed in the presence of fresh water. Calculations of the degrees of saturation of the common carbonates (Chapter II) suggests that alteration of aragonite to calcite would be expected between 40 to 60 wt. % marine water [also, it can occur due to the action of fresh water alone, Kinsman (1969)]. For a mixed solution with 10 to 40 wt. % marine water in the mixture dolomitization is preferred. For less than 10 wt. % marine water in the mixture the solution would be under-saturated with respect to the common carbonates and dissolution

would be anticipated. When the fresh water component is one in which minerals more soluble than calcite (e.g., gypsum) could have dissolved such water could be as much as two fold saturated with respect to calcite (Plummer, 1975, p. 228). In such a case for very low proporations of marine water in the mixture, calcitization of dolomite is feasible (see section on effect of dilution, Chapter II). In other words, dolomitization and calcitization could be regarded as natural consequences of mixing "fresh water" (of locally varying composition) with marine water; variable proportions of the mixture resulting in differing geochemical behavior.

Fine-Grained Dolostones (Fd)

Individual dolomite crystals that comprise fine-grained dolostones are generally 0.02 to 0.05 mm in diameter. Mostly the crystals are anhedral and occur in a fitted fabric (xenotopic—Friedman, 1965). Some stain blue in acidified potassium ferricyanide solution indicating that they are ferroan dolomite. They luminesce shades of darker red. Generally they show no luminescent zonation. However, at the contacts of some crystals brighter red luminescence is observed. Electron microprobe analyses on some crystals show a nearly stoichiometric Ca/Mg ratio (Table 4-4, p. 74). Their Mn content is very low, below the detectability limit of the microprobe. Their Fe content is variable, about 1000 ppm, but sometimes reaching up to 1800 ppm. However, reddish dolomites, such as those near the post-Knox unconformity tend to have a higher Fe content, about 2300 ppm.

Although there are interlayered dark gray horizons, the fine-grained dolostones are generally light gray or greenish gray. Some beds, near the post-Knox unconformity at the River Ridge section are reddish. This reddish coloration may have resulted from aerobic decomposition of algal mats shortly after deposition of sediments (e.g., aerobic decomposition of Holocene intertidal algal laminites has resulted in the production of reddish sediments—Golubic, 1976). However, abundant wavy and planar laminae marked by contrast in coloration are preserved. These cryptalgal laminae are very thin (mm.-sized), although sometimes they are as thick as 1 cm (Fig. 4-4). Often, discontinuous quartz-rich lenses occur parallel to the laminae. The grain size of the quartz is about 0.04 mm. In addition, rounded and coarser quartz grains (0.6 mm) occur scattered in some of the beds. Opaques, some of them pyrite cubes, occur in laminae which are often parallel to bedding, but sometimes at oblique angles to it. Frequently, fine-grained dolostones may show grain-size mottling, and some of them show size grading. Rarely, ripple laminated sandstones and intra-formational conglomerates occur interbedded with the wavy laminated dolostones (e.g., at River Ridge section). Other current indicators such as scour and fill features are preserved in some of the beds—some beds and laminae surfaces preserve mudcracks (Fig. 4-5). Birdseye infilled by coarse grained dolomites are also observed. Nodular shaped vugs are generally infilled by very coarse grained, often ferroan dolomite crystals which tend to have arcuate cleavages and wavy extinction. Sometimes such vug-fills are associated with length-slow



Figure 4-4. Wavy laminae at Joe Mill Creek-Rucker Branch section. (Photo taken about 76 meters above the Kingsport-Mascot contact.) Discontinuous, lensoid wavy laminae, some of them up to 1 cm thick, occur as ridges on weathered surfaces.



Figure 4-5. Polygonal mudcracks. (Photo taken at River Ridge from the top of unit 135 of Harris, 1969.)

chalcedony. Where the chalcedony occurs as an outer lining of the vug-fill, the nodules stick out on weathered surfaces (Fig. 4-6). Some of the nodular features (Fig. 4-7) are infilled by what appears to be vadose silt (e.g., Dunham, 1969a). Rarely, some vugs have an earlier lining of drusy cement, probably of vadose origin, and are finally infilled by blocky dolomite. Chert nodules and layers, some of them preserving oolitic textures, occur inside of some of the beds and along bedding separations.

Although some of the oolitic-textured cherts appear to be a product of the silicification of oolitic limestones, it is possible that some of them are of caliche origin. Greenish shaly material occurs between bedding planes. Analysis of some of the shaly material shows a higher K/Na ratio (about 150:1—Table 3-3, p. 39) in comparison to shales from both platforms (5:1) and geosynclines (2.5:1) as calculated from data given by Wedepohl (1969, p. 260). Other features observed include microfaulting, loadcasts, and bed aligned stylolites. These probably resulted from over-burden pressure.

Contrary to the suggestion of Harris (1973) that the Upper Knox dolostones are a product of incipient processes in a subtidal environment, presumably due to refluxion of hypersaline solutions, the following features indicate an intertidal to supratidal origin for the fine-grained dolostones.

Fine-grained nature of the dolostones. In his field description of the River Ridge section, Harris (1969) distinguished between various grain sizes of dolostones. In his dolomitization model, where he



Figure 4-6. Nodular vug fills at Joe Mill Creek-Rucker Branch Creek section. Scale is given by the 25 cent coin at arrow. (Photo taken about 113 meters stratigraphically above the Kingsport-Mascot contact.) The vug fill is primarily of coarse-grained, baroque-type dolomite with an outer lining of length-slow chalcedony. The outer lining silica makes the nodules resistant to weathering so that they stick out on weathered surfaces.



Figure 4-7. Nodular and lensoid features with geopetal sediment fill at Joe Mill-Rucker Branch section. Scale is given by the 25-cent coin. (Photo taken about 124 meters stratigraphically above the Kingsport-Mascot contact.)

proposed that dolomites were formed by incipient subtidal processes, Harris (1973) did not distinguish between the grain sizes of dolomites. However, since Harris (1971) argued that the coarse-grained dolostones were formed by ground waters that were transported through an interconnected paleoaquifer system, and he did not disclaim this conclusion in his later paper (1973), presumably his dolomitization model of 1973 referred to the fine-grained dolostones.

As will be discussed later, the fine-grained dolostones in the Copper Ridge district are not composed of grain sizes (less than 5 μ) equivalent to those of Holocene dolomites (e.g., Shinn et al., 1965; Illing et al., 1965). But they are of the size (e.g., 20 to 80 μ— Mazzulo and Friedman, 1977) that have been previously interpreted by others to have formed in peritidal environments. This suggests that the grain size of the dolostones may be used as a corroborative evidence of their formation in peritidal environments.

Algal laminae. Harris (1973, p. 67) reported, "beds consisting of nearly parallel paper-thin laminae, similar to those described (Black, 1933, p. 170-171) as the result of rhythmic alteration of Holocene carbonate sediments and dark algal films are common in the Knox Group." However, instead of relying on modern analogs he chose to conclude that these organosedimentary structures were formed subtidally; the organic layers being a result of mass mortality of phytoplankton (Harris, 1973). He suggested a subtidal environment of deposition, based on the presumed occurrence of abundant vertically stacked hemispheroidal stromatolites (Harris, 1969). Such stromatolitic occurrences were not

confirmed in this study. Even if they were present, based on modern analogs they are also indicative of intertidal origin (e.g., Logal et al., 1964).

The most abundant feature in the fine-grained dolostones are planar to wavy laminae. In thin-sections, under a transmitted-light microscope, the laminar features are marked by presence of lighter and darker horizons sometimes associated with differences in grain sizes of dolomite. Sometimes 0.04 mm.-sized quartz grains occur as discontinuous and lenticular laminae in the lighter horizons. Dispersed opaque material is in many instances more prevalently aligned in the laminae. However, in some cases the laminar features are only faintly preserved, and may be only discernible by the naked eye while holding the thin-sections against light. The laminar features are sometimes observed in the field. On weathered surfaces, they may stick out as ridges (e.g., Fig. 4-4, p. 82). In polished slabs the laminar features are nearly parallel. They consist of darker laminae alternating with thicker and lighter zones. These features resemble the cryptalgal laminites observed in Holocene peritidal deposits. For example, in the intertidal zone of Abu Dhabi, cryptalgal laminites are documented in which the laminated fabric resulted from thicker, sediment-rich layers alternating with thinner, organic-rich laminae (Monty, 1976). The abundant occurrence of planar to wavy laminae in the fine-grained dolostones in the Copper Ridge district suggests the early presence of algal mats that trapped and bound sediments as documented in Holocene peritidal deposits (e.g., Ginsburg, 1955; Shinn et al., 1965; Ginsburg

Hardie, 1975; Schneider, 1975; Monty, 1976; Golubic, 1976). Cryptalgal laminites similar to those found in the Upper Knox have been ascribed to algal activity in ancient peritidal environments (e.g., Thompson, 1975; Wanless, 1975; Mazzulo and Friedman, 1977). Mazzulo and Friedman (1977) reported that the Lower Ordovician Great Meadows and Fort Ann formations of New York state have abundant cryptalgal laminites and proposed that they formed in intertidal to supratidal environments. These carbonates are of similar age and palaeolatitude to the Lower Ordovician carbonates of the Copper Ridge district.

Planar algal mats were also recorded from the Holocene subtidal environment of Bermuda (Gebelein, 1969), but do not commonly lead to formation of laminated sediments (Awramik et al., 1976). At any rate, Holocene algal mats are found in areas where grazing fauna are rare (Gebelein, 1976). In the Early Ordovician intertidal to supratidal environment of the Copper Ridge district, grazing fauna (such as trilobites—Mazzulo and Friedman, 1977) could have been precluded by hypersalinity of the environments and also by the ozone free Early Ordovician atmosphere which may have led to high incidence of ultraviolet radiation (e.g., McAlester, 1968; Garrels et al., 1973). However, blue-green algae are adapted to withstand high fluxes of ultraviolet radiation (Awramik et al., 1976).

Desiccation indicators. Harris (1973) has noted the presence of mudcracks in the dolostones and limestones of the Upper Knox. But he argued that they could have resulted from contraction and expansion of shales in subtidal environments. However, the polygonal shapes of the

cracks in plan view (e.g., Fig. 4-5, p. 83) and their wedge shaped nature (tapering downward) in cross-section is diagnostic of mudcracks that resulted from desiccation due to subarial exposure. In places where these mudcracks are associated with shaly material, the cracks are not infilled by shale. This suggests that the fine-grained dolostones were infilled before the shaly material was deposited. However, it should be noted that preserved mudcracks are not abundant. Another indication of subarial exposure of some of the beds includes the presence of birdseyes (see Shinn, 1969).

Paucity of fauna. Except for the presence of organosedimentary structures fossils are absent or rare. When it is noted that a relict fossil fauna is discernible in the coarser than fine-grained dolostones, absence of fossils in the fine-grained dolostones indicates that the environments of deposition of the precursor lime mud were probably not conducive to a normal marine fauna.

Evaporites. Sulfate evaporites, filling nodular vugs are known to be associated with dolomites in recent intertidal to supratidal sediments of the Persian Gulf (Curtis et al., 1963; Bush, 1973). The possible early presence of gypsum in the Early Ordovician peritidal environments is inferred from the following indirect lines of evidence.

(a) The nodular shapes of vugs (e.g., Curtis et al., 1963).

(b) The wavy extinction and arcuate cleavages of the coarser grained dolomite vug-fills ("baroque dolomite"—Folk and Assereto, 1974).

(c) The association of the dolomite vug-fills in some cases with length-slow chalcedony (e.g., Folk and Pittman, 1971; Siedlecka, 1972).

(d) The occurrence of brecciated beds (e.g., Mazzulo and Friedman, 1977) particularly when underlain and overlain by undistrubed beds.

Additional but very indirect clues to the possible early presence of gypsum would include, the paleolatitude (20° to 30° south of the equator—Smith et al., 1973) as well as the presence of two distinct grain sizes of quartz (decimicron, and centimicron). Although not abundant, the bimodal distribution of quartz grains could indicate possible aridity of the region (e.g., Folk and Siedlecka, 1974). However, the absence of rarity of preserved gypsum or anhydrite would indicate that the environment was probably periodically flushed by fresh water. It should be noted though, that in some brecciated and sphalerite mineralized zones anhydrite vug-fills have been reported; for example from the Puncheon Camp Creek area (Hill, 1971) and from the Idol and Flat Gap mines (Mantooth and Morris, 1979, personal communication). But, such anhydrites might have been precipitated from mineralizing solutions as suggested by Anderson (1973, 1975).

Chert. Some of the chert nodules and layers have oolitic textures. In many instances, the oolitic textures are composed of concentric laminae and radial fabrics, much like aragonitic ooids. They are also similar in size to the ooids (about 0.5 mm) in oolitic limestones (e.g., RR 49, Appendix G). Similar fabrics could also result from caliche origin

(James, 1972). However, those of caliche origin could probably be distinguished by the criteria discussed by Dunham (1969b). These criteria include: geotropic lengthening, in situ brecciation, and fitted polygonal structures of adjacent pisolites. Additionally, the diameters of pisolites range from 2 mm to 5 cm (Read, 1976). On the basis of these criteria most of the oolitic textures do not seem to be of caliche origin. However, some of the ooids of unit 109 (Appendix G) show downward lengthening. In one of the oolitic textured units minute beads of oolitic fabric are observed (Fig. 4-8). It appears that these textures are of caliche origin.

Nonetheless, the presence of chert within beds and as bed partings in most cases aligned to bedding strongly suggests that chertification was a synsedimentary or very early diagenetic phenomenon. The inference that allochems (e.g., ooids, intraclasts, peloids) are preserved by chert suggests that in these particular cases chertification was very early diagenetic and preceded dolomitization. However, there are many instances where chert occurs as a matrix (cement) in dolostones. Thus, the overall impression is that chertification is broadly contemporaneous with dolomitization, or there may have been more than one period of chert formation. Prior to the formation of chert, the diagenetic solution ought to have silica in solution, in other words it should have been alkaline (Peterson and Von Der Borch, 1965; Mason, 1966; Krauskopf, 1975) and possibly hypersaline (Krauskpof, 1959; Eugster, 1973; Zamarino, 1975). The point to be made here is that the environment under which chert lenses and layers in the fine-grained dolostones formed was probably not normal marine.

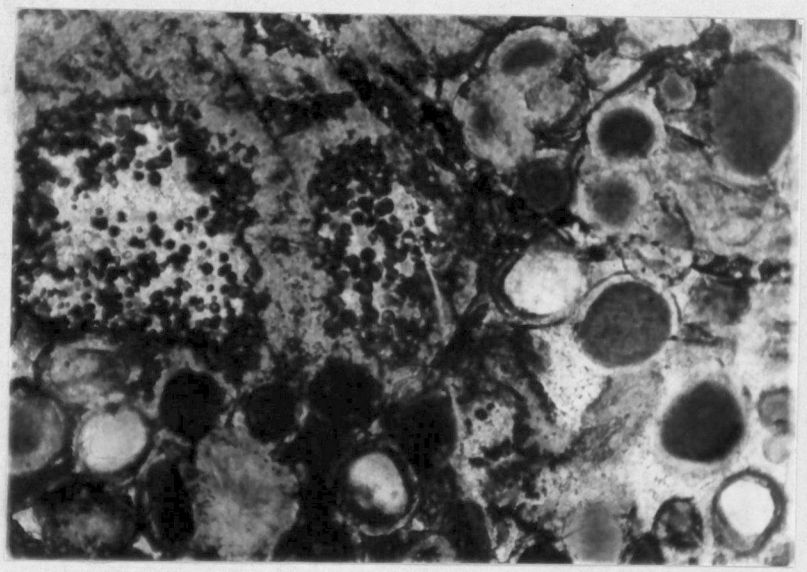

1 mm

Figure 4-8. Photomicrograph of an oolitic chert (Sample RR-44A). Notice the several rounded beads in two pockets. These beads are brownish in color and oolitic in fabric.

In short, the evidence of solutions of elevated salinities suggested by the presence of chert, absence of normal marine fauna, indirect evidence of the early presence of gypsum, coupled with presence of planar to wavy cryptalgal laminae as well as the presence of mudcracks and birdseyes suggest that the environments in which the fine-grained dolostones formed were comparable to the intertidal to supratidal regimes of modern analogs. However, as discussed below, there are differences between Holocene analogs and the fine-grained dolostones in the Copper Ridge district.

1. In Holocene peritidal environments, the grain sizes of dolomites are reported to range from 1-5 μ, i.e., $\leq$ 0.005 mm (e.g., Shinn et al., 1965; Illing et al., 1965). The fine-grained dolomites in Copper Ridge district are an order of magnitude coraser (0.02 to 0.05 mm). However, as discussed above, the fine-grained dolostones preserve primary sedimentary structures such as mudcracks, wavy to planar laminae. This suggests that the grains have aggraded. Although the criteria for recognizing aggraded grains and the reason for aggradation were not given, Folk (1965) has discussed aggradation of grain sizes in calcites.

2. Holocene dolomites are disordered and have greater than 56 mole percent Ca^{++} (Shinn et al., 1965). On the other hand, the Copper Ridge fine-grained dolomites have a nearly stoichiometric Ca/Mg ratio (Table 2-3, p. 17).

Fine-grained dolomites are generally regarded to be penecontemporaneous to sedimentation. Probably the best clue to the

penecontemporaneity of their formation is obtained by reference to Holocene analogs. In Holocene peritidal deposits C^{14} chronology gave recent ages for dolomites indicating penecontemporaneity of their formation (Shinn et al., 1965; Illing et al., 1965). Considering that the environments in which the fine-grained dolomites of the Copper Ridge district occur were peritidal, it may be assumed that they were formed penecontemporaneously. On the other hand, the fine-grained dolostones at Copper Ridge district have probably undergone considerable alteration from their presumed "primary" state (i.e., nonstoichiometric composition and $\leq$ 5 μ grain size).

Coarser than Fine-Grained Dolostones (CFd)

Dolostones of this group consist of dolomites belonging to the medium, coarse, and very coarse grain size categories of Folk (1965). In the Copper Ridge district such dolostones are medium gray to brown in color. Often, the crystals are zoned with a cloudy center and clearer rim when viewed under transmitted light petrographic microscope (Fig. 4-9). In acidified potassium ferricyanide solution CFd crystals stain blue either in alternating bands or only at the crystal rims. Using cathodoluminescence as many as eight growth zones are observed. Figure 3-1 (p. 30) gives a summary of the luminescent patterns observed in these dolomites. Some of the dolomites show wavy extinction under crossed nicols. Dolomites which show the above characteristics are observed in both mineralized and unmineralized sections.

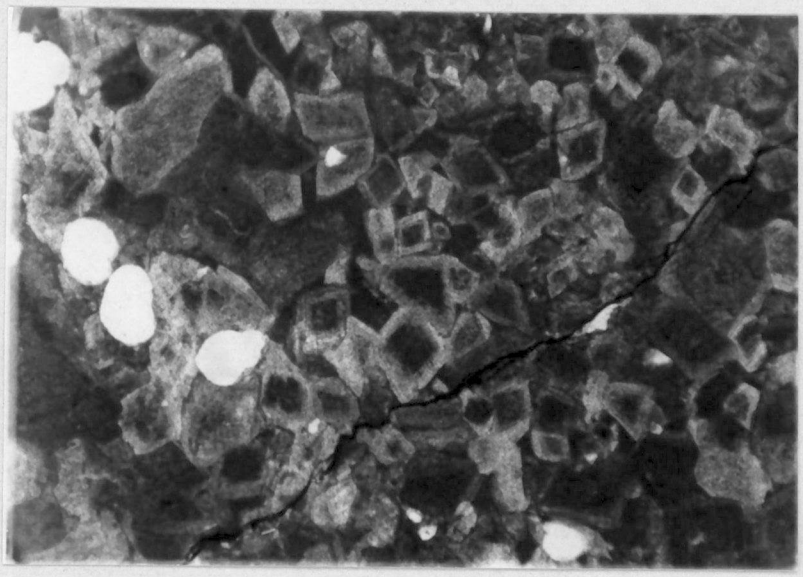

1 mm

Figure 4-9. Photomicrograph of zoned dolomite (Sample RR-59B). Dolomite crystals appear cloudy-centered and clearer-rimmed.

Electron microprobe analysis of some of the grains show that the composition of the dolomites is variable. In general they have a higher Ca/Mg ratio (Table 3-1, p. 32) than ideal ordered dolomites. High Mg-calcite sometimes occurs as inclusions in the centers of dolomite rhombs. There is a tendency for Fe to increase from core to rim, but Mn may not show a sympathetic variation. On the whole the Mn content is very low, but at some points in a crystal it can be of the order of thousands of ppm. Although the Fe concentration is also variable, the overall Fe content of a dolomite crystal is 1000 to 4000 ppm.

Descriptions of the fabrics of the dolostones are given using Friedman's (1965) terminology. Tightly packed CFd sometimes consists entirely of anhedral dolomite crystals and displays a xenotopic fabric. In other instances, it consists of anhedral and subhedral crystals, and is therefore hypidiotopic. Often, the dolomite crystals are also poikilotopic, frequently with inclusions of calcite in proximity to limestones, and generally quartz, finer dolomite crystals and insoluble residue elsewhere. Mostly CFd is porphyrotopic due to the occurrence of scattered coarser grained crystals in a ground mass of less coarse crystals. In some cases it is color-mottled, and sometimes size-mottled due to the occurrence of one grain size group as patches in another grain size group. Sometimes, ghost features of fossils (fauna) and peloids are observed. Another feature of the CFd is the occurrence of lens-shaped vugs infilled by mostly ferroan dolomite, with wavy extinction.

Where some fine-grained dolomite pods and lenses occur in CFd units field relationships suggest that such CFd units formed by aggradation of fine-grained dolomites, unless the Fd patches indicate microenvironments conducive for their formation. The processes of aggradation may be similar to those suggested by Folk (1965) for calcite, and may consist of two types: one involving porphyroid growth, the other involving coalescive growth. The coalescive growth was thought to result in uniform grain sizes. The CFd units at Copper Ridge district are in almost all cases porphyrotopic so that they probably were not a product of coalescive growth. The porphyroid type of aggradation yielding CFd units from originally Fd units could apply to some beds. In those units where fossil fauna are discernible it is unlikely that the CFd units formed by aggradation of Fd units because unaltered Fd units contain no fossils. Even in other cases where fossils are not observed, the evidence to suggest aggradational processes is equivocal, for the precursor limestones might not have had fossils or any present may have been completely destroyed. Moreover, it is difficult to explain how zoned dolomites could result from aggradational processes.

More information on the origin of CFd may be obtained from partially dolomitized limestones that occur at the gradational contact between limestones and CFd. Petrographic study of the partially dolomitized limestones shows the following relationships. The dolomite grain sizes are of the type that belong to the coarser than fine-grained category. The dolomite crystals do not seem to have any preference as to where they grow. They grow across fossils

(Figures 4-10 and 4-11), and interallochem pores (Fig. 4-12). They appear clearer on interallochem pore space as well as where they intersect fossils, and cloudier on peloidal and intraclastic allochems, and as such preserve relict features. Such ghost features in totally dolomitized limestones are better seen under diffused light such as may be obtained by inserting the condenser lens after putting a piece of transparent paper between a microslide and the stage of the microscope (Delagado, 1977). Some dolomite crystals maintain a sharp contact with low Mg-calcite cement (Fig. 4-3, p. 76) on interallochem pore space, although they sometimes have serrated edges on micritic material. Some dolomites grow in a void after a lining of calcite cement (Fig. 4-13) or silica. Frequently authigenic quartz is associated with dolomite. Another observed feature is the presence of stylolites, and in many cases dolomite crystals are corroded by and terminate at stylolites (Fig. 4-10), suggesting that sylolitization post dates dolomitization. However, some "stylo-corroded" dolomite crystals have overgrowths (Fig. 4-14) indicating separate stages of dolomite-growth, or broad contemporaneity of stylolitization and dolomitization. In general, dolomite crystals which grew on micrite are less coarse than those that grew on sparite. In the latter case they sometimes attain diameters up to 2.0 mm. Ostensibly the dolomitization of an interlaminated micrite and sparite, and/or a burrowed micrite could result in size mottled as well as porphyrotopic dolostone. The interpretation that a bioturbated precursor limestone could result in a mottled dolostone was previously suggested by Mazzulo and Friedman (1977).



1 mm

Figure 4-10. Photomicrograph of partially dolomitized biopelsparitic packstone (Sample RR-60C). The outline of the brachiopod can be discerned even on the part where dolomite has grown across it. Note also that some dolomite crystals are truncated by stylolites.



1 mm

Figure 4-11. Photomicrograph of partially dolomitized biopelsparitic packstone (Sample RR-72). The outline of the trilobite can be discerned even where dolomite has grown across it.



1 mm

Figure 4-12. Photomicrograph of partially dolomitized intrapelsparitic grainstone (Sample RR-68A). Dolomite appears clearer across interallochem pore space. Drusy calcite lining around an intraclast can be traced through the dolomite in the middle part of the photomicrograph.

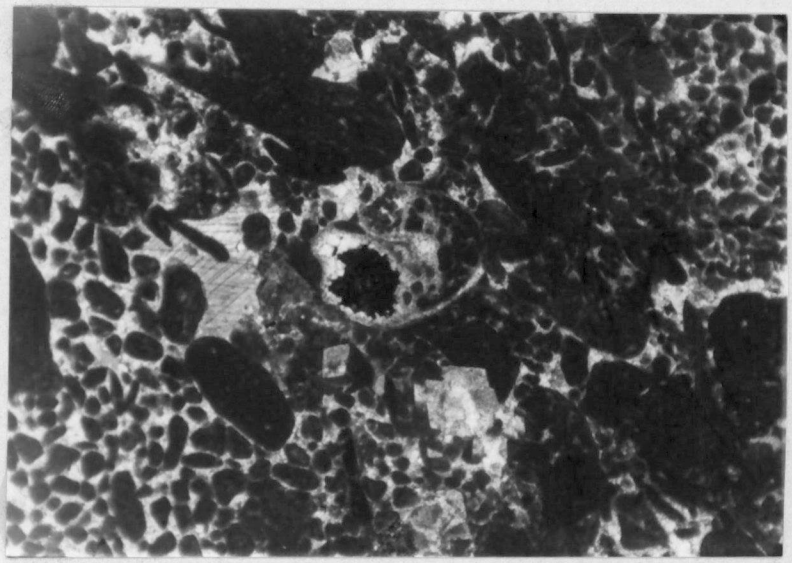

1 mm

Figure 4-13. Photomicrograph of a slightly dolomitized biointrapelsparitic grainstone (Sample RR-70C). Photo taken under crossed nicols. Stratigraphic up direction is indicated by the geopetal fill in gastropod. The middle part of the gastropod is infilled by crystal silt (e.g., Dunham, 1969a). The top part has a lining of calcite followed by blocky dolomite (dark) cement.



1 mm

Figure 4-14. Photomicrograph of a slightly dolomitized limestone (Sample RR-68C). Stylolite winds through a dolomite crystal suggesting that stylolitization and dolomitization were broadly contemporaneous.

Previous workers who studied the Upper Knox dolostone (e.g., Hill, 1969, 1971; Harris, 1971; West, 1974; Snyder, 1975) have suggested that the coarser than fine-grained dolostones are a replacement product of limestones. The processes suggested include dolomitization by mineralizing fluids (e.g., Hill, 1969; West, 1974) and dolomitization by ground waters that had abundant Mg^{++} ions from the erosion of the Mascot dolostone during the post-Knox unconformity (Harris, 1971). The regional extent of the CFd units and the fact that sphalerite mineralization occurs in fractures and breccias (including fragments of CFd) do not support the suggestion that CFd units were formed from mineralizing fluids (although some of the vug-fill dolomite associated with sphalerite probably originated from mineralizing solutions—see Chapter V). Also limestones occur in close proximity to sphalerite deposits. Moreover, the characteristics (textural and chemical) of CFd adjacent to mineralized zones such as at Shiloh and the Joe Mill Creek area are similar to those in unmineralized areas such as at River Ridge. This indicates that the formation of CFd did not result from mineralizing fluids.

The occurrence of high Mg-calcite inclusions in dolomite crystals suggests an early stage of dolomitization, since high Mg-calcite alters to low Mg-calcite rather quickly (Chave and Shamalz, 1966; Gavish and Friedman, 1969). As discussed in the geochemistry section the luminescent zoning of dolomite probably indicates different rates of growth of different increments of the same crystal as it grows from a mixture of fresh and marine water. Cloudy-centered, clearer-rimmed

zoning was suggested to be a product of a mixing zone environment (Sibley, 1979). The same environment is also indicated by low Na contents and low Sr/Ca ratios (e.g., Badiozamani, 1973; Land, 1973), and the increase of Fe towards rims of crystals, as well as the correlation patterns discussed in Chapter III. Furthermore, the limestones were interpreted to have been stabilized in the presence of fresh water. Some dolomite crystals in the limestones appear to be cements (e.g., Fig. 4-7, 4-12, pp. 86, 101). This suggests that like the calcite cements the dolomites were formed in the presence of fresh water. Also, it does not appear unlikely that stylolites could form in a mixing environment. The mixing model requires marine pore water as the source of Mg^{++} for dolomitization. Thus the CFd is interpreted to be the product of early diagenetic alteration.

V. SEDIMENTARY AND DIAGENETIC SETTING

The Upper Knox carbonate rocks at Copper Ridge are predominantly diagenetically altered. The environments of deposition of the lime muds which were precursors of the dolostones can only be inferred from indirect lines of evidence. As discussed earlier, the fine-grained dolostones are interpreted to be a product of penecontemporaneous (very early diagenetic) dolomitization in supratidal and upper intertidal environments; the preserved limestones were deposited in intertidal to subtidal environments; and the coarser than fine-grained dolostones probably resulted from early diagenetic dolomitization of intertidal and subtidal limestones. The lateral and

vertical relationships of these lithologies can give a clue as to the environments of deposition of the precursor lime muds. Such a view of relationships may be obtained from the construction of a fence diagram.

The published columnar sections in the study area are given in Fig. 4-15. The correlation of these sections is shown as determined by Harris (1969). He used a certain chert-matrix sandstone and SH-V stromatolitic horizons as stratigraphic markers. He reported that the SH-V horizons are easy to recognize in the field. But their presence could not be confirmed even at the River Ridge section where SH-V letters are still painted on the rocks.

In the three sections measured during this study, no marker horizons were identified to be traceable through all three localities. Shaly bed partings are abundant, but in many cases they probably are accumulated insoluble residue from pressure solution. From the greenish color of some of the shales, their high K/Na ratios (obtained from three samples) it was suspected that they could be bentonitic. However, the sporadic nature of these shales precluded their use for correlation (e.g., several greenish shales in the Thorn Hill section were described by Hall and Amick (1934), but only a few were observed at Joe Mill Creek). Chert nodules and layers are interpreted here to be of diagenetic origin, and are, thus, probably of little use as marker horizons over long distances. The chert matrix sandstone shown to be traceable through three sections in Fig. 4-15 (and herein regarded to correspond to unit 96 at River Ridge) was not observed at Joe Mill Creek area either by Harris (1969) or during this study. This

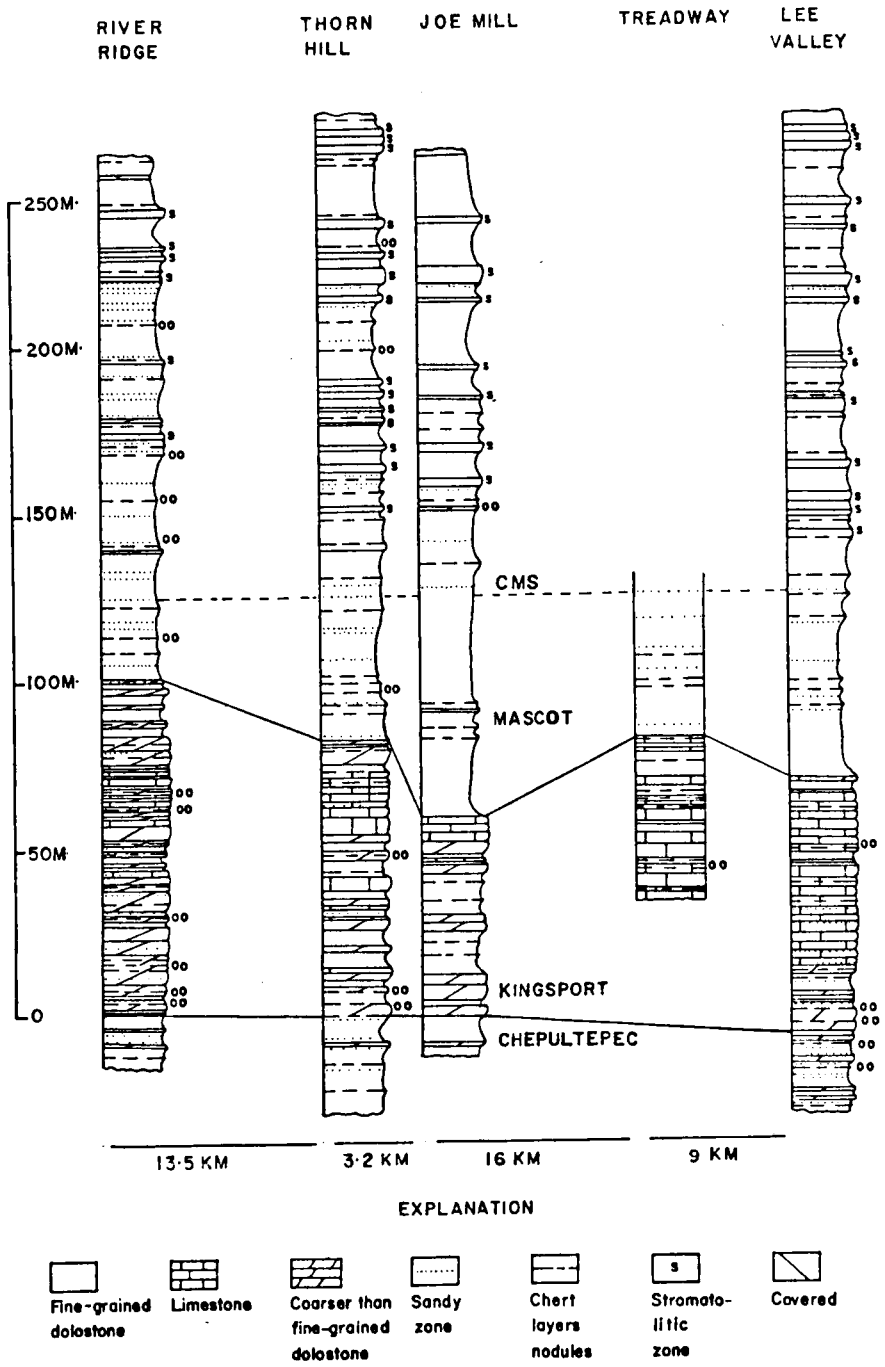

Figure 4-15. Columnar section of the Upper Knox in the Copper Ridge district.

poses a problem about the correlation of the sections, particularly of the Joe Mill Creek area.

The River Ridge section, as measured by the present author, showed a good agreement in terms of units and thicknesses (though not necessarily description of units) with that given by Harris (1969). Portions of the Upper Knox were measured along a dirt road parallel to Rucker Branch and along the stream bed below the confluence of Joe Mill Creek and Rucker Branch. The Kingsport lithologies below the confluence of the two creeks measured during this study are not identical to those given by Harris (1969). The Kingsport lithologies as measured during this study show a high correlation with the adjacent Lee Valley section. For comparison, sections remeasured during this study in conjunction with others, and put in their position shown in Fig. 4-15, are given in Fig. 4-16. Figure 4-16 also includes the Shiloh section measured during this study. Its stratigraphic position is not ascertained by any marker beds. But its correlative position was judged by lithologic types.

A marker horizon that is traceable through all the sections was not identified. However, the reasonable correlation of lithologic types of adjacent sections indicates that the stratigraphic positions shown in Fig. 4-16 are probably correct. Based on this assumption, a fence diagram (Fig. 4-17) was constructed. Obviously, more stratigraphic sections would be required to come up with a better controlled fence diagram. However, based on the available data, the constructed fence diagram is used to suggest the following interpretations. The

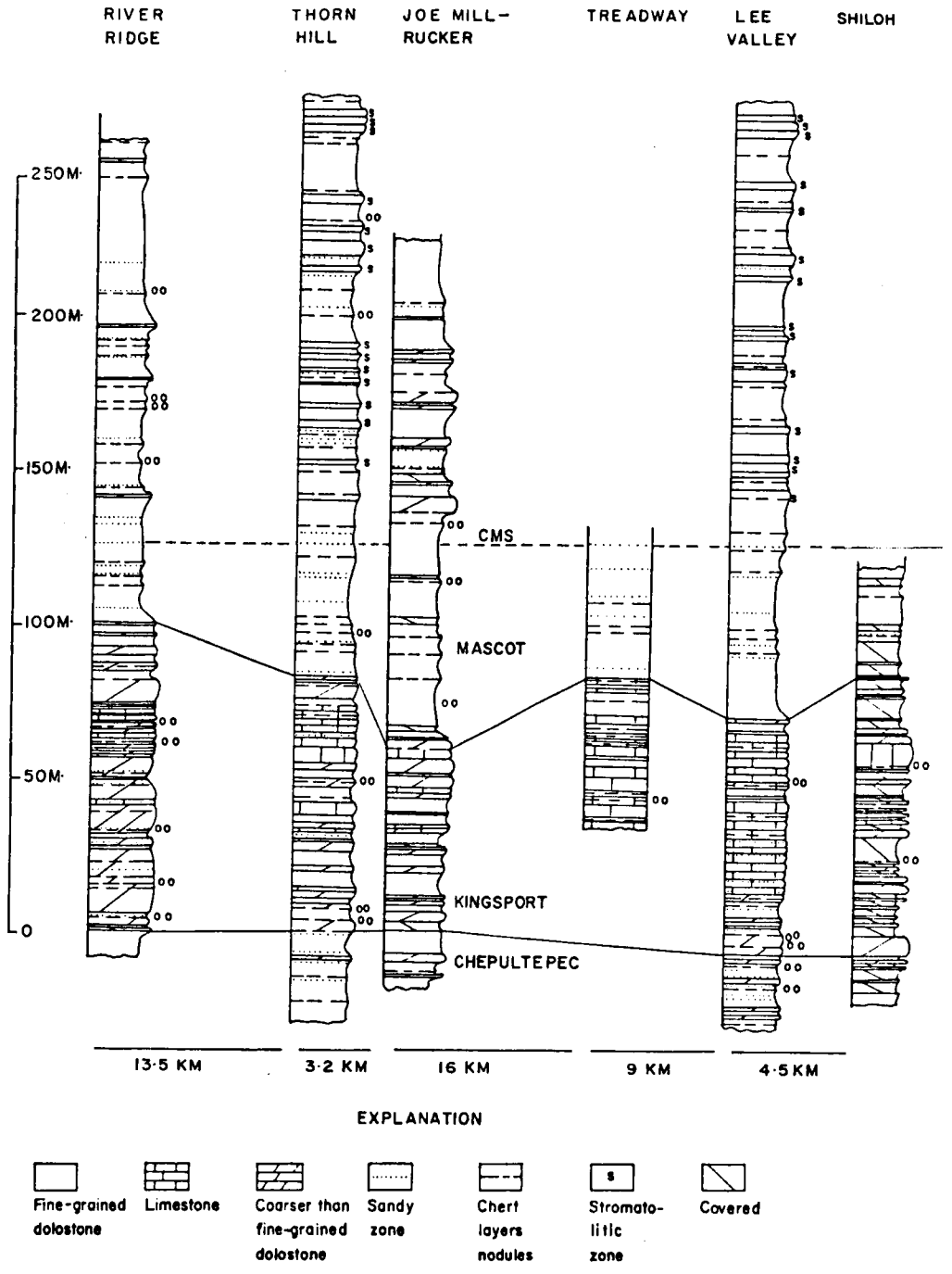

Figure 4-16. Columnar section of part of the Upper Knox in the Copper Ridge district. (River Ridge, Joe Mill-Rucker Branch and Shiloh sections as measured during this study.)

Figure 4-17. Fence diagram of the Lower Mascot and Kingsport formations in the Copper Ridge district.

The top dashed line corresponds to the chert-matrix sandstone shown in Figure 4-16. The base of the fence diagram is the contact between the Kingsport and the Chepultepec. For ease of demonstration the location of River Ridge section is displaced. Its palinspastically restored location is 13.5 km north of Thorn Hill. RR. River Ridge; TH. Thorn Hill; JMCRB. Joe Mill Creek-Rucker Branch; T. Treadway; LV. Lee Valley; S. Shiloh; CC. location of Copper Creek fault.

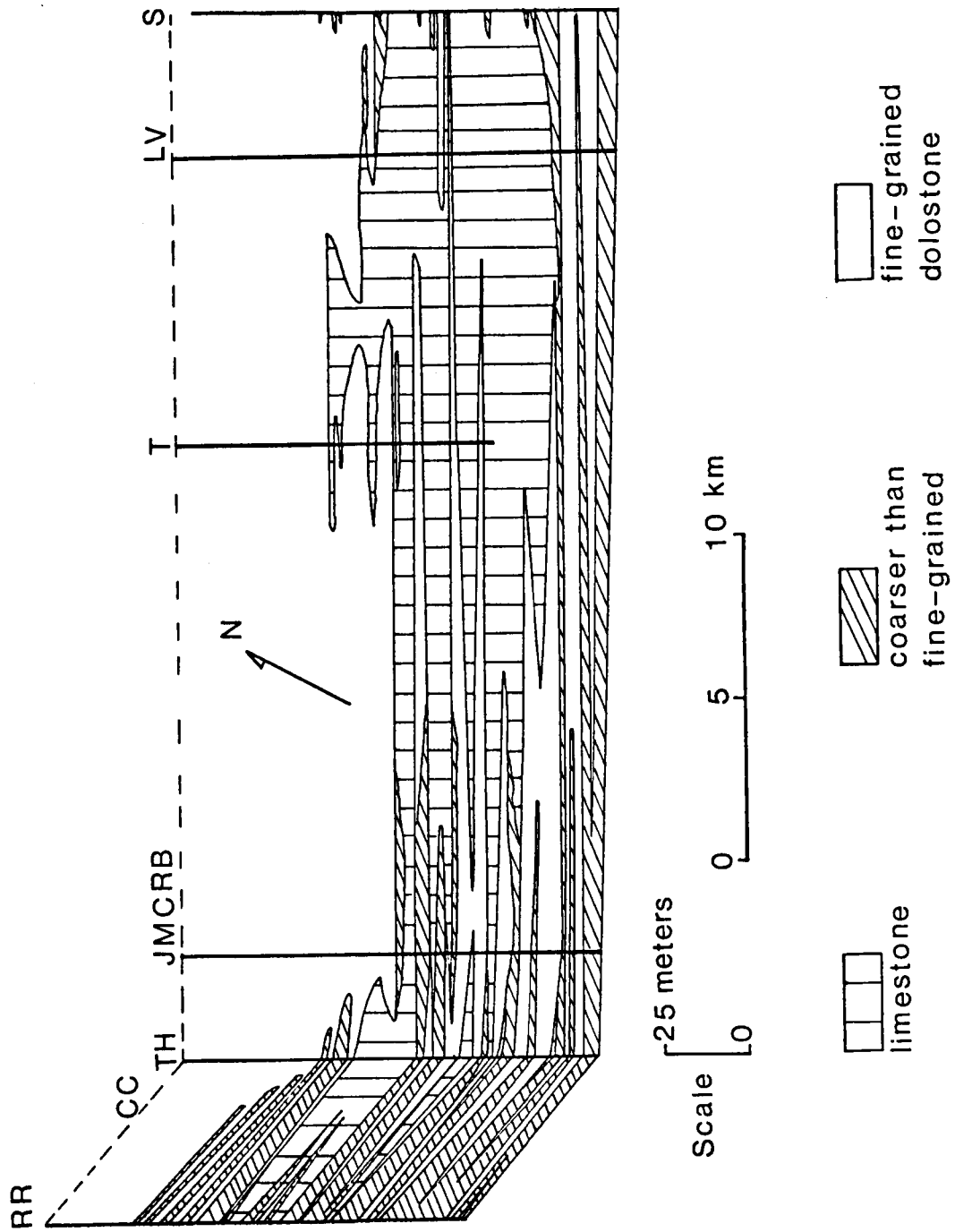
RR
CC
TH
JMCRB
T
LV
S
N
Scale
25 meters
0
0
5
10 km
limestone
coarser than fine-grained dolostone
fine-grained dolostone

Figure 4-17

fine-grained dolostones in the record of the Kingsport thin as they are traced northwestward (i.e., toward the River Ridge section). This suggests that these fine-grained dolostones are records of islands. During progradational episodes, the islands expanded, and during retrogradational periods, the islands shrunk. Such expansion and shrinking of islands gives rise to a thicker sequence of dolostones (fine-grained) towards the centers of islands, whereas limestones thin. This intertonguing relationship is better seen (Fig. 4-17) near the Joe Mill Creek area, an area where the productive Idol mine is located. Such thinning of limestones and thickening of dolostones towards mineralized localities was observed by previous workers (e.g., Wedow and Marie, 1965; Harris, 1969). They explained this phenomenon to be due to different solubilities of carbonates and the action of aqueous solutions. They proposed that limestones which are more soluble were thinned by dissolution, whereas overlying fine-grained dolostones were thickened by dilation and sag. According to Harris (1969) about 100 feet of dolostone section could correspond to thickening by dilation. However, even in the Joe Mill Creek area where several brecciated horizons occur, sufficient fracture-fill dolomites to account for such thickening were not observed. Moreover, the brecciation appears to be restricted to certain horizons, as there are unbrecciated intervening horizons. Dilation of carbonate units as postulated by previous workers for the Knox has not been observed anywhere else and is logically unlikely.

Overall, the fence diagram suggests that the depocenter was a broad tidal flat environment (the Mascot) adjacent to a very shallow marine environment dotted with islands (the Kingsport). A sedimentologic setting that has a broad supratidal flat adjacent to a marine environment with scattered islands in a modern environment could serve as an analog to the Early Ordovician environment. Based on paleomagnetic data and geometric considerations, Smith et al. (1973) reconstructed the disposition of continents throughout the Phanerozoic. During the Cambrian and Early Ordovician, the Valley and Ridge Physiographic Province of Eastern United States was shown to be 20° to 30° south-latitude. Presently, the Persian Gulf with its islands and coastal sabkha (Illing et al., 1965; Purser, 1973; Bathurst, 1975; pp. 181-212 and pp. 525-530) is within 20° to 30° north-latitude. Probably, the Persian Gulf could serve as a guide to the environmental setting of an Early Ordovician Copper Ridge District. Lown (1978) has also used the Persian Gulf as a guide to explain some of the features observed in the Mascot of Middle Tennessee. Nonetheless, the Persian Gulf is not as extensive as the Early Ordovician environment in Tennessee (Harris, 1973; Lown, 1978).

Harris (1973) used a variation of the epeiric sea model of Shaw (1964) and Irwin (1965) to explain the environment of deposition of the Knox Group carbonates in East Tennessee. He suggested that they were deposited in a subtidal zone of an epi-continental sea. Irwin (1965) distinguished the environments of an epeiric sea as the X-zone referring to the environment above wave base and up to the higher

reaches of tidal activity; and the Z-zone, for the portion landward and beyond the higher reaches of tidal action. Yet, most of the Z-zone, in a sense supratidal because it is landward and beyond tidal activity, was thought to have been covered by a very shallow water that might be agitated only by wind stress. Restricted water movement of the shallow water cover over the extremely broad (tens- to hundreds-of-miles wide) Z-zone coupled with evapoconcentration of ions, and possible formation of Ca-minerals was thought to have caused direct precipitation of dolomite (Irwin, 1965).

However, if as Textoris (1969) remarked, the moon was closer to the earth in the Early Palaeozoic, greater tidal activity should have prevailed in seas at that time. Even when uniformitarian concepts are used, Klein and Ryer (1978) suggested that ancient epeiric seas should have been tide dominated, since broad continental shelves of modern shallow seas are associated with tides of high amplitude, greatest tidal ranges and greatest tidal current velocities. They considered that astronomical forces that operate today were also operative in the past and that modern shallow seas such as the East China and Yellow Seas, the Arafura Sea, the Java Sea, and Hudsons Bay could serve as guides to ancient epeiric seas. The locations of these shallow seas may not be comparable to the latitude of the Valley and Ridge Province in the Early Ordovician epeiric seas. However, using these shallow seas as guides, it appears that a shallow water cover on a broad shelf, such as the Z-zone of Irwin (1965), could not be tideless. Also the fine-grained dolostones in the Copper Ridge district have

evidence of mudcracks (indicative of subaerial exposure) as well as wavy laminae documenting that the dolostones resulted from replacement but not from direct precipitation. Thus, the need for a relatively permanent water cover in the Z-zone of the epeiric sea model leading to direct precipitation of dolomite does not become apparent in the case of the Copper Ridge district. On the other hand, the regional extent and imperceptible slope of the epeiric sea model is attractive. As indicated in the fence diagram (Fig. 4-17, p. 109) a shallow and broad normal marine environment with islands, and an adjacent extensively broad tidal flat environment was the depositional setting in the Copper Ridge district. An extensively broad intertidal zone (probably broader than that conceived by Irwin (1965) probably was a result of the imperceptible slope of the terrain and the greater tidal activity associated with such broad shelves.

The supratidal environment was probably occasionally flooded by marine water driven by strong winds and hurricanes. Hurricanes have the potential of depositing lime mud on supratidal flats (Ball et al., 1967; Perkins and Enos, 1968). In southern Florida, Ball et al. (1968) estimated that about 160 hurricanes occur in 1000 years. From a study of hurricane Donna, Ball et al. (1968) noted that lime mud picked up from marine environments was suspended in stormy water. As the storm ebbed, the suspension was deposited as a continuous soupy mud on supratidal flats. Furthermore, they showed photographs of slabs of laminated supratidal sediments of the recent hurricane deposits from Crane Key, Florida, that compared with the San Andres dolomite and the

Ordovician El Paso limestone. Probably the fine-grained dolostones in the Copper Ridge district represent lime muds that were deposited in peritidal environments due to normal tidal activities and occasional storm and hurricane activities.

Chemical evidence and textural data suggest that the coarser than fine-grained dolostones were probably formed by mixing of fresh and marine water. Probably fresh water lenses were entrapped on certain parts of the peritidal environment including the islands. Mixing of such fresh water and marine pore water has the potential of resulting in dolomitization or increased porosity depending on the proportion of the mixture (see Chapter II).

A low Sr/Ca ratio and low Na content were obtained from the fine-grained dolostones of the Copper Ridge district. This suggests that they were formed in the presence of fresh water. On the other hand, the palaeolatitude coupled with the sedimentologic setting as well as the paucity of marine fauna in the fine-grained dolostones suggest that the environment of deposition of the precursor lime muds ought to have been hypersaline. The explanation for the formation of the fine-grained dolomite crystals for many of the Holocene peritidal occurrences include the following: Evaporation of pore waters leads to concentration of ions (e.g., Shinn et al., 1965). Ground waters ascend to replace loss by evaporation (e.g., Hsü and Schneider, 1973). Gypsum and calcium carbonates (aragonite, high Mg-calcite) precipitate (e.g., Illing et al., 1965) leading to a high Mg/Ca ratio of solution and the formation of protodolomites that have grain sizes of 1-5 microns

(e.g., Shinn et al., 1965). However, the fine-grained dolomites in Copper Ridge district are an order of magnitude coarser. Also, there are lines of evidence suggestive of both hypersaline conditions and the presence of fresh water. Probably dilution of hypersaline water by fresh water results in the production of fine-grained dolomite crystals (whereas, dilution of normal marine water with fresh water results in coarser-grained dolomite crystals—Land, 1973). The only modern analog where it was suggested that tidal flat dolomites formed from mixing of fresh and hypersaline waters was given by Gebelein (1977, 1979). He reported that tidal flat sediments of west and southwest Andros, Bahamas, had higher concentrations of protodolomites to those portions which were flushed by fresh water. Based on measurements of salinities, he found that small ridges (up to 2 meters above mean tide level) trapped fresh water lenses. Alternatively, very fine-grained dolomites could have formed as explained in the case of many Holocene analogs; and they coarsened to fine-grained dolostones in the presence of fresh water. This interpretation is slightly at variance with the schizohaline mixing model (Folk and Siedlecka, 1974) in that the fine-grained dolostones themselves appear to have formed in the presence of fresh water. Folk and Siedlecka (1974) suggested that fine-grained dolostones result from hypersaline conditions in environments of fluctuating hypersaline to fresh water conditions.

VI. SUMMARY AND CONCLUSIONS

In summary, the carbonate lithologies at Copper district allow the following observations and conclusions.

(a) The fine-grained dolomites have a Ca/Mg weight % ratio much closer to an ideal ordered dolomite than the coarser than fine-grained dolomites do.

(b) The fine-grained dolomites are generally unzoned and have anhedral shapes. In contrast, the dolomites of CFd are zoned and can be subhedral to anhedral. The zoning in CFd is generally cloudy centered and clearer rimmed, when stained with acidified potassium ferricyanide solution, in many instances the rims of the crystals are stained blue. Under the Luminoscope more growth zones are observed. Bright luminescence corresponds to a higher Mn/Fe ratio.

(c) Chemical data and textural evidences suggest that the neomorphism of the limestones and the formation of the coarser than fine-grained dolomite crystals was probably due to mixing of fresh and normal marine water. Chemical data obtained from the fine-grained dolostones suggests that fine-grained dolostones formed either due to dilution of hypersaline pore water with fresh water or very fine-grained crystals initiated in hypersaline environments coarsened to fine-grained sizes in the presence of fresh water.

(d) The fence diagram shows that the Kingsport Formation formed in a normal marine environment dotted with islands, and that the Mascot Formation formed in an adjacent peritidal environment.

CHAPTER V

SPHALERITE MINERALIZATION IN THE COPPER RIDGE DISTRICT

I. INTRODUCTION

The Copper Ridge zinc district of East Tennessee occurs in the Copper Creek thrust-fault block of the Valley and Ridge province of the Appalachian physiographic division. Ore-grade mineralization occurs in brecciated zones, but it is stratabound, because it is found over a limited stratigraphic interval, straddling the contact of the Mascot and Kingsport Formations (Hill, 1969, 1971; Maher, 1971). The occurrence of laminated sediments with detrital sphalerite between breccia fragments in which the laminae are parallel to the bedding of the country rock showed that the mineralization occurred prior to Appalachian tectonic activity (Kendall, 1960, 1961).

The host carbonate rocks consist of dolostones and limestones of the Mascot and Kingsport formations. The dolostones are subdivided into fine-grained and coarser than fine-grained varieties. Some features suggest that the fine-grained dolostones are of the type that have been reported from Holocene peritidal environments (e.g., Shinn et al., 1965; Illing et al., 1965). These criteria include: presence of mudcracks, birdseyes, planar to wavy cryptalgal laminae, indirect evidence of the former presence of gypsum, rarity of fauna, and the fine-grained nature of the constituent dolomite crystals (see Chapter IV for detail). In contrast, the coarser than fine-grained

dolostones are characterized by concentrically zoned (luminescent zones), poikilotopic dolomite crystals, and often preserve ghost features of fossil fragments suggestive of their formation from dolomitization of subtidal to intertidal limestones. Textural relationships and chemical evidence such as low Sr/Ca ratios and low Na contents as well as correlation patterns of some trace elements suggest that the coarser than fine-grained dolostones (CFd) formed in the presence of a mixture of fresh and marine water. The preserved limestones are interpreted to be subtidal to intertidal in origin (see Chapter IV for detail).

Breccia bodies associated with ore-grade mineralization often occur in dolostones overlying limestones. In the opinion of many geologists (e.g., Wedow and Marie, 1965; Wedow, 1971, Hoagland et al., 1965; Hill, 1969; Harris, 1971; Laurence, 1971; Maher, 1971), the brecciation is believed to be a consequence of the action of meteoric waters that descended from the post-Knox erosional surface. These meteoric waters are thought to have been responsible for the dissolution of limestones and foundering of the overlying dolostones. In some instances, such foundering is thought to be vertically extensive, and its effect propagated as crackle breccia in overlying thicker sequences of fine-grained dolostones (e.g., Harris, 1969). The action of meteoric solutions was also used to explain the thinning of limestones and thickening of dolostones towards mineralized horizons (e.g., Wedow and Marie, 1965; Wedow, 1971; Harris, 1969). However, in Chapter IV, it was proposed that this phenomenon could be due to the depositional setting in which the thicker portions of the dolostones represent

centers of islands. Furthermore, as there is evidence of several emergence episodes in the Upper Knox, some of the units could have been brecciated prior to the post-Knox erosional period.

This chapter deals with the description and interpretation of the mode of occurrence of sphalerite observed during this study. The mineralogy of the ore deposits is simple, but the detailed relationships of the minerals are complex. The ore textures suggest more than one episode of mineralization. But, this may also be due to fluctuations in the geochemistry of an ore-solution. Probably the ore-solution was initially acidic. Among other reasons, this is suggested by the presence of primary marcasite. According to Ramdohr (1969) the presence of marcasite would also indicate that the ore deposition associated with marcasite occurred at shallow depth.

II. ORE TEXTURES AND CHARACTERISTICS OF SULFIDES AND DOLOMITE

The paragenetic sequence of minerals observed from the Flat Gap mine, Copper Ridge district, as given by Hill (1969) is: brown sphalerite → galena → yellow sphalerite → marcasite → pyrite → dolomite → barite → fluorite → calcite → quartz → anyhydrite and gypsum. Some of the above minerals were not present in the samples collected during this study, hence a complete verification of the paragenetic sequence given by Hill (1969) was not possible. The textural relationships that will be discussed below are for iron and zinc sulfides and dolomite.

Iron Sulfides

Both coarse and fine crystals of pyrite and marcasite occur in association with sphalerite (Fig. 5-1). The surfaces of the pyrite crystals, particularly the coarser ones, are not smoth throughout. In some crystals irregular surfaces alternate with smooth surfaces, giving a banded appearance. In other cases, the irregular surfaces occur in the central portions of crystals, and thus pyrite appears zoned (Fig. 5-2). The reasons for this textural appearance is not clear. However, it appears to be unlikely that these textural variations are due to detectable variations in Ni or Co content, as electron microprobe analyses for these elements show that they are below detection limits (< 0.05 wt. %).

Pyrite and marcasite do not always have a common boundary. Textural relationships do not suggest replacement of pyrite by marcasite. Actually, in some instances where pyrite and marcasite have common boundaries, marcasite occurs towards the center of the grains (Fig. 5-3).

The relationships of the iron sulfides to dolomite and sphalerite are complex. Some of the iron sulfides occur near the boundary of a fine-grained dolostone breccia fragment and vug-fill dolomite (Fig. 5-4). They also appear to have formed after the brecciation of the vug-fill dolomite itself (Fig. 5-5). Some pyrite crystals formed in fractures of sphalerite (Fig. 5-6). In many instances, iron sulfides occur near the boundary between sphalerite and vug-fill dolomite, where they tend to be engulfed by the sphalerite (Fig. 5-7). Some textures also indicate that vug-fill dolomite has replaced pyrite. Thus, an

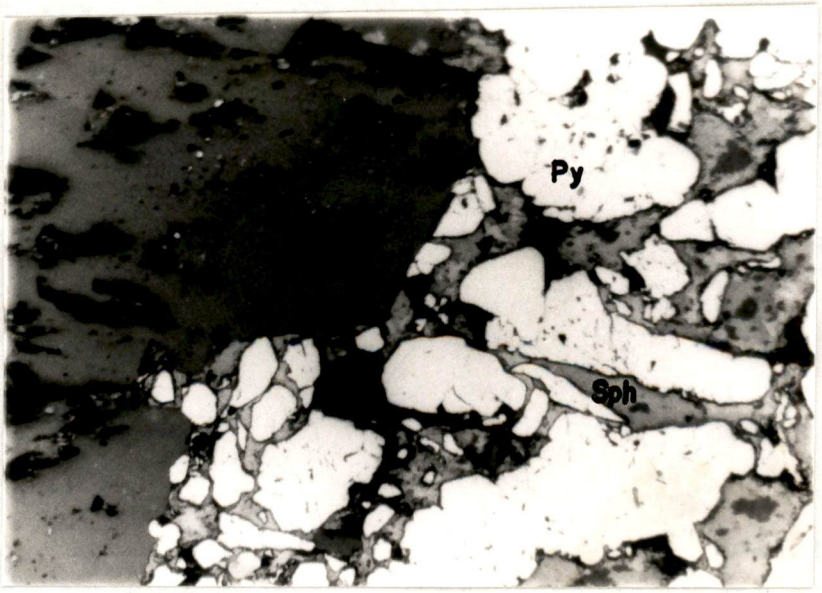

10 μm

Figure 5-1. Photomicrograph (plane-polarized reflected light) showing sphalerite (Sph) replacing pyrite (Py). Part of the pyrite has irregular surfaces (Sample ID-19).

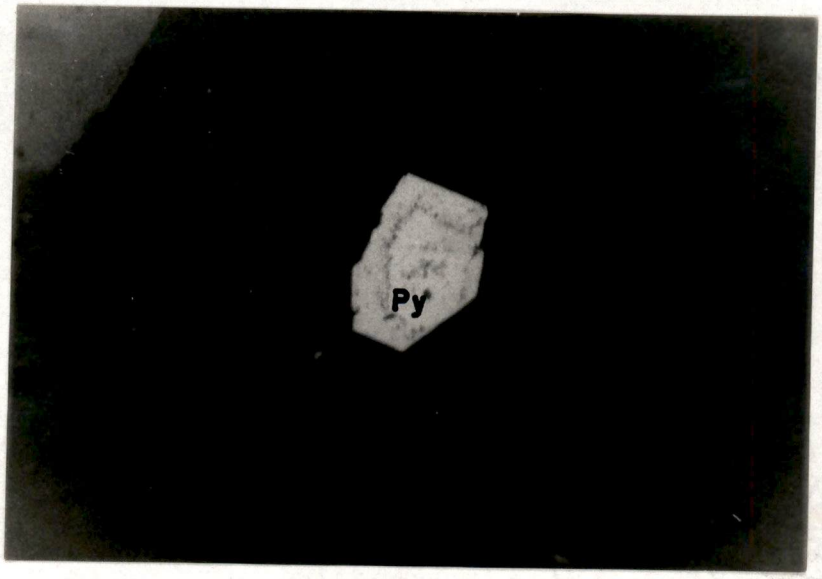

10 μm

Figure 5-2. Photomicrograph (plane-polarized reflected light) of a zoned pyrite (Sample Idol-51).

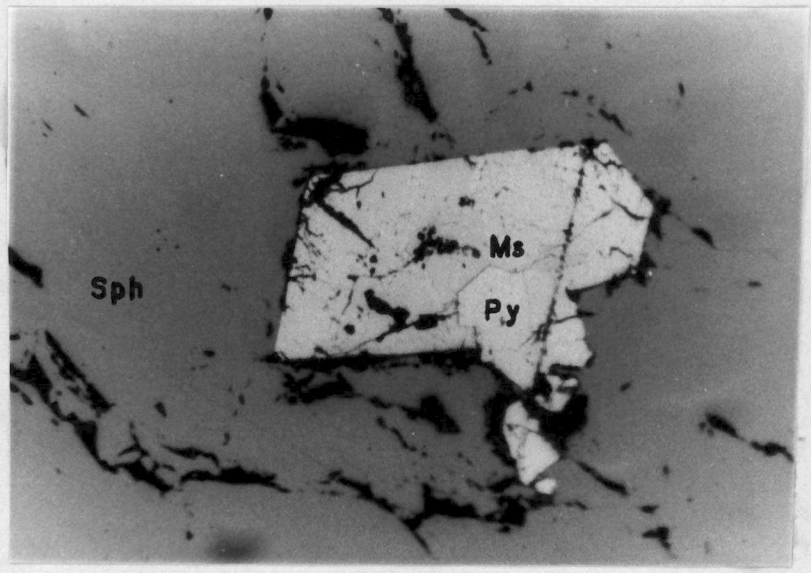

10 μm

Figure 5-3. Photomicrograph (plane-polarized reflected light) showing pyrite (Py) and marasite (Ms) relationships (Sample Ido1-51).

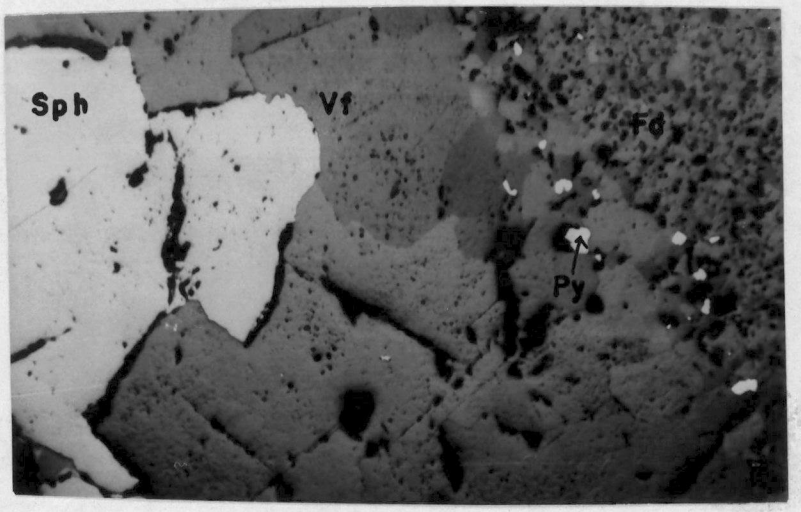

100 μm

Figure 5-4. Photomicrograph (plane-polarized reflected light) showing iron sulfides (Py) occurring near the boundary of fine-grained dolomite fragment (Fd) and vug-fill dolomite (V_S) (Sample Tandy Dalton-1).



100 mm

Figure 5-5. Photomicrograph (plane-polarized reflected light) showing that iron sulfide (Py) formed after brecciation of vug-fill dolomite (Sph) (Sample Idol-11).

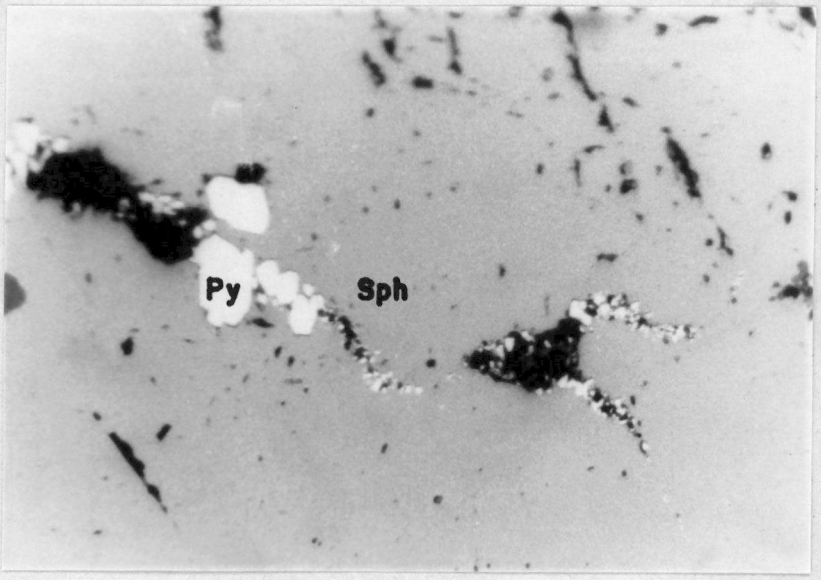

10 μm

Figure 5-6. Photomicrograph (plane-polarized reflected light) showing pyrite (Py) occurring in fractures of sphalerite (Sph) (Sample Shiloh-52).

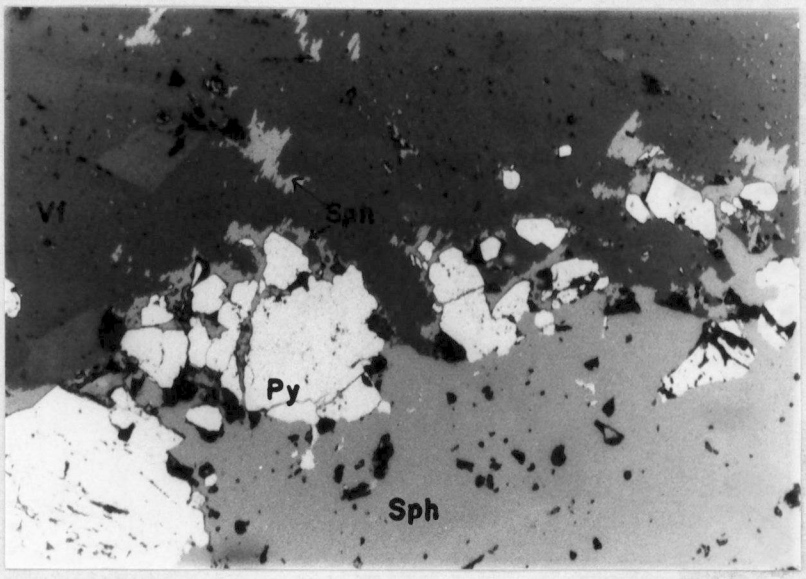

10 μm

Figure 5-7. Photomicrograph (plane-polarized reflected light) showing iron sulfides (Py) engulfed by sphalerite (Sph) (Sample Idol-19).

interchanging paragenetic sequence between vug-fill dolomite and iron sulfides is common and probably indicates that the geochemistry of the ore solution fluctuated.

Sphalerite

The sphalerite observed during this study is predominantly of the yellow variety, although black sphalerite occurs in some rosettes, and as patches. The Fe and Cd contents of sphalerite are quite variable. On the average, Fe is less than 0.5 wt. %; and Cd contents are about 0.15 wt. %, although in some spots Cd reaches up to 3 wt. %. The Cu content is below detection limit of the electron microprobe. The circular black bands in sphalerite rosettes do not show any distinctive features in reflected plane-polarized light, but under crossed nicols they may appear dark and with no internal reflection. These bands are not associated with higher Fe content, but sometimes they are associated with higher Cd content.

The relationships between sphalerite and dolomite crystals are complex. Dolomite crystals are of a variety of origins. Some of them form dolostones, and others occur in vugs, fractures and between breccia fragments of dolostones. The latter could be of detrital origin or of nondetrital origin. Those of detrital origin are often unstratified and are called fine-rock matrix and coarse-rock matrix (Hill, 1969; Hill et al., 1971). Rarely there are laminated internal sediments (Kendall, 1960, 1961). The dolomite crystals of nondetrital origin are very coarse-grained, mostly white and sometimes pink crystals, and are variously called gangue dolomite, sparry dolomite,

recrystalline, or vug-fill dolomite. In the present study, the author refers to them as vug-fill dolomite. As suggested by Hill (1969), the vug-fill dolomite is younger than the detrital matrix fracture fills.

Relationships between sphalerite and dolostones. Commonly a rind of dolomite crystals separates sphalerite crystals from breccia fragments of fine-grained dolostones (Fig. 5-4, p. 123). In some instances, sphalerite occurs in direct contact with fine-grained dolostone fragments. In the latter case, sphalerite has a replacive-boundary relationship. In some cases, sphalerite crystals may occur dispersed in coarser than fine-grained dolostones. However, sphalerite predominantly has a replacive-boundary relationship with the dolomite crystals.

Relationships between sphalerite and detrital matrix. Sphalerite may occur in alternate laminae of internal sediments (Fig. 5-8). Such sphalerite crystals were interpreted by Kendall (1960, 1961) to be of detrital origin. Often vug-fill dolomite occurs between sphalerite and dolomite crystals of the unstratified detrital matrix. In those cases where sphalerite occurs in direct contact with the dolomite crystals of the detrital matrix it predominantly has a replacive relationship.

Relationships between sphalerite and vug-fill dolomite. Vug-fill dolomite and sphalerite crystals often show replacive-boundary relationships (Fig. 5-9). According to Bernard and Samama (1967), such textures are indicative of the diagenetic growth of sphalerite. Some



100 μm

Figure 5-8. Photomicrograph (plane-polarized reflected light) showing sphalerite crystals (Sph) occurring in alternate laminae of internal sediments (Sample Idol-1).

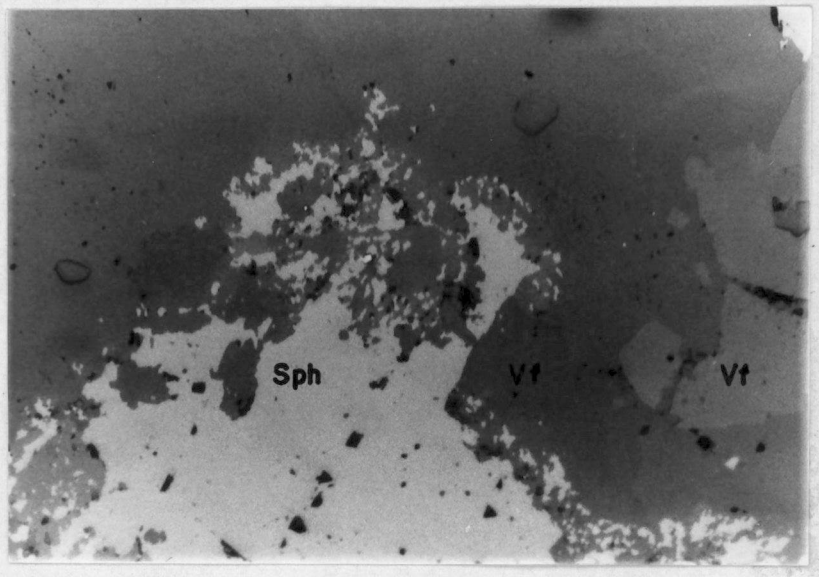

10 μm

Figure 5-9. Photomicrograph (plane-polarized reflected light) showing sphalerite (Sph) replacing vug-fill dolomite (Vf) (Sample Joe Mill-60).

of this replacive-type sphalerite appears to have been re-replaced by dolomite (Fig. 5-10). This texture suggests that zinc was remobilized. In other instances, sharp boundaries between sphalerite and dolomite are observed (Fig. 5-11). Such textures are indicative of equilibrium conditions (Anderson, 1975; Kyle, 1976), and the possible cogenesis of the two phases. However, sharp boundaries on one side and replacive relationships on the other side of the same dolomite crystal are not uncommon (Fig. 5-12). This texture probably suggests that the geochemistry of the ore-forming solution had fluctuated from one in which sphalerite and vug-fill dolomite were supersaturated to another in which dolomite was not supersaturated.

Relationships between sphalerite and iron sulfides. Photomicrographs showing relationships between sphalerite and iron sulfides was given earlier (Figs. 5-1, 5-6, 5-7, pp. 122, 124, 125). In many instances, where iron sulfides and sphalerite have common boundaries, the iron sulfides occur in that zone where sphalerite has not completely replaced vug-fill dolomite (Fig. 5-6, p. 124).

Vug-Fill Dolomite

By far the most common mineral associated with sphalerite is vug-fill dolomite. Under transmitted-light microscope some arcuate cleavages are observed in the dolomite crystals. Also, the dolomite crystals display wavy extinction and resemble the baroque-type dolomite described by Folk and Assareto (1974) as suggestive of a sulfate-rich environment of formation. Under the Luminoscope they may

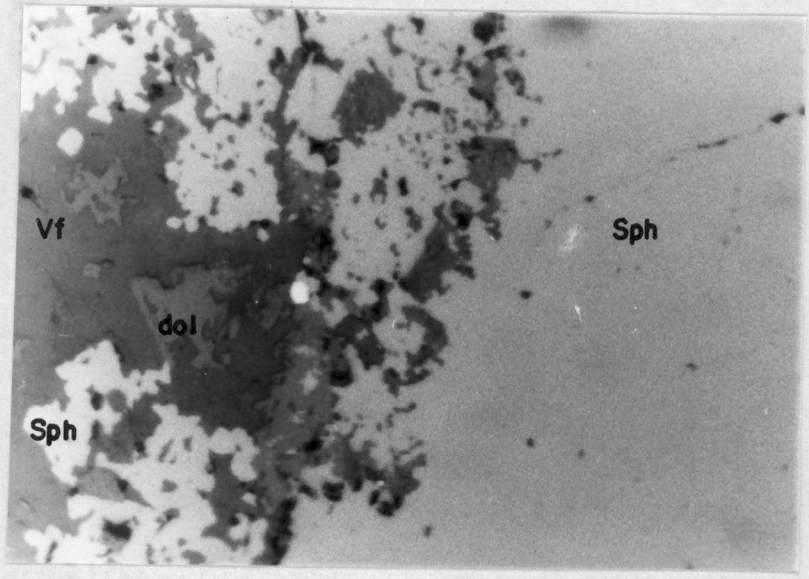

10 μm

Figure 5-10. Photomicrograph (plane-polarized reflected light) showing dolomite (Vf) replacing sphalerite (Sph) (Sample Joe Mill-50).

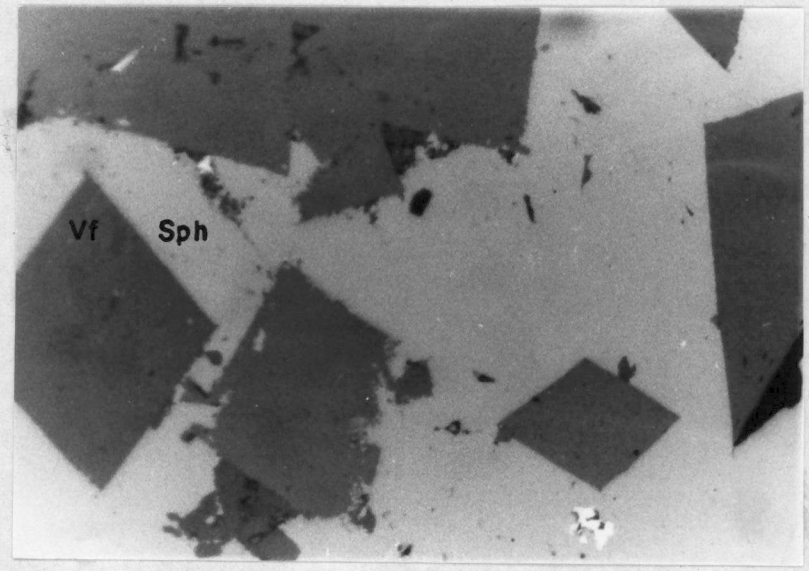

10 μm

Figure 5-11. Photomicrograph (plane-polarized reflected light) showing sharp boundaries between sphalerite (Sph) and vug-fill dolomite (Vf) (Sample Idol-51).

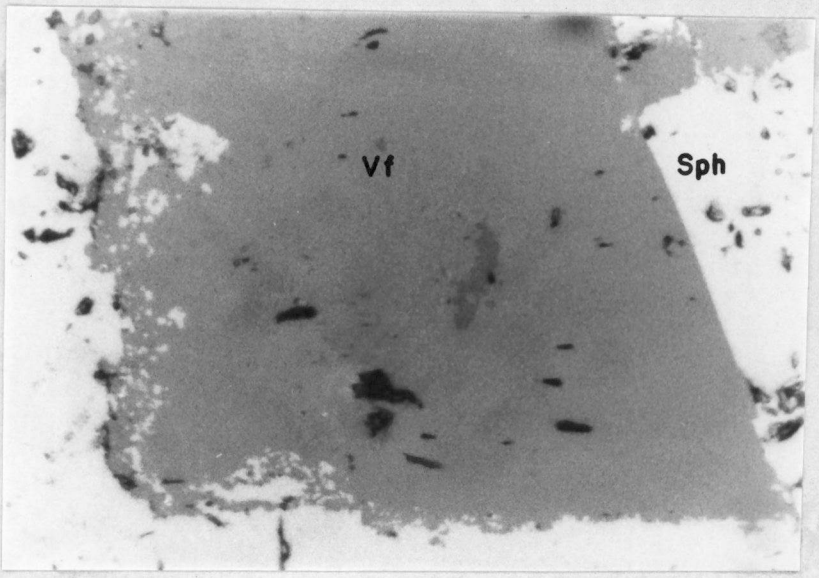

10 μm

Figure 5-12. Photomicrograph (plane-polarized reflected light) showing sharp and replacive boundary relationships between sphalerite (Sph) and vug-fill dolomite (Vf) rhomb (Sample Joe Mill-50).

display several luminescent bands of shades of red. Ebers (1976) and Ebers and Kopp (1979) observed similar patterns in the gangue dolomites of the Mascot-Jefferson City zinc mines. These features are also seen in vug-fill dolomites, such as in the River Ridge dolostones, with which sphalerite was not observed. Study of vug-fill dolomites using the Luminoscope also shows that some of them formed after the brecciation of previous vug-fill dolomites. Both generations of dolomite show growth zones related to compositional variation in Mn/Fe ratios, with low values corresponding to the darker zones. Study of luminescent patterns confirms observations in the field that calcite is the latest vug-fill mineral.

Paragenesis

The textural relationships suggest at least two stages of sphalerite mineralization: a stage where vug-fill dolomite and sphalerite were in equilibrium with one another, and another where vug-fill dolomite was replaced by sphalerite. A probable paragenetic sequence of the phases described above is depicted below.

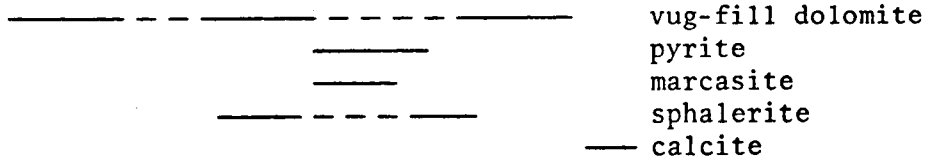

The occurrence of at least two stages of mineralization may also be inferred from field observations which show that some sphalerite ore is brecciated prior to the deposition of later ore (e.g., Hoagland, 1976).

III. FIELD OCCURRENCES OF SPHALERITE

Field and petrographic relationships were studied from the Joe Mill Creek-Rucker Branch section, the Tandy Dalton prospect, the Shiloh prospect, and a few stops at Idol mine (Fig. 2-1, p. 20). In each case, the mineralization occurs in the Upper Knox carbonate rocks of Copper Creek fault block, localized in various types of breccia. The nomenclature of breccia types described by Hill (1969) is used in the following description of mineral occurrences.

Idol Mine

The author had the opportunity to visit the Idol mine and collect samples from a few stops. The mineralization occurs in the upper part of the Kingsport and the lower Mascot formations.

Some striking features were observed in the mine walls and pillars. For example, breccia fragments appear to be "floating" in a matrix of vug-fill dolomite. This implies that some breccia structure is not fragment supported, unless the vug-fill dolomites are of various generations and the early generation vug-fill dolomites along with the fragments of the country rock are rebrecciated. The author suggests that such rubble breccia structure is an evidence of more than one generation of vug-fill dolomite crystals. Some specimens collected from about six meters above the Mascot-Kingsport contact show that sphalerite grows directly from a fine-grained dolostone breccia fragment without a rind of vug-fill dolomite between sphalerite and the breccia fragment. This indicates either that sphalerite replaced

an early generation of vug-fill dolomite which surrounded the fine-grained dolostone fragment, or that ore solutions caused the brecciation of the country rock. From a hand specimen (e.g., Sample 14), the observed paragenetic sequence of minerals is sphalerite → white dolomite → pink dolomite → calcite.

One of the striking features of sphalerite at Idol mine is the occurrence of rosette textures marked by circular black bands often near the edges of crystals. As discussed in the previous section the cause of the black bands is not known. The significance of the rosette textures is not clear either. Perhaps they are a variety of colloform texture and suggestive of faster rates of growth (e.g., Anderson, 1975).

Joe Mill Creek-Rucker Branch Section

The Joe Mill Creek-Rucker Branch exposure is very close to Idol mine. Sphalerite exposures were observed at the Joe Mill prospect at the top of the Kingsport formation, and in some horizons of the Mascot Formation.

The mineralization at the top of the Kingsport occurs at two prospect sites on both sides of the Joe Mill Creek. The mineralization at the prospect near a dirt road occurs in fractures of dolostones (both the fine-grained and the coarser than fine-grained varieties). Some of the coarser than fine-grained dolostones are laterally traceable to limestones. Even in close proximity to the dolostones, these subtidal limestones are barren of sphalerite.

In the other prospect site, sphalerite occurs in the fractures of crackle-brecciated fine-grained dolostones. Between the fractures of bigger breccia fragments, smaller-sized (about 1 mm) fragments of fine-grained dolostone occur in a matrix of brownish gray coarse-grained dolomite crystals. This matrix is fractured and infilled by white gangue dolomite and minor sphalerite.

Brecciated zones also occur towards the middle of the Kingsport, but no mineralization was observed in them.

Several crackle-breccia zones exposed on a roadside adjacent to Rucker Branch are in the Mascot Formation. However, intervening strata are not brecciated. Some of the crackle-brecciated zones are mineralized, and sphalerite was observed up to 133 meters above the Mascot-Kingsport contact. Although coarse-grained dolomite also occurs in nodules of the fine-grained dolostones, sphalerite is associated only with fracture-fill dolomite crystals.

Tandy Dalton Prospect

According to Secrist (1924), the mineralization in this prospect occurs about 207 meters below the post-Knox unconformity. The prospect is plotted on the wrong hill in the 7-1/2-minute geologic quadrangle map of the area. The prospect is located on the north side of a little hill, southeast of Cedar Springs Creek, 0.35 miles from Cedar Springs Baptist Church. The lithologies at the site of the prospect are covered. Judging from the incomplete exposure of the Upper Knox rocks on the side of a nearby dirt road, the mineralization appears to be at the bottom of the Mascot Formation. On the side of this road, which is

on the northeast side of Cedar Springs Creek, the bottom of the Mascot is also brecciated and the breccia fragments cemented by vug-fill dolomite and calcite, but no mineralization was observed. The beds immediately below this zone are not brecciated. At the site of the prospect, sphalerite was observed in blocks of rubble-breccia from the prospect dump. From hand specimens sphalerite and vug-fill dolomite appear contemporaneous, whereas calcite is the latest vug-fill.

Shiloh Prospect

Mineralized hybrid breccia is well exposed in the walls of the Shiloh prospect, and is stratigraphically at the top of the Kingsport Formation. The hybrid breccia consists of detrital matrix breccia (fine-rock matrix, and coarse-rock matrix breccia) and precipitate- or replacive-matrix of white gangue dolomite and sphalerite. The breccia fragments consist mostly of fine-grained dolostone and are of various sizes, some chert and greenish shale. The breccia is transected by a fault that dips to the north at 65°. The beds above the breccia zone are not well exposed, and it is not possible to determine how far up section the brecciation extends. The brecciated and mineralized horizon is laterally traceable to limestone that is exposed at the closely adjacent Bird Creek. The limestone is of subtidal to intertidal origin and has abundant criss-crossing stylolites marked by greenish residue.

IV. COMPARISON OF MINERALIZED AND BARREN SECTIONS

The field relationships discussed above confirm previous suggestions that the occurrence of sphalerite in the Copper Ridge district is epigenetic (e.g., Hill, 1969; Maher, 1971). Even in those localities that occur far removed from reported mineralized sections, such as at River Ridge, some sphalerite is observed (e.g., samples 45, 53A, 59B, 83—Appendix G). These sphalerite crystals are very few and fine-grained as observed in polished thin sections. Although not observed by this author, minor amounts of sphalerite were also reported from the otherwise barren Lee Valley section (Rodgers and Kent, 1948).

Brecciation

A common explanation of brecciation in the Upper Knox carbonate rocks in East Tennessee is dissolution of underlying limestones causing foundering of overlying dolostones. The dissolution of the limestones was considered to be due to meteoric waters that descended from the erosional surface during the Knox Chickamauga time interval (e.g., Hoagland et al., 1965; Harris, 1971; Hill et al., 1971; Laurence, 1971; Wedow, 1971). Brecciation by action of meteoric waters that descended from the post-Knox unconformity is a well-documented occurrence, particularly in those cases where the brecciation can be traced to the erosional surface, such as in the sinkhole at Douglas Lake (Harris, 1969). It is also possible that such meteoric waters could have penetrated deeper as suggested by many geologists (see the references above). However, the author believes that brecciation could also have

developed during the deposition of the Upper Knox, and later enlarged by ore solutions. The reasons for this interpretation are given below.

In the essentially barren sections such as at Lee Valley and River Ridge, brecciated zones are rare. At the River Ridge section, Unit 83 of Harris (1969) is conspicuously brecciated, although it was not reported by him. The breccia consists of rotated and displayed angular fragments of fine-grained dolostone with a matrix of pink and white vug-fill dolomite crystals. The beds above and below this unit are not affected by the brecciation. As dissolution did not cause the overlying beds to founder, the brecciation probably predated their deposition. Since, the underlying beds are not affected, the brecciation postdated their deposition. Similarly, other units in the River Ridge section, which were brecciated on a very local scale, are synsedimentary to early diagenetic in origin.

The Joe Mill Creek-Rucker Branch section is not as well exposed as the River Ridge section, but it is better exposed than the other prospect localities. Several zones in this section are brecciated with unbrecciated intervening units, suggesting that the brecciation in each unit probably occurred prior to the deposition of immediately overlying beds. I interpret these breccia bodies as having developed during the deposition of the Upper Knox from activity of fresh water in subaerially exposed parts of the environmental complex. This is better appreciated from an inspection of facies relationships displayed in the fence diagram described in Chapter IV (Fig. 4-17, p. 110).

Facies Relationships

Since mineralization in this district occurs near the Mascot-Kingsport contact, the facies relationships near this boundary are more relevant to this chapter. The facies easily recognizable in this district are fine-grained dolostones, coarser than fine-grained dolostones and the limestones. The fine-grained dolostones represent supratidal to intettidal environments, and the corrser than fine-grained dolostones (CFd) and limestones represent subtidal to intertidal environments (see Chapter IV).

In the fence diagram (Fig. 4-17, p. 110) the Mascot formation is represented by fine-grained dolostones, on the top parts of the fence. In some localities the lower part of the Mascot is a record of peninsulas, or that of islands. Between the Thorn Hill and Treadway (Flat Gap) sections the Mascot-Kingsport contact is probably the base of an island. The rate of sedimentation exceeding the rate of basin subsidence may have caused the emergence of the island. Tidal and storm activities supplied lime muds and sustained the growth of the island. The lime muds were dolomitized penecontemporaneously with their deposition resulting in fine-grained dolostones. Differential rates of sedimentation between the island and the adjacent marine environment resulted in fine-grained dolostones being juxtaposed to limestones, some of which were later dolomitized to the CFd lithology.

Fresh water on such islands could cause brecciation. For example, vadose dissolution of sediments on Sabkha islands of the Trucial Coast, Persian Gulf, has been reported by Purser and Evans (1973).

Similarly, islands of the Kingsport could have been sites of brecciation. Possibly storm wash could have been introduced between breccia fragments, and their record could resemble some of the detrital breccia. More probably, the origin of the detrital-matrix breccia could have been the action of strong wind-driven currents that could deeply incise islands of low relief. Such deeply incised recent washover channels were reported from the barrier flats along the upper Texas coast (Morton, 1979). Fulweiler and McDougal (1971) reported the common occurrence of channel structures at the Jefferson City mine, about 50 kilometers southeast of the Copper Ridge district, and suggested the detrital-matrix deposits were of synsedimentary origin. They also noted that where mineralization was intense the channel outlines were obliterated by solution activity.

Other significant points can be made using the fence diagram. First, the Mascot-Kingsport contact as redefined by Harris (1969) is not a contemporaneous surface throughout East Tennessee. Thus, ore deposits in the lower Mascot Formation, for example at Idol mine, may not be at stratigraphically higher positions than those which occur in the top part of the Kingsport formation elsewhere. Second, and importantly, the two productive ore deposits in the Copper Ridge district, the Idol mine and Flat Gap mine, are located near the Joe Mill Creek-Rucker Branch and Treadway sections, respectively. These occurrences are near facies boundaries, between the record of an island, and adjacent shallow marine environments.

V. DISCUSSION ON THE GENESIS OF SPHALERITE DEPOSITS

The genesis of ore deposits involves the source of metals, mechanisms of dissolving the metals, mechanisms of transporting the ore solution to sites of localization, availability of sites of localization, and precipitation (Krauskopf, 1967; Stanton, 1972; Skinner and Barton, 1973). Study of the ore minerals and their relationships to others as well as the type of host rock helps to assess the genesis of ore deposits (Stanton, 1972). From the previous sections it is clear that sphalerite is associated with vug-fill dolomite and in dolostones, and that ore-grade mineralization is related to facies boundaries.

Relationships of Vug-Fill Dolomite and Sphalerite: Nature of Ore-Solution

Vug-fill dolomite crystals in the country rock, far removed from ore deposits and unassociated with sphalerite, have similar characteristics to those associated with sphalerite. This suggests that the composition of the ore solution was similar to formation waters, i.e., mixed fresh and marine waters.

Metals are hardly soluble in aqueous solutions, but substantial amounts of metals could be dissolved by forming complex-ion species (Barnes and Czamanske, 1967). The abundance of chloride ion in formation waters, and the dominance of sulfate over sulfide ions in fluid inclusions of sphalerite (Roedder, 1967, 1971, 1976), as well as analyses of solutions from environments in which sulfide precipitation occurs in the present day such as the central Mississippi region (Carpenter, 1974), the Salton Sea, and the Red Sea Deeps (White, 1968),

support Helgesen's (1964) suggestion that the metals are dissolved as chloride complexes in slightly acidic solutions. For temperatures and compositions obtained from fluid inclusion data, Anderson (1973, 1975) has shown stabilities of sulfide and carbonate minerals in f O_2-pH space which could help in deciphering textural relationships between sulfide and carbonate minerals.

According to Anderson (1973, 1975) equilibrium boundary relationships between sphalerite and dolomite are evidence that the mechanism of precipitation of sphalerite is addition of reduced sulfur to the ore solution. Before the introduction of reduced sulfur, the ore solution is considered to be acidic and therefore capable of increasing the porosity in the carbonate rocks into which it is introduced. This acidic condition may not continue for long, however, since the carbonate environment will buffer the solution. If reduced sulfur is introduced in sufficient amount, the ore solution can be highly oversaturated with respect to sphalerite and enhance faster growth of sphalerite. This condition will be evidenced by fine grain sizes, as well as dendritic and colloform textures. If the amount of introduced reduced sulfur is low, the oversaturation of the solution with respect to sphalerite may not be high and the consequent slower growth rate of sphalerite results in coarser crystals. Also, as may be seen from the following relationships

$$H_2S + 2O_2 \rightleftharpoons 2H^+ + SO_4^=$$

and

$$a_H^+ = 10^{-pH}$$

for the same Eh, if the amount of reduced sulfur is increased the pH of the solution will be decreased so that sphalerite can replace dolomite. On the other hand, if the amount of reduced sulfur is decreased, sphalerite can be replaced by dolomite. Thus, fluctuations in the amount of introduced reduced sulfur to an ore solution could result in the formation of several generations of sphalerite and dolomite crystals, as well as result in equilibrium and disequilibrium boundary relationships between sulfide and dolomite crystals. The textures between vug-fill dolomite and sulfide crystals, as described in a previous section, could have formed due to fluctuations in the amount of reduced sulfur introduced to an ore solution.

The above explanation does not rule out the possibility that some of the vug-fill dolomite crystals in contact with sphalerite formed from solutions other than the ore-forming solution. All it indicates is that disequilibrium boundary relationships do not necessarily imply that the phases formed from different solutions. With regard to this, because some coarser than fine-grained dolostones (CFd) have disseminated sphalerite crystals in some locations, it might be suggested that the CFd formed from ore-forming solutions (e.g., Hill, 1969; Hoagland, 1971). However, it must be cautioned that much as vug-fill calcites do not form limestones, so too vug-fill dolomites do not form dolostones; and relationships derived from vug-fill dolomite crystals may not be useful in deciphering the formation of dolostones. It is interesting to note that although the occurrence of sphalerite is

predominantly limited to dolostones, some sphalerite crystals replace limestones (Hoagland, 1976), for example in the Jefferson City mine. Also, in the Copper Ridge district the occurrence of sphalerite is limited to dolostones, but limestones occur in close proximity to mineralized dolostones (e.g., at the Shiloh and Joe Mill Creek prospects), whereas farther away from any reported occurrences of ore deposits the limestones are dolomitized to CFd (e.g., at the River Ridge section). These lines of evidence, together with those discussed in Chapters III and IV suggest that the CFd did not form from ore solutions.

Facies Relationships: Speculation on Sources of Metals

It is interesting to note that ore grade mineralization in the Copper Ridge district, like that of the southeast Missouri lead belt (Gerdmann and Myers, 1972) and the Pine Point district, Canada (Skoll, 1975) is related to facies boundaries. The facies boundaries in these districts are from sediments that formed in topographic highs and adjacent shallow marine environments. In the Copper Ridge district the topographic highs were sabkha islands, and in the other districts they were reef structures. The ore deposits in the three districts occur in breccias and in dolostones. Some interesting speculations can be derived from such relationships.

Speculation 1: Dolomitization related to source of metals

It is known that marine plants can concentrate base metal several fold with respect to their concentrations in marine water, e.g., Zn up

to 150 ppm, Cu up to 11 ppm, Pb up to 8 ppm (Trudinger, 1976). During dolomitization of algal-rich limestones metals may be released to the environment. Organic reduction of sulfate could produce H_2S so that sulfides could precipitate. Davis (1977) has elaborated on such a process and has proposed it to explain the mineralization in the Missouri Pb-Zn district.

In the Copper Ridge district, this could be the origin of some of the sphalerite, and could easily explain the minor occurrences of sphalerite in the country rock, but, it may not explain the ore grade mineralization because:

1. Algal-rich limestones were not reported from this district by previous workers nor observed during this study except for cryptalgal laminae preserved in the fine-grained dolostones.
2. Marine plants also concentrate Cu and Pb, but Cu minerals are absent in East Tennessee (Hoagland, 1976) or very rare (Wedow, 1979, personal communication), and Pb minerals are rare, although an early generation of mineralization at the Flat Gap mine had some galena (Hill, 1971b).
3. Fluid inclusion homogenization temperatures (Roedder, 1971) indicate higher temperatures than would be expected in normal diagenetic environments. To account for the higher temperatures of formation, Davis (1977) proposed that organic reduction of sulfate aided by bacterial activity is sufficiently exothermic to generate temperatures of the order of 100°C. However, it is not clear how such locally generated

temperatures could be uniformly sustained for the duration of time in which coarse sphalerite crystals formed.

Speculation 2: Introduction of heated solutions

Topographic highs afford catchment areas of fresh water. Fresh water could increase porosities in the vadose zone, and when mixed with marine water it could cause dolomitization depending upon the proportion of the mixture (Badiozamani, 1973; Land, 1973; see also Chapter II). In such depositional setting early diagenetic porosities could be enveloped in dolostones. Thus, the fact that ore deposits occur in breccias which are limited to dolostones may only be because the breccias are favorable sites for ore formation, and not because mineralization is related to dolomitization.

A necessary condition for ore deposition is the abundant availability of reduced sulfur. Anderson (1975) pointed out that thermal degradation of organic matter in carbonate rocks that may be brecciated by ore forming solutions is inadequate for the formation of ore deposits. The association of coarse-grained dolostones with sphalerite (e.g., in bedded ore occurrences) may be an evidence of coincidence of mineralization and dolomitization. Sufficient reduced sulfur may be generated in anoxic pockets in the shallow marine environment adjacent to the topographic highs. It may well be that ore-forming solutions from deeper basins (such as the site of the present Piedmont) rising due to temperature contrasts were localized in some breccias at the time of the diagenesis of the limestones.

VI. CONCLUSIONS

The ore deposits in the Copper Ridge district are related to facies boundaries. The facies resulted from sediments deposited on sabkha islands and adjacent shallow marine environments. The sabkha islands could have been sites for the formation of several of the breccia types described from this district. It appears that the breccia features associated with mineralization may not be the result of a mere coincidence of action of meteoric waters descending from the post-Knox errosional surface. The associations of sphalerite with coarse-grained dolostones, as well as the need for a sufficient amount of reduced sulfur to precipitate sulfides from ore-forming solutions is used to speculate that mineralization and dolomitization were coincidental without implying that the ore-forming solutions produced dolostones.

CHAPTER VI

SUMMARY AND CONCLUSIONS

Harris (1973) proposed that the Lower Ordovician dolostones formed subtidally, presumably due to refluxed brines. Several workers (e.g., Hill, 1969; West, 1974) suggested that the coarser-grained dolostones of the Upper Knox carbonate rocks in the Copper Ridge district formed from alteration of limestones by ore-forming solutions. Laboratory as well as field studies, conducted during the present investigation on the relationships of dolomitization to sphalerite mineralization, do not support those interpretations.

A portion of the research concerned the investigation of dolomitization processes. This included a critical review of the dolomitization models available in the literature and a theoretical treatment of dolomitization involving mixing of fresh and marine water. Some of the main points from this portion are as follows.

1. The seepage refluxion model involving downward movement of brines has no demonstrated modern analog. Laboratory demonstration and field measurements indicate that motion of saline water in an evaporative supratidal environment is directed upward to replace loss by evaporation.
2. Higher Mg/Ca ratio in solutions speed up reactions leading to the formation of dolomite.

3. Although marine water in equilibrium with dolomite is oversaturated with respect to dolomite, marine water in equilibrium with aragonite may be undersaturated with respect to dolomite.
4. As determined from a theoretical mixing model by the author, aragonite and calcite are undersaturated, and dolomite is supersaturated for 10-40 wt. % marine water in mixtures of fresh and marine waters; thus, dolomitization is feasible for this range of mixtures.

Another portion of the study dealt with the evaluation of trace element data obtained from Knox Group dolostones. The difficulty of precipitating dolomite in the laboratory under low temperature conditions does not allow experimental determination of partition coefficients of trace elements between dolomite and coeval solution. However, approximate partition coefficients were calculated. The ordering of trace elements according to their partition coefficients is similar to those for calcite, and in decreasing order, is Pb, Mn, Cd, Fe, Zn, Cu, Sr, Ba, and Ni. This ordering was used to assess the types of solutions from which dolomite crystals formed.

A major portion of the research was devoted to studying the Upper Knox lithologies. Sections were measured at the Shiloh, Joe Mill Creek and River Ridge localities. Samples were collected from these localities as well as from the Lee Valley exposure, Tandy Dalton prospect and Idol mine. The following are summaries based on field and laboratory investigations.

Limestones are quantitatively rare, and they occur only in the Kingsport Formation. They consist of interlaminated biointrapelsparitic grainstones/wackestones and biomicritic wackestones with some grapestones and rarely ooids. The recognized fossil fragments, in order of abundance, are trilobites, gastropods, ostracods, pelmatozoans, and sponges. Most of the allochems have micritic envelops due to fungal and/or algal microborings. The limestones were probably deposited in subtidal to intertidal environments but were neomorphosed in the presence of mixtures of fresh and marine water.

Dolostones are most abundant in the district. They were subdivided into two easily recognizable groups, each representing a different depositional facies. The distinguishing characteristics of the two groups is given in Table 4-3, p. 72.

The features in Table 4-3 suggest that the fine-grained dolostones formed in supratidal to intertidal environments, and the low Na and Sr contents suggest that their formation also involved presence of fresh water. The CFd dolostones probably formed from dolomitization of subtidal to intertidal limestones due to mixing of fresh and marine water. This interpretation was also corroborated by the correlation matrices of trace elements (Zn, Fe, Cd, Sr). In terms of depositional facies, although the CFd did not form subtidally, the precursor limestones probably did, and the CFd are equivalent to the preserved limestone facies.

Sections measured during this study in conjunction with those reported by Harris (1969) were used to construct a fence diagram that

shows the temporal and spatial relationships of the lithologies. The following are conclusions based on lithologic interpretations and the fence diagram.

1. The Kingsport Formation represents a shallow marine environment dotted with sabkha islands.
2. Most of the Mascot represents a broad tidal fault environment.
3. Ore deposits in the Copper Ridge district occur at facies boundaries. The facies boundaries resulted from sediments deposited on islands and in adjacent shallow marine environments.

Dissolution of sediments on islands could have caused brecciation, and unidirectional wind-driven currents could have developed deeply-incised channels that might have been filled with sedimentary rubble. These synsedimentary features probably served to localize ore-grade mineralization.

Study of ore textures suggest that some of the vug-fill dolomite crystals and the associated sphalerite are cogenetic. This, in turn, indicates that the mechanism of precipitation of sphalerite was addition of reduced sulfur. Fluctuation in the amount of introduced sulfur to an ore solution causes disequilibrium and equilibrium grain-boundary relationships between dolomite and sphalerite. Thus, from a study of grain-boundary relationships it is difficult to determine whether some dolomite crystals formed from ore-forming or other solutions. However, in close proximity to mineralized breccias some limestone beds are not dolomitized, but farther away the same beds

are dolomitized. This indicates that dolomitization was not caused by ore-forming solutions. On the other hand, in bedded-ore deposits, dolomite crystals of CFd occur intimately associated with sphalerite. This gives a clue about the timing of mineralization. Based on facies relationships, and association of sphalerite with CFd in bedded-ore deposits, as well as the need for sufficient reduced sulfur it is speculated that the mineralization was probably earlier than the post-Knox unconformity.

Recommendations for Further Work

1. It appears that an analysis of the depositional environment of the host carbonates serves to delimit sites of ore deposition. Within the Copper Ridge district other localities could be investigated along similar lines. Even within the studied area more columnar sections could give more detailed information. From such detailed investigations it may even be possible to understand why some breccia bodies are practically barren of ore. Similar studies could be done for the Mascot-Jefferson City zinc district in order to further investigate the relationships of ore deposits to facies boundaries, and to establish the procedure as an ore-guide.

2. As is observed in some mine pillars at Idol mine, some dolostone breccia fragments do not seem to be touching each other. This suggests two stages of brecciation, the second being probably due to ore-forming solutions. It would be interesting to determine the trace element contents of the vug-fill dolomites between breccia fragments that are widely separated. Samples could be collected along traverses

between breccia fragments. This may give an idea about the trace element chemistry of the ore solution as well as indicate if the first generation precipitate matrix, which may be unrelated to ore solutions, can be distinguished based on trace element contents.

3. More chemical data such as oxygen and carbon isotope data from dolomites and calcite crystals should be obtained for further assessment of the origin of the dolostones.

4. Trace element values from dolostones could only be evaluated semi-quantitatively. More trace element data may be obtained from dolostones, in order to evaluate their origin using the ordering of partition coefficients of trace elements suggested in Chapter III.

BIBLIOGRAPHY

BIBLIOGRAPHY

Adams, J. E., and Rhodes, M. L., 1960, Dolomitization by seepage refluxtion: Bull. Am. Assoc. Petrol. Geol., v. 44, pp. 1912-1920.

Alberstadt, L. P., and Reesman, A. L., 1978, Significance of authigenic k-feldspar in Cambro-Ordovician Carbonate rocks of the proto-Atlantic shelf in North America: Additional comments regarding the southeastern United States: Jour. Sed. Pet., v. 48, pp. 679-683.

Alvarez, W., Engelder, T., and Geiser, P., 1978, Classification of solution cleavage in pelagic limestones: Geology, v. 6, pp. 263-266.

Anderson, G. M., 1973, The hydrothermal transport and deposition of galena and sphalerite near 100°C: Econ. Geol., v. 68, pp. 480-492.

Anderson, G. M., 1975, Precipitation of Mississippi Valley-type ores: Econ. Geol., v. 70, pp. 937-942.

Awramik, S. M., Margulis, L., and Barghoorn, E. S., 1976, Evolutionary processes in the formation of stromatolites: in Walter, M. R. (ed.),

Badiozamani, K., 1973, The dorag dolomitization model - application to the Middle Ordovician of Wisconsin: Jour. Sed. Pet., v. 43, pp. 965-984.

Badiozamani, K., Mackenzie, F. T., and Thorstenson, D. C., 1977, Experimental carbonate cementation: salinity, temperature and vadose-phreatic effects: Jour. Sed. Pet., v. 47, pp. 529-542.

Ball, M. M., Shinn, E. A., and Stockman, K. W., 1967, The geologic effects of hurricane Donna in South Florida: Jour. Geol., v. 75, pp. 583-597.

Barnes, H. L., and Czamanski, G. K., 1967, Solubilities and transport of ore minerals, in Barnes, H. L. (ed.), Geochemistry of hydrothermal ore deposits: New York, Rinehart and Winston, Inc., New York, pp. 334-381.

Barr, J. A., Goodnight, J. H., Sall, J. P., and Helwig, J. T., 1976, A user guide to SAS 76, SAS Institute Inc., North Carolina, 329p.

Barton, P. B., 1967, Possible role of organic matter in the precipitation of the Mississippi Valley ores: in Brown, J. S. (ed.), Genesis of stratiform galena-zinc-barite-fluorite deposits: Econ. Geol., Mono., 3, pp. 371-379.

Bathurst, R. G. C., 1975, Carbonate sedimentation and their diagenesis: Elsevier, New York, 2nd edition, 658p.

Beales, F. W., 1975, Precipitation mechanism for Mississippi Valley-type ore deposits: Econ. Geol., v. 70, pp. 943-948.

Behrens, S. W., and Land, L. S., 1972, Subtidal Holocene dolomite, Baffin Bay, Texas: Jour. Sed. Pet., v. 42, pp. 155-161.

Bernard, A. J., and Samama, J. C., 1976, Summary of the French school of studies of ores in sedimentary and associated volcanic rocks - Epegenesis versus syngenesis: in Wolf, K. H. (ed.), Handbook of strata-bound and stratiform ore deposits: Elsevier, New York, pp. 299-338.

Berner, R. A., 1971, Principles of chemical sedimentology, McGraw-Hill, New York, 240p.

Boyd, F. R., Finger, L. W., and Chayes, F., 1969, Computer reduction of electron probe data: Carnegie Inst. Wash. Yb., v. 67, pp. 210-215.

Bricker, O. P. (ed.), 1971, Carbonate cements, Johns Hopkins University studies in geology, No. 19: Johns Hopkins Press, Baltimore, 376p.

Bush, P., 1973, Some aspects of the diagenetic history of the sabkha in Abu Dhabi, Persian Gulf: in Purser, B. H. (ed.), The Persian Gulf, Springer-Verlag, New York, pp. 395-407.

Carpenter, A. B., 1974, Preliminary report on the origin and chemical evolution of lead- and zinc-rich oil field brines in central Mississippi: Econ. Geol., v. 69, pp. 1191-1206.

Chave, K. E., and Schamlz, R. F., 1966, Carbonate-sea water reaction: Geochim. Cosmochim. Acta., v. 30, pp. 1037-1048.

Churnet, H. G., and Misra, K. C., 1978, Implications of the sedimentary and diagenetic fabrics in the Lower Ordovician Upper Knox dolostones at River Ridge, East Tennessee: GSA abstracts with programs, southeastern section, v. 70, No. 4, p. 165.

Churnet, H. G., and Misra, K. C., 1979, Sphalerite mineralization in the Upper Knox carbonates, Copper Ridge district, East Tennessee: GSA abstracts with programs, southeastern section, v. 11, No. 4, p. 174.

Cobb, L. B., 1974, A study of the distribution of trace elements and cathodoluminescent zonation in mineral fracture fillings: Unpublished M.S. Thesis, Univ. of Tenn., Knoxville, 39p.

Crawford, J., and Hoagland, A. D., 1968, The Mascot-Jefferson City zinc district, Tennessee: in (Granton-Sales volume), Ore deposits of the United States: Am. Inst. Mining, Metal. Petrol. Engineers, New York, pp. 242-256.

Crocket, J. H., and Winchester, J. W., 1966, Coprecipitation of zinc with calcium carbonate: Geochim. Cosmochim. Acta, v. 30, pp. 1093-1100.

Curtis, R., Evans, G., Kinsman, D. J. J., and Shearman, D. J., 1963, Association of dolomite and anhydrite in recent sediments of the Persian Gulf: Nature, v. 197, pp. 679-680.

Davis, A. R., 1977, Principles of oceanography, 2nd ed., Addison-Wesley Pub. Co., pp. 167-172.

Davis, J. H., 1977, Genesis of South Missouri lead deposits: Econ. Geol., v. 72, pp. 443-450.

Deffeyes, K. S., Lucia, F. J., and Weyl, P. K., 1965, Dolomitization of recent and Plio-Pleistocene sediments by marine evaporite waters on Bonaire, Netherland Antilles: in Pray, L. C., and Murray, R. C. (ed.), Dolomitization and limestone diagenesis: a symposium - Soc. Econ. Paleontologists Mineral., Spec. Publ., v. 13, pp. 71-88.

Delgado, F., 1977, Primary textures in dolostones and recrystallized limestones: A technique for their microscopic study: Jour. Sed. Pet., pp. 1339-1342.

Dunham, R. J., 1962, Classification of carbonate rocks according to depositional texture: in Ham, W. E. (ed.), Classification of carbonate rocks: Am. Assoc. Petrol. Geologists, Tulsa, Okla., pp. 108-121.

Dunham, R. J., 1969a, Early vadose silt in Townsend Mound (reef), New Mexico: in Freidman, G. M. (ed.), Depositional environments in carbonate rocks: a symposium - Soc. Econ. Paleontologists Mineral., Spec. Publ., v. 14, pp. 139-181.

Dunham, R. J., 1969b, Vadose pisolite in the Capitain Reef (Permian), New Mexico and Texas: in Friedman, G. M. (ed.), Depositional environments in carbonate rocks: a symposium - Soc. Econ. Paleontologists Mineral., Spec. Publ., v. 14, pp. 182-191.

Ebers, M. L., 1967, A study of gangue dolomite mineralization in the Mascot-Jefferson City zinc district, using cathodoluminescence: Unpublished M.S. Thesis, Univ. of Tenn., Knoxville, 82p.

Ebers, M. L., and Kopp, O. C., 1979, Cathodoluminescent microstratigraphy in gangue dolomite, the Mascot-Jefferson City district, Tennessee: Econ. Geol., v. 74, pp. 908-918.

Eugster, H. P., and I-Ming, C., 1973, The depositional environment of Precambrian Banded Iron-Formations of the World: Econ. Geol., v. 68, pp. 1144-1168.

Evamy, B. D., 1963, The application of a chemical staining technique to a study of dolomitization: Sedimentology, v. 2, pp. 164-170.

Feazel, C. T., 1978, A phenomenon glows: Geotimes, v. 23, No. 7, pp. 16-17.

Folk, R. L., 1959, Practical petrographic classification of limestones: Bull. Am. Assoc. Petrol. Geologists, v. 43, pp. 1-38.

Folk, R. L., 1965, Some aspects of recrystallization in ancient limestones: in Pray, L. C., and Murray, R. C. (ed.), Dolomitization and limestone diagenesis: A symposium - Soc. Econ. Paleontologists Mineral., Spec. Publ., No. 13, pp. 14-48.

Folk, R. L., and Assererето, R., 1974, Giant aragonite rays and baroque white dolomite in tepee-fillings, Triassic of Lombardy, Italy (abs.): Am. Assoc. Petrol. Geologists, Soc. Econ. Paleontologists Mineral., Annual Mtg., Abstracts with programs, v. 1, pp. 34-35.

Folk, R. L., and Land, L. S., 1975, Mg/Ca ratio and salinity: Two controls over crystallization of dolomite: Am. Assoc. Petrol. Geologists, v. 59, pp. 60-68.

Folk, R. L., and Pittman, J. S., 1971, Length-slow Chalcedony: A new testament for vanished evaporites: Jour. Sed. Pet., v. 41, pp. 1045-1058.

Folk, R. L., and Siedlecka, A., 1974, The "schizohaline" environment: its sedimentary and diagenetic fabrics as exemplified by late paleozoic rocks of Bear Island, Svalbard: Sed. Geology, v. 11, pp. 1-15.

Freeman, T., 1971, Magnesium-rich water from evaporite-bearing shales, and diagenesis of subjacent carbonates-keuper-Muschelkalk, Iberian Range, Spain (abs.): Am. Assoc. Petrol. Geol. Bull., v. 55, pp. 338-339.

Friedman, G. M., 1965, Terminology of crystallization textures and fabrics in sedimentary rocks: Jour. Sed. Pet., v. 35, pp. 643-655.

Friedman, G. M., 1969, Trace elements as possible environmental indicators in carbonate sediments: in Friedman, G. M. (ed.), Depositional environments in carbonate rocks - Soc. Econ. Paleontologists Mineral., Spec. Publ., No. 14, pp. 193-198.

Friedman, G. M., and Sanders, J. E., 1967, Origin and occurrence of dolostones: in Chilingar, Bissell, and Fairbridge (ed.), Developments in sedimentology-carbonate rocks, Elsevier, New York, pp. 267-348.

Fyfe, W. S., Bischoff, J. L., 1965, The calcite-aragonite problem: in Pray, L. C., and Murray, R. C. (ed.), Dolomitization and limestone diagenesis: A symposium - Soc. Econ. Paleontologists Mineral., Spec. Publ., No. 13, pp. 3-13.

Garrels, R. M., and Christ, C. L., 1965, Solutions, minerals, and equilibria, Harper and Row Publ., New York, 450p.

Garrels, R. M., Perry, E. A., and Mackenzie, F. T., 1973, Genesis of Precambrian iron-formations and the development of atmospheric oxygen: Econ. Geol., v. 68, pp. 1173-1179.

Garrels, R. M., and Thompson, M. E., 1962, A chemical model for sea water at 25°C and one atmosphere total pressure: Am. Jour. Sci., v. 26, pp. 57-66.

Garrels, R. M., Thompson, M. E., and Siever, R., 1960, Stability of some carbonates at 25°C and one atmosphere total pressure: Am. Jour. Sci., pp. 402-418.

Garrels, R. M., Thompson, M. E., and Siever, R., 1961, Control of carbonate solubility by carbonate complexes: Am. Jour. Sci., pp. 24-45.

Gavish, E., and Friedman, G. M., 1969, Progressive diagenesis in Quaternary to Late Tertiary carbonate sediments: sequence and time scale: Jour. Sed. Pet., v. 39, pp. 980-1006.

Gebelein, C. D., 1969, Distribution, morphology, and acretion rate of recent subtidal algal stromatolites, Bermuda: Jour. Sed. Petrol., v. 39, pp. 49-69.

Gebelein, C. D., 1976, Open marine subtidal and intertidal stromatolites (Florida, The Bahamas and Bermuda): in Walter, M. R. (ed.), Stromatolites, Elsevier, New York, pp. 381-388.

Gebelein, C. D., 1977, Mixing-zone dolomitization of Holocene tidal-flat sediments, southwest Andros Island, Bahamas (abs.): Am. Assoc. Petrol. Geol. Bull., v. 61, No. 15, pp. 787-788.

Gebelien, C. D., 1979, Mixing zone dolomite in tidal flat sediments of central West Andros Island, Bahamas: (Abs.): Assoc. Am. Petrol. Geol. - Soc. Econ. Paleontologists Mineral. annual mtg., p. 93.

Gebelein, C. D., and Hoffman, P., 1973, Algal origin of dolomite laminations in stromatolitic limestones: Jour. Sed. Pet., v. 43, pp. 603-613.

Gerdmann, P. E., and Meyers, H. E., 1972, Relationships of carbonate facies patterns to ore distribution and to ore genesis in the southeast Missouri lead district: Econ. Geol., v. 67, pp. 426-433.

Ginsburg, R. N., and Hardie, L. A., 1975, Tidal and storm deposits, northwestern Andros Islands: in Ginsburg, R. N. (ed.), Tidal deposits, Springer Verlag, New York, pp. 201-208.

Goldsmith, J. R., 1953, A "simplexity principle" and its relation to "ease of crystallization": Jour. Geol., v. 61, pp. 439-451.

Golubic, S., 1976, Organisms that build stromatolites: in Walter, M. R. (ed.), Developments in sedimentology 20 - Stromatolites, Elsevier, New York, pp. 113-126.

Goodell, H. G., and Garman, R. K., 1969, Carbonate geochemistry of superior deep test well, Andros Island, Bahamas: Am. Assoc. Petrol. Geol. Bull., v. 53, pp. 513-536.

Hall, G. M., and Amick, H. C., 1934, The section on the west side of the Clinch mountain, Tennessee: Tenn. Acad. Sci. Jour., v. 9, pp. 157-168, 195-220.

Hanshaw, B. B., Back, W., and Deike, R. G., 1971, A geochemical hypothesis for dolomitization by ground water: Econ. Geol., v. 66, pp. 710-724.

Harris, L. D., 1969, Kingsport Formation and Mascot dolomite (Lower Ordovician) of East Tennessee: Tenn. Div. Geology, Rept. Invest. 23, pp. 1-39.

Harris, L. D., 1971, A Lower Paleozoic Paleoaquifer - the Kingsport Formation and Mascot dolomite of Tennessee and southwest Virginia: Econ. Geol., v. 66, pp. 735-743.

Harris, L. D., 1973, Dolomitization model for Upper Cambrian and Lower Ordovician carbonate rocks in the eastern United States: Jour. Research U.S. Geol. Survey, v. 1, pp. 63-78.

Helgeson, H. C., 1964, Complexing and hydrothermal ore deposition, Pergamon, New York.

Helgeson, H. C., 1967, Solution chemistry and metamorphism: in Abelson, P. H. (ed.), Researches in Geochemistry, v. 2: New York: John Wiley and Sons, pp. 362-404.

Helgeson, H. C., 1969, Thermodynamics of hydrothermal systems at elevated temperatures and pressures: Am. Jour. Sci., v. 267, pp. 729-804.

Hewett, D. F., 1928, Dolomitization and ore deposition: Econ. Geol., v. 23, pp. 821-863.

Hill, W. T., 1969, Mine geology of the New Jersey zinc company's Flat Gap mine at Treadway in the Copper Ridge district: Tenn. Div. Geology, Rept. Invest. No. 23, pp. 76-90.

Hill, W. T., 1971, The geology, applied geochemistry, and drilling results in the Puncheon Camp Creek area, Grainger County, Tennessee: Unpublished Ph.D. Diss., Univ. of Tenn., Knoxville, 106p.

Hill, W. T., and McCormic, J. E., and Wedow, H., Jr., 1971, Problems on the origin of ore deposits in the Lower Ordovician Formations of East Tennessee: Econ. Geol., v. 66, pp. 799-804.

Hill, W. T., Morris, R. G., Hagegeorge, C. G., 1971, Ore controls and related sedimentary features at the Flat Gap mine, Treadway, Tennessee: Econ. Geol., v. 66, pp. 748-756.

Hoagland, A. D., 1967, Interpretations relating to the genesis of East Tennessee zinc deposits: in Brown, J. S. (ed.), Genesis of stratiform lead-zinc-barite-fluorite deposits: Econ. Geol., Mono. 3, pp. 52-58.

Hoagland, A. D., 1971, Appalachian strata-bound deposits: their essential features, genesis and exploration problem: Econ. Geol., v. 66, pp. 805-810.

Hoagland, A. D., 1976, Appalachian zinc-lead deposits, in Wolf, K. H. (ed.), Handbook of strata-bound and stratiform ore deposits, v. 6, Elsevier, New York, pp. 495-534.

Hoagland, A. D., Hill, W. T., and Fulweiler, R. E., 1965, Genesis of the Ordovician zinc deposits in East Tennessee: Econ. Geol., v. 60, pp. 693-714.

Holland, H. D., 1967, Gangue minerals in hydrothermal deposits: in Barnes, H. L. (ed.), Geochemistry of hydrothermal ore deposits: Holt, Rinehart and Winston, Inc., New York, pp. 382-436.

Hsü, K. J., and Schneider, J., 1973, Progress report on dolomitization - hydrology of the Abu Dhabi sabkha, Arabian Gulf: in Purser, B. H. (ed.), The Persian Gulf, Springer-Verlag, New York, pp. 409-422.

Hsü, K. J., and Siegenthaler, C., 1969, Preliminary experiments on hydrodynamic movements induced by evaporation and their bearing on the dolomite problem: Sedimentology, v. 12, pp. 11-25.

Ichikuni, M., 1973, Partition of strontium between calcite and solution effect of substitution by manganese: Chem. Geol., v. 11, pp. 315-319.

Ilich, M., 1974, Hydrothermal-sedimentary dolomite: The missing link?: Am. Assoc. Petrol. Geol. Bull., v. 58, pp. 1331-1347.

Illing, L. V., Wells, A. J., and Taylor, J. C. M., 1965, Penecontemporary dolomite in the Persian Gulf: in Pray, L. C., and Murray, R. C. (ed.), Dolomitization and limestone diagenesis: a symposium - Soc. Econ. Paleotologists Mineral., Spec. Publ., No. 13, pp. 89-111.

Irwin, M. L., 1965, General theory of epeiric clear water sedimentation: Am. Assoc. Petrol. Geol. Bull., v. 49, pp. 445-459.

James, N. P., 1972, Holocene calcareous crust (caliche) profiles: criteria for subaerial exposure: Jour. Sed. Pet., v. 42, pp. 817-836.

Kahle, C. F., 1965, Possible roles of clay minerals in the formation of dolomite: Jour. Sed. Pet., v. 35, pp. 448-453.

Katz, A., 1971, Zoned dolomite crystals: Jour. Geol., v. 79, pp. 35-51.

Katz, A., and Mathews, A., 1977, The dolomitization of $CaCO_3$: an experimental study at 252-295°C: Geochim. Cosmochim. Acta., v. 41, pp. 297-308.

Katz, A., Sass, E., Starinsky, A., and Holland, H. D., 1972, Strontium behavior in aragonite calcite transformation: an experimental study at 40-98°C: Geochim. Cosmochim. Acta., v. 36, pp. 381-496.

Kendall, D. L., 1960, Ore deposits and sedimentary features. Jefferson City mine, Tennessee: Econ. Geol., v. 55, pp. 985-1003.

Kendall, D. L., 1961, Ore deposits and sedimentary features in Tennessee: Econ. Geol., v. 56, pp. 1137-1139.

Kern, R., and Weisbrod, A., 1967, Thermodynamics for geologists, Freeman, Cooper and Co., San Francisco, 304p.

Kinsman, D. J. J., 1969, Interpretation of Sr^{++} concentrations in carbonate minerals and rocks: Jour. Sed. Pet., v. 39, pp. 486-508.

Kinsman, D. J. J., and Holland, H. D., 1969, The co-precipitation of cations with $CaCO_3$ IV, the co-precipitation of Sr^{2+} with aragonite between 16 and 96°C: Geochem. Cosmochim. Acta., v. 33, pp. 1-17.

Klein, G. V., and Ryer, T. A., 1978, Tidal circulation patterns in Precambrian, Paleozoic, and Cretaceous epeiric and mioclinal shelf seas: Geol. Soc. Am. Bull., v. 89, pp. 1050-1058.

Krauskopf, K. B., 1959, The geochemistry of silica in sedimentary environments: in Ireland, H. A. (ed.), Silica in sediments: Soc. Econ. Paleontologists Mineral., pp. 4-19.

Krauskopf, K. B., 1967, Source rocks for metal bearing fluids: in Barnes, H. L. (ed.), Geochemistry for hydrothermal ore deposits, Holt, Rinehart and Winston, Inc., New York, pp. 1-33.

Krauskopf, K. B., 1975, Introduction to geochemistry, McGraw-Hill, New York, 617p.

Kyle, J. R., 1976, Brecciation, alteration and mineralization in the central Tennessee zinc district: Econ. Geol., v. 71, pp. 892-903.

Land, L. S., 1967, Diagenesis of skeletal carbonates: Jour. Sed. Pet., v. 37, pp. 914-930.

Land, L. S., 1972, Contemporaneous dolomitization of Middle Pleistocene reefs by meteoric water, north Jamaica (abs.): Am. Assoc. Petrol. Geol. Bull., v. 56, p. 635.

Land, L. S., 1973, Contemporaneous dolomitization of Middle Pleistocene reefs by meteoric water, north Jamaica: Bull. Marine Sci., v. 23, pp. 64-92.

Laporte, L. F., 1971, Paleozoic carbonate facies of the Central Appalachian shelf: Jour. Sed. Pet., v. 41, pp. 724-740.

Laurence, R. A., 1971, Evolution of thoughts on ore controls in East Tennessee: Econ. Geol., v. 66, pp. 696-700.

Legrand, H. E., and Stringfield, V. T., 1971, Tertiary limestone aquifer in southeastern states: Econ. Geol., v. 66, pp. 701-709.

Lindholm, R. C., and Finkleman, R. B., 1972, Calcite staining: semi-quantitative determination of ferrous iron: Jour. Sed. Pet., v. 42, pp. 239-242.

Linvingston, D. A., 1963, Chemical composition of rivers and lakes: U.S. Geol. Survey Prof. Paper 440-G, 41p.

Logan, B. W., Rezak, R., and Ginsburg, R. N., 1964, Classification and environmental significance of algal stromatolities: Jour. Geology, v. 72, No. 3, pp. 68-83.

Logan, B. W., and Semeniux, V., 1976, Dynamic metamorphism, processes and products in Devonian carbonate rocks, Canning Basin, Western Australia: Geol. Soc. Australia, Spec. Publ., No. 6, 180p.

Long, J. V. P., and Agrell, S. D., 1965, The cathodo-luminescence of minerals in thin section: Mineral. Mag., v. 34, pp. 318-325.

Lovering, T. S., 1969, The origin of hydrothermal and low temperature dolomite: Econ. Geol., v. 64, pp. 743-754.

Lucia, F. J., 1968, Recent sediments and diagenesis of South Bonaire, Netherland Antilles: Jour. Sed. Pet., v. 38, pp. 845-858.

Lyon, W. S., Jr., 1964, Guide to activation analysis, D. Von Nostrand Co. Inc., New Jersey, 186p.

Maher, S. W., 1971, Regional distribution of mineral deposits beneath the pre-Middle Ordovician unconformity in the Southern Appalachian: Econ. Geol., v. 66, pp. 744-747.

Mason, B., 1966, Principles of geochemistry, John Wiley & Sons, Inc., New York, 329p.

Mazzulo, S. J., and Friedman, G. M., 1977, Competitive algal colonization of peritidal flats in a schizohaline environment: The Lower Ordovician of New York: Jour. Sed. Pet., v. 47, pp. 398-410.

McAlester, A. L., 1968, The history of life, Foundation of earth science series, Prentice-Hall Inc., Englewood Cliffs, N.J., 151p.

Meyers, W. J., 1974, Carbonate cement stratigraphy of the Lake Valley Formation (Mississippian) Sacramento Mountains, New Mexico: Jour. Sed. Pet., v. 44, pp. 837-861.

Meyers, W. J., Lohmann, K. C., 1978, Microdolomite-rich syntaxial cements: proposed meteoric-marine mixing-zone phreatic cements from Mississippian limestones, New Mexico: Jour. Sed. Pet., v. 48, No. 2, pp. 475-488.

Monty, C. L. V., 1976, The origin and development of cryptalgal fabrics: in Walter, M. R. (ed.), Developments in Sedimentology 20 - Stromatolites, Elsevier, New York, pp. 196-249.

Morton, R. A., 1979, Subaerial storm deposits formed on barrier flats by wind-driven currents: sedimentary geology, v. 24, pp. 105-122.

Murray, R. C., 1969, Hydrology of South Bonaire, N. A. - A rock selective dolomitization model: Jour. Sed. Pet., v. 39, No. 3, pp. 1007-1013.

Nickel, E., 1978, The present status of cathodoluminescence as a tool in sedimentology: Minerals Science and Engineering, South Africa, v. 10, No. 2, pp. 73-100.

Oglesby, T. W., 1976, A model for the distribution of manganese, iron, and magnesium in authigenic calcite and dolomite cements in the Upper Smackover Formation in Eastern Mississippi: M.S. Thesis, Univ. of Missouri, 122p.

Perkins, R. D., and Enos, P., 1968, Hurricane Betsy in the Florida-Bahama area - Geologic effects and comparison with hurricane Dona: Jour. Geol., v. 76, pp. 710-717.

Perkins, R. D., and Halsey, S. D., 1971, Geologic significance of microboring fungi and algae in carolina shell sediments: Jour. Sed. Pet., v. 41, pp. 843-853.

Peterson, M. N. A., and Von Der Borch, C. D., 1965, Chert: modern inorganic deposition in a carbonate precipitating locality: Science, v. 149, pp. 1501-1503.

Pingitori, N. E., Jr., 1978, The behaviour of Zn^{+2} and Mn^{+2} during carbonate diagenesis: theory and application, Jour. Sed. Pet., v. 48, No. 3, pp. 799-814.

Playford, P. E., and Lowry, D. C., 1966, Devonian reef complexes of the Canning Basin, Western Australia: Bull. Geol. Survey, Western Australia 118, 150p.

Playford, P. E., Cockbain, A. E., Druce, E. C., and Wray, J. L., 1976, Devonian stromatolites from the Canning Basin, Western Australia: in Walter, M. R. (ed.), Developments in Sedimentology 20 - Stromatolites, Elsevier, New York, pp. 543-563.

Plummer, L. N., 1975, Mixing of sea water with calcium carbonate ground water: in Whitten, E. H. T. (ed.), Quantitative studies in geological sciences: Geol. Soc. Am. Mem. 142, pp. 219-238.

Potosky, R. A., and Kopp, O. C., 1970, Application of cathodoluminescence to petrographic studies: Compass, v. 47, pp. 63-69.

Purser, B. H., 1973, Sedimentation around bathymetric highs in the Southern Persian Gulf: in Purser, B. H. (ed.), The Persian Gulf, Springer-Verlag, New York, pp. 157-178.

Purser, B. H., and Evans, G., 1973, Regional sedimentation along the Trucial Coast, SE Persian Gulf: in Purser, B. H. (ed.), The Persian Gulf, Springer-Verlag, New York, pp. 211-232.

Read, J. F., 1976, Calcretes and their distinction from stromatolites: in Walter, M. R. (ed.), Developments in sedimentology 20 - Stromatolites, Elsevier, New York, pp. 55-72.

Reeves, R. D., and Brooks, R. R., 1978, Trace element analyses of geologic materials, John Wiley & Sons, New York, 421p.

Ridge, J. D., 1968, Comments on the development of the ore-bearing structures of the Mascot-Jefferson City district and on the genesis of the ores contained in them: Inst. Mining and Metallurgy Trans., Sec. B, v. 77, Bull. 735, pp. B6-B17.

Ridge, J. D., 1972, Annotated bibliographies of mineral deposits in the Western Hemisphere: Geol. Soc. Am., Inc., Memoir, v. 131, pp. 501-505.

Roedder, E., 1967, Environment of deposition of stratiform (Mississippi Valley-type ore deposits, from studies of fluid inclusion: in Brown, J. S. (ed.), Genesis of stratiform lead-zinc-barite-fluorite deposits: Econ. Geol., Mono. 3, pp. 349-362.

Roedder, E., 1971, Fluid inclusion evidence on the environment of formation of mineral deposits of the Southern Appalachian Valley: Econ. Geol., v. 66, pp. 777-791.

Roedder, E., 1976, Fluid-inclusion evidence on the genesis of ores in sedimentary and volcanic rocks: in Wolf, K. H. (ed.), Handbook of strata-bound and stratiform ore deposits, v. 2, Elsevier, New York.

Roeder, D., Gilbert, D. E., and Witherspoon, W. D., 1978, Evolution and microscopic structure of Valley and Ridge thrust belt, Tennessee and Virginia: Univ. of Tenn., Structure in Geology 2, Knoxville, 25p.

Roeder, D., and Witherspoon, W. D., 1978, Palinspastic map of East Tennessee: Am. Jour. Sci., v. 278, pp. 543-550.

Sass, E., 1965, Dolomite-calcite relationships in sea water: theoretical considerations and preliminary experimental results: Jour. Sed. Pet., v. 35, pp. 339-347.

Schneider, J. F., 1975, Recent tidal deposits, Abu Dhabi, UAE, Arabian Gulf: in Ginsburg, R. N. (ed.), Tidal deposits, Springer-Verlag, New York, pp. 209-214.

Secrist, M. H., 1924, Zinc deposits of East Tennessee: Tenn. Div. Geol. Bull. 31, 165p.

Shaw, A. B., 1964, Time in stratigraphy: Mc-Graw Hill, New York, 365p.

Shinn, E. A., 1968, Practical significance of birdseye structures in carbonate rocks: Jour. Sed. Pet., v. 38, pp. 215-223.

Shinn, E. A., 1973, Carbonate coastal accretion in an area of longshore transport, NE Qatar, Persian Gulf: in Purser, B. H. (ed.), The Persian Gulf, Springer-Verlag, New York, pp. 179-192.

Shinn, E. A., Ginsburg, R. N., and Lloyd, R. M., 1965, Recent supratidal dolomite from Andros Island, Bahamas: in Pray, L. C., and Murray, R. C. (ed.), Dolomitization and limestone diagenesis: a Symposium - Soc. Econ. Paleontologists Mineral., Spec. Publ., 13, pp. 112-123.

Sibley, D. F., 1979, Dolomitization of Plio-Pleistocene carbonate sediments, Bonaire, Netherlands Antilles (abs.): Am. Assoc. Petrol. Geologists - Soc. Econ. Paleontologists Mineral. Annual Mtg., p. 164.

Siedlecka, A., 1972, Length-slow chalcedony and relicts of sulphates: evidences of evaporitic environments in the Upper Carboniferous and Permian beds of Bear Island, Svalbard: Jour. Sed. Pet., v. 42, No. 4, pp. 812-816.

Skall, H., 1975, The paleoenvironment of the Pine Point lead-zinc district: Econ. Geol., v. 70, pp. 22-47.

Smith, G. A., Briden, J. C., and Drewry, G. E., 1973, Phanerozoic world maps: in Hughes, N. F. (ed.), Organisms and continents through time: Spec. Papers in Paleontology, Paleontological Assoc. London, v. 12, pp. 1-42.

Snyder, J. F., 1975, Petrography and minor element distribution in wall rocks from the Mascot-Jefferson City zinc district: Unpublished Ph.D. Diss., Univ. of Tenn., Knoxville, 209p.

Skinner, H. C. W., 1963, Precipitation of calcian dolomites and magnesian calcites in the southeast of South Australia: Am. Jour. Sci., v. 261, pp. 449-472.

Skinner, B. J., 1967, Precipitation of Mississippi Valley-type ores: A possible mechanism: in Brown, J. S. (ed.), Genesis of stratiform lead-zinc-barite-fluorite deposits: Econ. Geol., Mono. 3, pp. 363-370.

Skinner, B. J., and Barton, P. B., Jr., 1973, Genesis of mineral deposits: Annl. Rev. Earth and Planet Sci. Leh., v. 1, pp. 183-211.

Stanton, R. F., 1972, Ore petrology: McGraw-Hill, New York, 713p.

Textoris, D. H., 1969, Supratidal origin of Appalachian Basin dolostone: Geol. Soc. Am., Abstracts for 1968, Spec. Paper No. 121, pp. 470-471.

Thompson, A. M., 1975, Carbonate coastal environments in Ordovician shoaling - upward sequences, Southern Appalchian: in Ginsburg, R. N. (ed.), Tidal Deposits, Springer-Verlag, New York, pp. 397-405.

Trudinger, P. A., 1976, Microbiological processes in relation to ore genesis: in Wolf, K. H. (ed.), Handbook of strata-bound and stratiform ore deposits, v. 2, Elsevier, New York, pp. 135-190.

Wanless, H. R., 1975, Carbonate tidal flats of the Grand Canyon Cambrian: in Ginsburg, R. N. (ed.), Tidal deposits, Springer-Verlag, New York, pp. 250-271.

Wanless, H. R., 1979, Limestone response to stress: Pressure solution and dolomitization: Jour. Sed. Pet., v. 49, pp. 0437-0462.

Wedephol, K. H., 1969, Composition and abundance of common sedimentary rocks: in Wedephol, K. H. (ed.), Handbook of Geochemistry I, Springer-Verlag,

Wedow, H., Jr., 1971, Models of mineralized solution-collapse structures from drilling statistics: Econ. Geol., v. 66, pp. 770-776.

Wedow, H., Jr., and Marie, J. R., 1965, Correlation of zinc abundance with stratigraphic thickness variations in the Kingsport Formation, west New Market area, Mascot-Jefferson City mining district, Tennessee: U.S.G.S. Prof. Paper 252-B, pp. B17-B22.

Weber, J. N., 1964, Trace element composition of dolostones and dolomites and its bearing on the dolomite problem: Geochim. Cosmochim. Acta., v. 28, pp. 1817-1868.

West, J., 1974, Trace element geochemistry of the coarse crystalline ore-breccia dolomite in the Flat Gap mine, Treadway, Tennessee: Unpublished Ph.D. Diss., Univ. of Tenn., Knoxville, 91p.

White, D. E., 1968, Environments of generations of some base metal deposits: Econ. Geol., v. 63, pp. 301-335.

Zamarreno, I., 1975, Peritidal origin of Cambrian carbonates in Northwest Spain: in Ginsburg, R. N. (ed.), Tidal deposits, Springer-Verlag, New York, pp. 289-298.

Zenger, D. H., 1972a, Dolomitization and uniformitarianism: Jour. Geol. Education, v. 20, pp. 107-127.

Zenger, D. H., 1972b, Significance of supratidal dolomitization in the geologic record: Geol. Soc. Am. Bull., v. 83, pp. 1-12.

APPENDIXES

APPENDIX A

ASSUMPTIONS AND PROCEDURE USED TO DETERMINE THE EFFECT OF DILUTION OF MARINE WATER BY FRESH WATER

The effect of dilution may be investigated by a theoretical mixing model. The steps taken for such a treatment are as follows:

Assumptions:

1. Mixing of solutions is in a closed system where the P_{CO_2} of the mixtures is equal to the P_{CO_2} of the stmosphere, and the total pressure of mixing is one atmosphere.

2. The mixing of solutions is at 25°C and there is no change of temperature.

3. The pH of marine water is 8.03 and that of fresh water is 7.34

4. The extended Debye-Hückel equation (Helgeson, 1969) which is good for dilute solutions, remains valid for obtaining activity coefficients of solutions of ionic strengths up to 0.7. See p. 179 for comparison of γ values of ions in sea water obtained by this method, and also by Garrels and Thompson (1962).

5. γ of monovalent ion pairs equals $\gamma_{HCO_3^-}$.

6. The carbonates are pure compounds.

7. The grain size of carbonates that may be related to such calculations are such that surface energy contributions can be neglected.

Procedure:

1. Concentrations of dissolved ionic species of fresh water and marine water are selected from the literature (Table 2-2, p. 16). For general applicability of the results, the mean composition of the river waters of the world (Livingston, 1963) is used to obtain the concentrations of dissolved ionic species in water. The composition selected for marine water is that given by Davis (1977).

2. Concentrations of dissolved ionic species in mixtures of marine and fresh water are computed for different proportions of mixing (by weight) of the two. For example, concentration of Cl^- in marine water = 19353 ppm and in fresh water = 7 ppm (Table 2-2, p. 16).

So, concentration of Cl^- in a 20 wt. % marine water in the mixture = $\{(20 \times 19353) + (80 \times 7)\}/100 = 3876.8$ ppm. Concentrations of the dissolved ionic species in the mixtures, so calculated are given in Table 2-2.

3. Concentrations of the dissolved ionic species (Table 2-2) are converted into molalities

$$\{\text{molality } (m) = \frac{\text{concentration of solute in ppm}}{\text{formula weight of the solute}} \times 10^{-3} \quad .$$

The calculated molal concentrations are given in Table A-1.

4. From the molalities, the ionic strengths of the various mixtures are computed using the formula:

$$I = 1/2 \; \Sigma_i m_i \; Z_i^2$$

where I is the ionic strength of the solution; m_i is the molality of the ith ion in the solution; and Z_i is the charge of the ith ion.

The values so obtained are given in Table A-2. Because Mg^{++}, Ca^{++}, Na^+, K^+, $SO_4^=$, $CO_3^=$, and HCO_3^- are the ionic species that are reported by Garrels and Thompson (1962) to form stable complexes, they are the only ionic species considered in the subsequent calculations.

5. The activity coefficient (γ_i) of the ith species is calculated from the extended Debye-Hückel equation (Helgeson, 1969):

Table A-1. Molalities $\times 10^5$ of dissolved ionic species for different weight percent marine water in the mixture

Dissolved Ionic Species	Atomic Weight	0%	5%	10%	15%	20%	30%	40%	50%	60%	70%	80%	90%	100%
Cl^-	35.45	22.0	2751	5479	8207	10934	16393	21844	27306	32762	38220	43677	49134	54591
$SO_4^=$	96.06	12.0	152	293	432	573	854	1135	1416	1697	1978	2258	2539	2820
HCO_3^-	61.00	96.0	103	110	116	123	136	150	164	178	192	205	219	233
$CO_3^=$	60.01	0.27	1.3	3	4	5	8	11	13	16	19	21	24	27
Na^+	22.99	27.0	2367	4706	7045	9384	14063	18741	23420	28098	32776	37455	42133	46812
Mg^{++}	24.31	17.0	283	547	812	1076	1608	2138	2669	3198	3728	4258	4789	5319
Ca^{++}	40.08	37.0	87	136	186	235	334	433	531	630	729	828	927	1025
K^+	39.10	6.0	57	107	158	209	310	412	513	615	716	818	919	1020
Br^-	79.91	@	4	8	13	17	25	34	42	51	59	67	76	84
H_3BO_3	61.83	@	@	@	@	1	2	3	4	4	5	6	6	7
Sr^{++}	87.62	@	@	@	1	2	3	4	5	5	6	7	8	9
F^-	19.00	@	@	@	1	1	2	3	4	4	5	5	6	7
NO_3^-	62.00	2.0	2	1	1	1	1	1	1	1	@	@	@	@
Fe^{++}	55.85	1.0	1	1	1	1	1	1	1	@	@	@	@	@
SiO_2	60.08	22	21	20	18	17	15	13	11	9	6	4	2	@

@ Calculated molalities less than 0.000010.

Table A-2. Ionic strengths (I) and $m\ell^2 \times 10^5$ of solutions for different weight percent marine water in the mixture

Dissolved Ionic Species	ℓ^2	0%	5%	10%	15%	20%	30%	40%	50%	60%	70%	80%	90%	100%
$C\ell^-$	1	22	2751	5479	8207	10934	16393	21844	27306	32762	38220	43677	49134	54910
$SO_4^=$	4	48	608	1172	1728	2292	3416	4540	5664	6788	7912	9032	10156	11280
HCO_3^-	1	96	103	110	116	123	137	150	164	178	192	205	219	233
$CO_3^=$	4	1	5	12	16	20	32	44	52	64	72	84	96	108
Na^+	1	27	2367	4706	7045	9384	14063	18741	23420	28098	32776	37455	42133	46812
Mg^{++}	4	68	1132	2188	3248	4304	6432	8552	10676	12792	14912	17032	19156	21276
Ca^{++}	4	148	348	544	744	940	1336	1732	2124	2520	2916	3312	3708	4100
K^+	1	6	57	107	158	209	310	412	513	615	716	818	919	1020
Br^-	1	@	4	8	13	17	25	34	42	51	59	67	76	84
H_3BO_3	0	-	-	-	-	-	-	-	-	-	-	-	-	-
Sr^{++}	4	@	@	@	4	8	12	16	20	20	24	28	32	36
F^-	1	@	@	@	1	1	2	3	4	4	5	5	6	7
NO_3^-	1	2	2	1	1	1	1	1	1	@	@	@	@	@
Fe^{++}	4	4	4	4	4	4	4	4	4	@	@	@	@	@
SiO_2	0	-	-	-	-	-	-	-	-	-	-	-	-	-
Ionic Strength		.00211	.0364	.07166	.10593	.14119	.21082	.28037	.34995	.41946	.48904	.55958	.62818	.69933

@ $m\ell^2$ less than .00001.

$$\log (\gamma_i) = \frac{-AZ_i^2\sqrt{I}}{1+a_i^oB\sqrt{I}} + bI$$

where A and B are Debye-Hückel constants whose values depend on temperature and the nature of the solvent; a_i^o has a value dependent on the "effective diameter" of the ith ion in solution, b is the deviation function.

The values used for A, B and b are obtained from Helgeson (1967, 1969; Table 2-2, p. 16), where A = 0.5095, B = 0.3284×10^8, b = 0.041. A value of $a^0 = 3.89 \times 10^{-8}$ indicated in the Helgeson's paper (1969) gives one value for all monovalent ions, and another for divalent ions. In order to get variability in the activity coefficients of ions of the same valence, the values of a_i^o and b are obtained from Berner (1971, p. 218). Calculated parameters used for the extended Debye-Hückel equations are listed in Table A-3; and the activity coefficients so computed are given in Table A-4. The activity coefficients of monovalent complexed ionic species are assumed to be equal to $\gamma_{HCO_3^-}$; and the activity coefficients of neutral species are found from the extended Debye-Hückel equation by putting Z equal to zero. The activity coefficients so obtained using the extended Debye-Hückel equation are considered reliable even for solutions for solution of higher ionic strengths. For example, for marine water (I = 0.7), the values obtained here compare reasonably well with those obtained using other methods by Garrels and Thompson (1962). A comparison of the two values is shown in Table A-5.

Table A-3. Calculated parameters for the extended Debye-Hückel equation: $\text{Log } \gamma_i = -\frac{W}{X} + Y$, where $W = AZ^2\sqrt{I}$, $X = 1 + a^\circ_i B\sqrt{I}$, and $Y = bI$

Ionic Species	$a^\circ_i B$		Weight percent of marine water in the mixture												
			0%	5%	10%	15%	20%	30%	40%	50%	60%	70%	80%	90%	100%
		$\sqrt{I}$	.04593	.19074	.26769	.32547	.37575	.45915	.52950	.59157	.64766	.69931	.74805	.79258	.83626
		W for Z=2	.09361	.38873	.54555	.66331	.76578	.93572	1.07912	1.20562	1.31993	1.42513	1.52453	1.61528	1.70430
		W for Z=1	.02340	.09718	.13639	.16583	.19144	.23394	.26978	.30140	.32998	.35630	.38113	.40382	.42607
		Y	.00009	.00143	.00294	.00434	.00579	.00864	.01144	.01435	.01720	.02005	.02294	.02576	.02867
$SO_4^=$		X	1.06033	1.25056	1.35164	1.42754	1.49359	1.60314	1.69555	1.77709	1.85077	1.91861	1.98264	2.0413	2.09851
	1.3136	$\frac{W}{X}$	.08828	.31084	.40362	.46465	.51271	.58368	.63644	.67842	.71318	.74279	.76894	.79137	.81215
HCO_3^-		X	1.06033	1.25056	1.35164	1.42754	1.49359	1.60314	1.69555	1.77709	1.85977	1.91861	1.98264	2.04113	2.09851
	1.3136	$\frac{W}{X}$	.02207	.07771	.10009	.11616	.12818	.14592	.15911	.16961	.17829	.18570	.19224	.19784	.20304
$CO_3^=$		X	1.00031	1.28187	1.39559	1.48098	1.55528	1.67853	1.78250	1.87422	1.95711	2.03344	2.10547	2.17127	2.23582
	1.4778	$\frac{W}{X}$	.09332	.30327	.39094	.44789	.49237	.55746	.60540	.64326	.67443	.70085	.72408	.74393	.76227
Na^+		X	1.06033	1.25056	1.35164	1.42754	1.49359	1.60314	1.69555	1.77709	1.85077	1.91861	1.98264	2.04113	2.09851
	1.3136	$\frac{W}{X}$	.02207	.07771	.10009	.11616	.12818	.14592	.15911	.16961	.17829	.18570	.19224	.19784	.20304
Mg^{++}		X	1.12067	1.5011	1.70328	1.85507	1.98717	2.20628	2.39110	2.55417	2.70153	2.83723	2.95528	3.08227	3.19702
	2.6272	$\frac{W}{X}$	.08353	.25896	.32029	.35757	.38536	.42412	.45131	.47202	.48859	.50230	.51413	.52406	.53309
Ca^{++}		X	1.09050	1.37583	1.52746	1.64131	1.74083	1.90471	2.04332	2.16563	2.27615	2.37792	2.47306	2.56190	2.64777
	1.9704	$\frac{W}{X}$	.08584	.28254	.355716	.40414	.44001	.49127	.52812	.55671	.57990	.59932	.61623	.63055	.64367
K^+		X	1.04525	1.18792	1.28373	1.32065	1.37019	1.45235	1.52167	1.58281	1.63807	1.68896	1.73698	1.78085	1.82388
	.9852	$\frac{W}{X}$	.02239	.08181	.10793	.12557	.13972	.16108	.17729	.19042	.20144	.21096	.21942	.22676	.23361

Table A-4. Calculated values of $\gamma_i \times 10^5$ and $a_i\ 10^5$ in mixtures for different weight percent of marine water in the mixture (γ_i is calculated using parameters listed in Appendix A, and $a_i = \gamma_i\ m_i$. Values of m_i are taken from Table A-1)

Dissolved Ionic Species		0%	5%	10%	15%	20%	30%	40%	50%	60%	70%	80%	90%	100%
$SO_4^{=}$	γ	81623	49044	39748	34689	31123	26605	23714	21674	20138	18935	17947	17155	16463
	a	10	75	116	150	178	227	269	307	342	375	405	436	464
HCO_3^-	γ	95065	83892	79956	77300	75441	72899	71175	69942	69010	68289	67717	67285	66931
	a	91	86	88	90	93	100	107	115	123	131	139	147	156
$CO_3^{=}$	γ	80681	49907	40926	36012	32615	28261	25471	23501	22018	20855	19900	19135	18467
	a	0.22	0.67	1.2	1.4	1.6	2.2	2.8	3.1	3.5	4.0	4.2	4.6	5.0
Na^+	γ	9506.5	83892	79956	77300	75441	72899	71175	69942	69010	68289	67717	67285	66931
	a	26	1986	3763	5446	7079	10252	13339	16380	19390	22382	25364	28349	31332
Mg^{++}	γ	82520	55268	48156	44338	41728	38417	36319	34860	33776	32942	32271	31747	31303
	a	14	156	263	360	449	619	776	930	1080	1228	1374	1520	1665
Ca^{++}	γ	82082	52347	44384	39829	36794	32913	30431	28684	27372	26347	25516	24843	24260
	a	30	46	60	74	86	110	132	152	172	192	211	230	249
K^+	γ	94995	83104	78525	75643	73463	70398	68257	66670	65427	64430	63609	62951	62382
	a	6	47	84	120	154	218	281	342	402	461	520	579	636

Table A-5. Comparison of activity coefficients for marine water (I=0.7)

Dissolved Ionic Species	Activity Coefficients Given by Garrels and Thompson (1962)	Activity Coefficients Obtained in the Present Study
$NaHCO_3^\circ$	1.13	1.07
$MgCO_3^\circ$	1.13	1.07
$CaCO_3^\circ$	1.13	1.07
$MgSO_4^\circ$	1.13	1.07
$CaSO_4^\circ$	1.13	1.07
Na^+	0.76	0.67
HCO_3^-	0.68	0.67
$NaCO_3^-$	0.68	0.67
$NaSO_4^-$	0.68	0.67
KSO_4^-	0.68	0.67
$MgHCO_3^+$	0.68	0.67
$CaHCO_3^+$	0.68	0.67
K^+	0.64	0.62
Mg^{++}	0.36	0.31
Ca^{++}	0.28	0.24
$SO_4^=$	0.12	0.16
$CO_3^=$	0.20	0.18

6. The activity of an ionic species (a_i) may then be computed from the relationship

$$a_i = \gamma_i m_i$$

As will be discussed later such an activity is an apparent activity, but may be computed from values of m_i (Table A-1, p. 174), and γ_i (Table A-4).

7. The value of $^{m}CO_3^{=}$ may be computed from the relationships:

1. $CO_2 + H_2O \rightleftharpoons H_2CO_3 \qquad K_1 = 0.7015$

2. $H_2CO_3 \rightleftharpoons HCO_3^- + H^+ \qquad K_2 = 4.26 \times 10^{-7}$

3. $HCO_3^- \rightleftharpoons CO_3^{=} + H^+ \qquad K_3 = 4.687 \times 10^{-11}$

Combining Equations 1, 2 and 3

$$CO_2 + H_2O \rightleftharpoons 2H^+ + CO_3^{=}$$

$$^{m}CO_3^{=} = \frac{K_1 K_2 K \, ^{P}CO_2}{a_H^2 + \gamma_{CO_3^{=}}} .$$

Remembering that $a_{H^+} = 10^{-pH}$, and obtaining values for $^{\gamma}CO_3^{=}$ by using the extended Debye-Hückel equation for fresh water (Ionic strength = 0.00211) and marine water (Ionic strength = 0.7), and the value of atmospheric $^{P}CO_2$ ($^{P}CO_2 = 10^{-3.5}$ atm., Kern and Weisbrod, 1967), for pH = 7.34 and 8.03 (assumption 3); $^{m}CO_3^{=}$ in fresh water = 2.7×10^{-6}, and in marine water $^{m}CO_3^{=} = 2.7 \times 10^{-5}$. These values of $^{m}CO_3^{=}$ are then entered into the computations for various parameters in the various

mixtures of the two solutions as stipulated in steps 1, 2, 3, 4, 5, and 6.

8. The distribution of dissolved ionic species in each of the mixtures may be found by the Garrels-Thompson (1962) model. As further elaborated by Berner (1971), the distribution of dissolved ionic species may be calculated by solving seven mass balance equations in conjunction with ten mass action equations.

The seven mass balance equations are:

(A) $m_{SO_4^{=}\ total} = m_{SO_4^{=}\ uncomplexed} + m_{MgSO_4^o} + m_{CaSO_4^o} + m_{NaSO_4^-} + m_{KSO_4^-}$

(B) $m_{CO_3^{=}\ total} = m_{CO_3^{=}\ uncomplexed} + m_{MgCO_3^o} + m_{CaCO_3^o} + m_{NaCO_3^-}$

(C) $m_{HCO_3^-\ total} = m_{HCO_3^-\ uncomplexed} + m_{NaHCO_3^o} + m_{MgHCO_3^+} + m_{CaHCO_3^+}$

(D) $m_{Ca^{++}_{total}} = m_{Ca^{++}_{uncomplexed}} + m_{CaHCO_3^+} + m_{CaCO_3^o} + m_{CaSO_4^o}$

(E) $m_{Mg^{++}_{total}} = m_{Mg^{++}_{uncomplexed}} = m_{MgHCO_3^+} + m_{MgCO_3^o} + m_{MgSO_4^o}$

(F) $m_{Na^+_{total}} = m_{Na^+_{uncomplexed}} + m_{NaHCO_3^o} + m_{NaCO_3^-} + m_{NaSO_4^-}$

(G) $m_{K^+_{total}} + m_{K^+_{uncomplexed}} + m_{KSO_4^-}$.

The ten mass action equations are:

$$(H) \quad K^{o}_{MgSO_4} = \frac{\gamma_{Mg^{++}}\, m_{Mg^{++}}\, \gamma_{SO_4^{=}}\, m_{SO_4^{=}}}{\gamma_{MgSO_4^{o}}\, m_{MgSO_4^{o}}}$$

$$(I) \quad K^{o}_{CaSO_4} = \frac{\gamma_{Ca^{++}}\, m_{Ca^{++}}\, \gamma_{SO_4^{=}}\, m_{SO_4^{=}}}{\gamma_{CaSO_4^{o}}\, m_{CaSO_4^{o}}}$$

$$(J) \quad K^{-}_{NaSO_4} = \frac{\gamma_{Na^{+}}\, m_{Na^{+}}\, SO_4^{=}\, m_{SO_4^{=}}}{NaSO_4^{-}\, m_{NaSO_4^{-}}}$$

$$(K) \quad K^{-}_{KSO_4} = \frac{\gamma_{K^{+}}\, m_{K^{+}}\, \gamma_{SO_4^{=}}\, m_{SO_4^{=}}}{\gamma_{KSO_4^{-}}\, m_{KSO_4^{-}}}$$

$$(L) \quad K^{o}_{MgCO_3} = \frac{\gamma_{Mg^{++}}\, m_{Mg^{++}}\, \gamma_{CO_3^{=}}\, m_{CO_3^{=}}}{\gamma_{MgCO_3^{o}}\, m_{MgCO_3^{o}}}$$

$$(M) \quad K^{o}_{CaCO_3} = \frac{\gamma_{Ca^{++}}\, m_{Ca^{++}}\, \gamma_{CO_3^{=}}\, m_{CO_3^{=}}}{\gamma_{CaCO_3^{o}}\, m_{CaCO_3^{o}}}$$

$$(N) \quad K^{-}_{NaCO_3} = \frac{\gamma_{Na^{+}}\, m_{Na^{+}}\, \gamma_{CO_3^{=}}\, m_{CO_3^{=}}}{\gamma_{NaCO_3^{-}}\, m_{NaCO_3^{-}}}$$

$$(O) \quad K^{o}_{NaHCO_3} = \frac{\gamma_{Na^{+}}\, m_{Na^{+}}\, \gamma_{HCO_3^{-}}\, m_{HCO_3^{-}}}{\gamma_{NaHCO_3^{o}}\, m_{NaHCO_3^{o}}}$$

$$(P) \quad K^{+}_{MgHCO_3} = \frac{\gamma_{Mg^{++}}\, m_{Mg^{++}}\, \gamma_{HCO_3^{-}}\, m_{HCO_3^{-}}}{\gamma_{MgHCO_3^{+}}\, m_{MgHCO_3^{+}}}$$

$$(Q) \quad K_{CaHCO_3^+} = \frac{\gamma_{Ca^{++}}\, m_{Ca^{++}}\, \gamma_{HCO_3^-}\, m_{HCO_3^-}}{\gamma_{CaHCO_3^-}\, m_{CaHCO_3^-}} .$$

The above 17 equations may be solved simultaneously for 17 unknowns after obtaining the dissociation equilibrium constants for the mass action equations. The dissociation constants can be found from the Gibbs Free energy of reaction (ΔG_R^o given on p. 188) for the standard state of reactants and products. $\Delta G_R^o = \Delta G_f^o$ (Products) - ΔG_f^o (Reactants); and $\Delta G_R^o = -RT \ln K$ where, ΔG_f^o is the standard free energy of formation (of compounds given on p. 188); ΔG_R^o is the free energy of reaction; R is the gas constant (Kcal degree^{-1} K mole^{-1}); T is the temperature in degree Kelvin (in these calculations T = 298.15 K); and K is the equilibrium constant of the reaction, in this case the dissociation or ionization constant. The reaction constants (K) relevant for the considered carbonate equilibria calculated by using the above relationships are given on page 188.

There is a recommended short cut (Garrels and Thompson, 1962) for solving the equations. First, it is assumed that cations are uncomplexed; and then a correction is applied for this assumption by calculating the cations tied to ion pairs.

As an illustration consider the mass balance equation (B) for the $m_{CO_3^=}$ and the corresponding mass action equations (L, M, N) for the carbonate complexes.

The mass action equations can be rewritten in terms of $m_{CO_3^=}$, thus:

$$(L') \quad {}^{m}MgCO_3^{o} = \left(\frac{\gamma_{Mg^{++}} \; {}^{m}Mg^{++} \; CO_3^{=}}{MgCO_3^{o} \; K_{MgCO_3^{o}}} \right) {}^{m}CO_3^{=}$$

$$(M') \quad {}^{m}CaCO_3^{o} = \left(\frac{\gamma_{Ca^{++}} \; {}^{m}Ca^{++} \; CO_3^{=}}{CaCO_3^{o} \; K_{CaCO_3^{o}}} \right) {}^{m}CO_3^{=}$$

$$(N') \quad {}^{m}NaCO_3^{-} = \left(\frac{\gamma_{Na^{+}} \; {}^{m}Na^{+} \; CO_3^{=}}{NaCO_3^{-} \; K_{NaCO_3^{-}}} \right) {}^{m}CO_3^{=} \; .$$

Substituting the above equations (L', M', N') in Equation B and factoring out ${}^{m}CO_3^{=}$ yields:

$$(B') \quad {}^{m}CO_3^{=}\ \text{total} = {}^{m}CO_3^{=} \left\{ 1 + \frac{\gamma_{Mg^{+}} \; {}^{m}Mg^{++} \; \gamma_{CO_3^{=}}}{\gamma_{MgCO_3^{o}} \; K_{MgCO_3^{o}}} + \frac{\gamma_{Ca^{++}} \; {}^{m}Ca^{++} \; \gamma_{CO_3^{=}}}{\gamma_{CaCO_3^{o}} \; K_{CaCO_3^{o}}} + \frac{\gamma_{Na^{+}} \; {}^{m}Na \; \gamma_{CO_3^{=}}}{\gamma_{NaCO_3^{-}} \; K_{NaCO_3^{-}}} \right\}$$

If the values of the cations in this equation (B') are assumed to be equal to their total values, then all terms can be evaluated. As an example, consider a mixture with 60 wt. % marine water. Substituting values from Tables A-1 and A-4 in Equation B' yields:

$$(B'') \quad .00016 = {}^{m}CO_3 \quad (1 + 5.7140 + 0.56876 + 1.14734)$$

from which ${}^{m}CO_3 = .00001898$. Substituting this value of ${}^{m}CO_3^{=}$ in Equations L', M', N' will give the concentrations of $MgCO_3^{o}$, $CaCO_3^{o}$, $NaCO_3^{-}$, respectively. Their values will be easily obtained by multiplying the numbers inside the brackets in Equation B'' by the value of ${}^{m}CO_3^{=}$ (=.00001898). Thus

(B''') .00016 = (.00001898 + .00010845 + .0000108 + .00002178) .

Note that Equations B, B', B'', and B''' are similar. The percentages of cations and anions tied to a complex can be calculated by dividing the concentrations of the complexed ion (as found in the Equation B''') by the total concentration on the cation and anion respectively, and multiplying the values obtained by 100. For example

$$\% \ Mg^{++} \text{ in } MgCO_3^o = \frac{m_{MgCO_3^o}}{m_{Mg \text{ total}}} = \frac{0.00010845}{0.03198} \times 100 = 0.3\%$$

$$\% \ CO_3^{=} \text{ in } MgCO_3^o = \frac{m_{MgCO_3^o}}{m_{CO_3^{=} \text{ total}}} = \frac{0.00010845}{0.00016} \times 100 = 67.8\%$$

A series of similar calculations will give the percentage distribution of ionic species in different complexes (Tables A-6 and A-7). Knowing the percentages of ionic species that exist as complexes will enable calculation of the percentages of ions that remain as free ions. Equilibrium reaction constants are given in Table A-8. The percentages of the different free ions are obtained simply by subtracting the percentages of ionic species that exist in complexes from 100 (Table 2-4, p. 19).

9. Using values in Table 2-4, the percentage of the total individual ionic species tied to various complexes can be plotted (Fig. 2-1, p. 20). Such plots show that percentages of the ionic species would be released or tied up as a result of dilution of marine water.

Table A-6. Percentage distribution of cationic species in complexes for different weight percent of marine water in the mixture

Cations Complexed to Anions	0%	5%	10%	15%	20%	30%	40%	50%	60%	70%	80%	90%	100%
Cation complexed to $SO_4^{=}$													
Mg^{++}	1.5	6.0	7.4	8.2	8.7	9.3	9.7	10.0	10.2	10.4	10.5	10.5	10.8
Ca^{++}	1.5	6.0	7.1	7.6	7.9	8.2	8.4	8.5	8.5	8.6	8.6	8.6	8.6
Na^{+}	0.1	0.6	0.9	1.1	1.2	1.5	1.6	1.7	1.8	1.9	2.0	2.1	2.2
K^{+}	0.0	0.5	0.7	0.8	0.9	1.1	1.2	1.3	1.4	1.4	1.5	1.5	1.6
Cation complexed to $CO_3^{=}$													
Mg^{++}	0.3	0.3	0.3	0.3	0.3	0.3	0.3	0.3	0.3	0.3	0.3	0.3	0.3
Ca^{++}	0.2	0.2	0.2	0.2	0.2	0.2	0.2	0.2	0.2	0.2	0.2	0.2	0.2
Na^{+}	0	0	0	0	0	0	0	0	0	0	0	0	0
Cation complexed to HCO_3^{-}													
Mg^{++}	1.1	0.8	0.7	0.7	0.7	0.7	0.7	0.7	0.7	0.7	0.7	0.7	0.7
Ca^{++}	1.9	1.0	0.9	0.8	0.7	0.7	0.7	0.7	0.7	0.7	0.7	0.7	0.7
Na^{++}	0	0	0	0	0	0	0	0	0	0	0	0	0
Total of cation complexed to anions													
Mg^{++}	2.9	7.1	8.4	9.2	9.7	10.3	10.7	11.0	11.2	11.4	11.5	11.5	11.8
Ca^{++}	3.6	7.2	8.2	8.6	8.8	9.1	9.3	9.4	9.4	9.5	9.5	9.5	9.5
Na^{+}	0.1	0.6	0.9	1.1	1.2	1.5	1.6	1.7	1.8	1.9	2.0	2.1	2.2
K^{+}	0.0	0.5	0.7	0.8	0.9	1.1	1.2	1.3	1.4	1.4	1.5	1.5	1.6

Table A-7. Percentage distribution of anionic species in complexes for different weight percent of marine water in the mixture

Anions Complexed to Cations	0%	5%	10%	15%	20%	30%	40%	50%	60%	70%	80%	90%	100%
$SO_4^=$ complexed to cations													
Mg^{++}	2.1	11.3	13.9	15.4	16.3	17.5	18.2	18.8	19.2	19.5	19.8	20.0	20.3
Ca^{++}	4.7	3.4	3.3	3.3	3.2	3.2	3.2	3.2	3.2	3.2	3.2	3.1	3.1
Na^+	0.24	10.1	14.7	17.8	20.2	23.8	26.5	28.6	30.5	32.1	33.4	34.7	35.9
K^+	0	0.2	0.3	0.3	0.3	0.4	0.4	0.4	0.5	0.5	0.5	0.6	0.6
$Co_3^=$ complexed to cations													
Mg^{++}	17.0	55.2	60.6	63.0	64.4	65.8	66.7	67.4	67.8	68.1	68.3	68.5	68.7
Ca^{++}	22.6	10.2	8.6	8.1	7.7	7.3	7.1	6.9	6.8	6.6	6.6	6.5	6.4
Na^+	0.2	6.2	8.1	9.3	10.2	11.4	12.3	13.0	13.6	14.1	14.6	15.0	15.2
HCO_3^- complexed to cations													
Mg^{++}	0.2	2.2	3.6	4.7	5.8	7.7	9.3	10.9	12.2	13.5	14.7	15.9	17.0
Ca^{++}	0.7	0.8	1.0	1.2	1.4	1.7	2.0	2.2	2.5	2.7	2.9	3.0	3.2
Na^+	0.0	1.1	1.8	2.5	3.1	4.2	5.1	5.9	6.6	7.3	8.0	8.6	9.1
Total of anion complexed to cations													
$SO_4^=$	7.04	25.0	32.2	36.8	40.0	44.9	48.3	51.0	53.4	55.3	56.9	58.4	59.9
$CO_3^=$	39.8	71.6	77.3	80.4	82.3	84.5	86.1	87.3	88.2	88.8	89.5	90.0	90.3
HCO_3^-	0.9	4.1	6.4	8.4	10.3	13.6	16.4	19.0	21.3	23.5	25.6	27.5	29.3

Table A-8. Equilibrium reactions and constants

*Standard State Free Energy of Formation (ΔG° kcal.)							
Cationic Species		Anionic Species		Neutral Species		Compounds	
H^+	0	$SO_4^=$	-177.34	$MgSO_4^\circ$	-289.23	Calcite	-269.98
Na^+	- 62.5	$CO_3^=$	-126.22	$CaSO_4^\circ$	-312.84	Aragonite	-269.75
K^+	- 67.47	HCO_3^-	-140.31	$MgCO_3^\circ$	-239.62	$CaMg(CO_3)_2$	-516.6
Mg^{++}	-108.76	$NaSO_4^-$	-241.38	$CaCO_3^\circ$	-262.93	CO_2	- 92.3
Ca^{++}	-132.35	KSO_4^-	-246.11	$NaHCO_3^\circ$	-202.56	H_2O	- 56.9
$MgHCO_3^+$	-250.65	$NaCO_3^-$	-190.54	H_2CO_3	-149.00		
$CaHCO_3^+$	-274.38						

Dissociation reactions and constants (K) of $SO_4^=$ species

$MgSO_4^\circ$	$Mg^{++} + SO_4^=$	$K_{MgSO_4^\circ}=0.00508$
$CaSO_4^\circ$	$Ca^{++} + SO_4^=$	$K_{CaSO_4^\circ}=0.00491$
$NaSO_4^-$	$Na^+ + SO_4^=$	$K_{NaSO_4^-}=0.08650$
KSO_4^-	$K^+ + SO_4^=$	$K_{KSO_4^-}=0.11143$

Dissociation reactions and constants (K) of $CO_3^=$ species

$MgCO_3^\circ$	$Mg^{++} + CO_3^=$	$K_{MgCO_3^\circ}=0.00040$
$CaCO_3^\circ$	$Ca^{++} + CO_3^=$	$K_{CaCO_3^\circ}=0.00064$
$NaCO_3^-$	$Na^+ + CO_3^=$	$K_{NaCO_3^-}=0.05392$
HCO_3^-	$H^+ + CO_3^=$	$K_{HCO_3^-}=4.687\times10^{-11}$

Dissociation reachons and constants (K) of HCO_3^- species

$NaHCO_3^\circ$	$Na^+ + HCO_3^-$	$K_{NaHCO_3^\circ}=1.52500$
$MgHCO_3^+$	$Mg^{++} + HCO_3^-$	$K_{MgHCO_3^+}=0.06946$
$CaHCO_3^+$	$Ca^{++} + HCO_3^-$	$K_{CaHCO_3^+}=0.05484$

Dissociation constants of carbonate compounds and reachons involving H_2CO_3

$CaCO_3$ (Calcite)	$Ca^{++} + CO_3^=$	$K_{Calcite}=4.3\times10^{-9}$
$CaCO_3$ (Aragonite)	$Ca^{++} + CO_3^=$	$K_{Aragonite}=6.4\times10^{-9}$
$CaMg(CO_3)_2$	$Ca^{++} + Mg^{++} + 2CO_3^=$	$*K_{CaMg(CO_3)_2}=10^{-17}$
H_2CO_3	$H_2O + CO_2$	$K_{1}=0.7015$
$HCO_3 + H^+$	H_2CO_3	$K_{2}=4.26\times10^{-7}$

*Thermodynamic data obtained from Berner (1971).

10. It is also possible to find the ionic activity products (IAP), for instance of dolomite, calcite and aragonite (Table 2-5, p. 21). It can be seen that there are two values of IAP for each mixture. The one, the apparent IAP, is based on the activities found from γ_M, where the values of γ are those calculated by the extended Debye-Hückel equation discussed above (Table A-4, p. 178); the other, the effective IAP, which can be calculated from the activities of ions after considering effects of formation of complexes. Activities for the latter case can be found by multiplying the apparent activity values by the percentages of the ions that are free in each mixture.

11. Dividing IAP values by Keq. for the same carbonate will give degrees of saturation of the carbonate in the mixture, such that: if IAP/Keq. > 1, the solution is oversaturated with respect to a carbonate; if IAP/Keq. = 1, the solution is just saturated; and if IAP/Keq. < 1, the solution is undersaturated with respect to a carbonate.

Again, two values of degrees of saturation, one apparent, the other effective based on using the apparent or effective activities are calculated (Table 2-5).

Curves of degrees of saturation for carbonates using the values in Table 2-5 are given in Fig. 2-2, p. 22).

APPENDIX B

ESTIMATION OF ERROR OF Mn AMOUNT USING THE ELECTRON MICROPROBE MAC (400-S)

Reproducibility of some trace elements, for example Mn in a dolomite sample, may not correspond to the repeatable values of standards which have high content of Mn. This is because the error bar obtained by such a method which is small for higher concentrations in standards may become a big number when extrapolated for smaller concentrations in samples.

In absence of standards of very low concentrations, an attempt was made to grow in the laboratory a crystal with 0.01 wt. % Mn. This was attempted by dissolving 10 gm of Zn $SO_4 \cdot 6H_2$ (monoclinic) in 12 ml of distilled water, then adding 0.001 gm of Mn $SO_4 \cdot H_2O$ (monoclinic and/or orthorhombic). After stirring and filtering, the filterate was allowed to evaporate to a volume of 8 ml by putting it in an oven set at 75°C. After that it was allowed to cool slowly to room temperature. After three weeks minute crystallites were formed. They were then mounted on glass and polished for electron microprobe analysis. However, the crystallites plucked upon polishing.

Another procedure makes use of the automation facility of the krisel control (Finger and Hadidacos, 1976). For an appreciation of the problem the values of two standards used at different times will be discussed. Thus:

(A) cossyrite: Mn = 0.89 wt%

peak	background
30.367	6.89

(B) rhodonite, Mn = 28.27 wt%

peak	background
1544.141	14.43

From the above, peak values become:

For cossyrite (30.367 - 6.89) = 23.477 cps

Thus 23.477 cps = 0.89 wt % Mn,

so that 1 cps = 0.0379 wt % Mn on $\sim$ 400 ppm.

Similarly for rhodonite 1 cps = 0.0184 wt % Mn.

Even after assuming perfect electronic working conditions a pertinent question would be if a variation of 1 cps or more would not arise from factors other than change in concentration of Mn in a sample? This appears possible if the background factor used is not correct. Doing a step scan for Mg, Ca, and Fe in a standard Dr. L. A. Taylor found an average slope of background such that if the background value 500 units away from that beneath a peak value is multiplied by 1.05 (background factor = BF), the background value beneath the peak position will adequately be approximated. In the case of low concentrations of Mn the BF is not known, but a value of 1.05 was used. Suppose the BF is 1.50 instead of 1.05, then the recorded value beneath the peak should have been:

for cossyorite $\frac{1.50}{1.05} \times 6.89 = 9.84$

and for rhodonite = 20.614

Thus the peak values would be (30.367-9.84) = 20.527 cps for cossyrite; and (1544.141-20.614) = 1523.526 cps for rhodonite. Because the BF for small amounts is not known, a variation of BF as above shows that for cossyrite the cps values vary from 23.477 to 20.527, a difference of 2.95 cps. This corresponds to (2.95 × 0.0379) - 0.118 wt % Mn; i.e., 1180 ppm Mn. Similarly for rhodonite such variations correspond to 1138 ppm Mn.

Under the circumstances it appears advantageous if both background and peak intensities for each point were printed out, so that variations in the background could be used as an estimate of the reproducibility of Mn. The automation of Krisel control allows for this.

Using the cossyrite 150 background counts on samples give a mean value of 4.79 ± 0.7572 cps. Using rhodonite standard 162 background points on samples give a mean value 8.60 ± 1.09 cps. Assuming that the standard deviations might correspond to uncertainties in the BF, and thereby to Mn content, then the above variations would correspond to (0.7572 × 0.0379 =) 0.0287 wt % Mn, and (1.09 × 0.0184 =) 0.020 wt % Mn for sample analyzed using cossyrite and rhodonite standards respectively. In other words, an absolute error of about 0.03 wt % Mn is indicated using such an approach. This implies that for Mn concentrations ranging from 0.04 to 0.1 wt %, the corresponding error ranges from ± 75% to ±30%; and for concentrations ranging from 0.1 to 0.2 wt % Mn, the corresponding error ranges from ±30% to 15%.

APPENDIX C

A GRAPHICAL METHOD OF REPRESENTING LUMINESCENT PATTERNS IN DOLOMITE CRYSTALS

When studied using cathodoluminescence coarser-grained dolomite crystals show growth zones that luminesce shades of red. The luminescent zones tend to have different widths and intensities. These two parameters can be shown graphically, based on a visual assessment. The intensities can be plotted on vertical axes, brighter luminescent zones being shown at higher levels than darker zones. The widths can be shown on horizontal axes. For example, a luminescent pattern of a dolomite rhomb with a broad darker core and a narrow brighter rim can be graphically represented as shown in Fig. C-1.

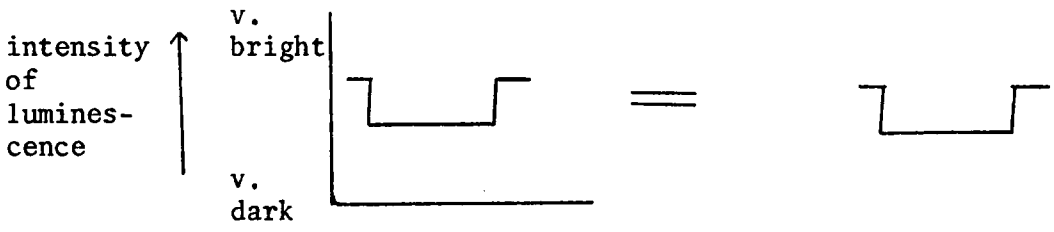

Fig. C-1. Graphical representation of a dolomite rhomb with darker core and brighter rim.

Another dolomite rhomb with a luminescent pattern of a narrow darker rim and a broader bright core can be represented as shown in Fig. C-2.

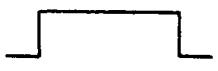

Fig. C-2. Graphical representation of a dolomite rhomb with brighter core and darker rim.

Even when quantitative measuring devices are not employed, a qualitative graphical approach could facilitate comparison of luminescent patterns. This approach does not require photographs, but as a further illustration, the luminescent pattern of a dolomite rhomb shown in the center of the photomicrograph (Fig. C-3) is depicted by the graphical method in Fig. C-3

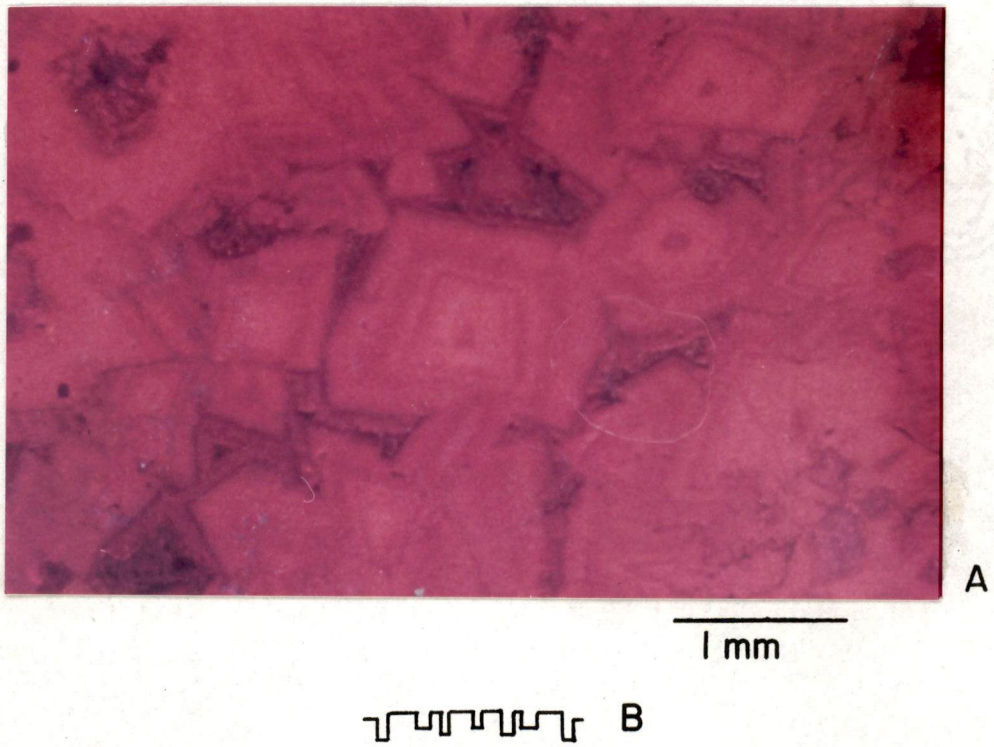

Fig. C-3. Negative photomicrograph of a partially dolomitized limestone (Sample RR-49D1).

Note: The zonal patterns of dolomites show much better when printed from the negative of a slide (above) than directly from a slide. However, the luminescent color of calcite, which in most cases is yellow, changes to a deep blue. The zonal pattern of dolomite at the center of the photograph (A) is shown by the graphical representation method (B).

APPENDIX D

CONCENTRATIONS OF TRACE ELEMENTS (ppm) IN CARBONATE MINERALS AT THE FLAT GAP MINE FROM WEST (1974)

Table D-1. Concentration of trace elements (ppm) in carbonate minerals at the Flat Gap mine from West (1974)

Sample	Cd	Zn	Fe	Mn	Sr	Fe/Mn
			A. Fine-Grained Dolomite			
P1	24	6	1472	127	50	11.5
P2	18	6	1471	200	50	7.3
P3	2	24	1424	91	7	15.6
P4	21	21	1587	225	43	7.0
P5	8	7	956	178	*	5.3
Average	15 ± 9	13 ± 9	1382 ± 246	164 ± 55	38 ± 21	9 ± 4
			B. Calcite			
L1	8	31	260	441	200	0.5
L2	8	45	81	400	188	0.2
L3	5	10	*	160	164	@
L4	7	21	167	427	141	0.39
L5	*	18	*	80	176	@
L6	12	52	310	684	173	0.4
L7	8	20	176	239	242	0.7
L8	5	26	500	551	117	0.9
L9	5	11	*	80	141	@
L10	9	29	559	160	239	3.4
L11	9	17	264	338	162	0.7
L12	5	9	*	223	200	@
L13	8	20	286	214	242	1.3
L14	8	20	168	222	247	0.7
Average	7 ± 2	24 ± 13	277 ± 150	301 ± 179	188 ± 142	0.9 ± 1.2
			C. Coarser than Fine-Grained Dolomite			
H1	14	17	1614	368	15	4.3
H2	14	9	1672	386	35	4.3
R1	30	7	2147	482	35	4.4
R2	31	22	1088	233	50	4.6
R3	16	9	2807	286	234	9.8
R4	14	9	2152	526	32	4.0
R5	8	4	3068	615	7	4.9
R6	14	9	630	200	14	3.1
R7	14	11	693	154	50	4.5
S1	11	9	1373	254	50	5.4
S2	14	7	3556	337	14	10.5
S3	37	30	1471	385	35	3.8
S4	38	77	1695	545	157	3.1
S5	24	9	2425	455	151	5.3
S6	8	*	2695	506	50	5.3
S7	14	24	1603	363	50	4.4

Table D-1 (continued)

Sample	Cd	Zn	Fe	Mn	Sr	Fe/Mn
	C. Coarser than Fine-Grained Dolomite (continued)					
S8	8	14	2217	280	36	7.9
S9	8	4	2068	297	36	6.9
S10	14	4	1931	361	15	5.3
S11	14	9	1693	501	36	3.3
S12	24	25	2530	697	50	3.6
S13	20	40	3952	626	51	6.3
S14	20	22	2902	470	14	6.1
S15	20	180	2847	459	68	6.2
T1	k4	7	977	255	50	3.8
T2	k4	7	1288	270	29	4.7
T3	24	6	993	385	29	2.5
T4	20	7	769	303	50	2.5
U1	14	9	1109	110	50	10.8
U2	20	39	1788	222	28	8.0
U3	24	12	1349	160	50	8.4
U4	*	64	2222	471	14	4.7
U5	24	260	1967	420	92	4.6
U6	55	605	1870	776	107	2.4
U7	4	*	2060	399	50	5.1
U8	10	4	1112	390	36	2.8
U9	35	34	3980	836	123	4.7
U10	14	8	1685	393	36	4.28
U11	4	11	1952	486	50	4.01
W1	24	6	1857	527	14	3.5
W2	8	6	1669	592	50	2.8
W3	20	6	2199	530	50	4.1
W4	14	6	1941	502	50	3.8
W5	14	8	2469	330	50	7.4
Average	18 ± 10	39 ± 101	1956 ± 790	412 ± 160	52 ± 43	5 ± 2

*Data not reported.

@Ratio not calculated.

Note that the Fe/Mn ratio in calcite is significantly lower than in coarser than fine-grained dolomite. This is because the Fe amount in dolomite is much higher than in calcite whereas Mn does not show such a major change. Averages are calculated based only on the number of samples for which data are reported.

APPENDIX E

STAINING TECHNIQUES

Mixing of acidified solutions of Alizarine Red S and potassium ferricyanide as described by Evamy (1963), Dickenson (1965), Friedman (1965) would help distinguish between ferroan and non-ferroan carbonates. But the mauve color that arises from such a mixed stain on ferroan dolomite is rather difficult to distinguish from the pinkish red color of calcite. It was found more useful to adopt the procedure of staining half of a slide in potassium ferricyanide and the other half in Alizarin Red S solutions. Potassium ferricyanide stain was prepared as per Lindholm and Finkleman's (1972) procedure. Deionized water (200 ml) was mixed with 2 ml of 2N HCl; i.e., a 1% HCl was prepared. Potassium ferricyanide powder (4 gm) was put in 200 ml of 1% HCl. Slides were etched in 1% HCl for 30 seconds and then inserted in the potassium ferricyanide solution for 2-3 minutes. Corners and backs were cleaned with tissue paper and the front of the slide air dried. Alizarine Red S stain was prepared using Dr. K. R. Walker's recipe. Alizarine Red S powder (1.25 gm) was dissolved in a solution of 2.5 ml of 12N HCl and 475 ml of deionized water. Slides etched in 1% HCl solution for 30 seconds were inserted in Alizarine Red S stain for 30 seconds after which they were rinsed in running water and then air dried.

APPENDIX F

COLUMNAR SECTIONS OF THE UPPER KNOX, COPPER RIDGE DISTRICT

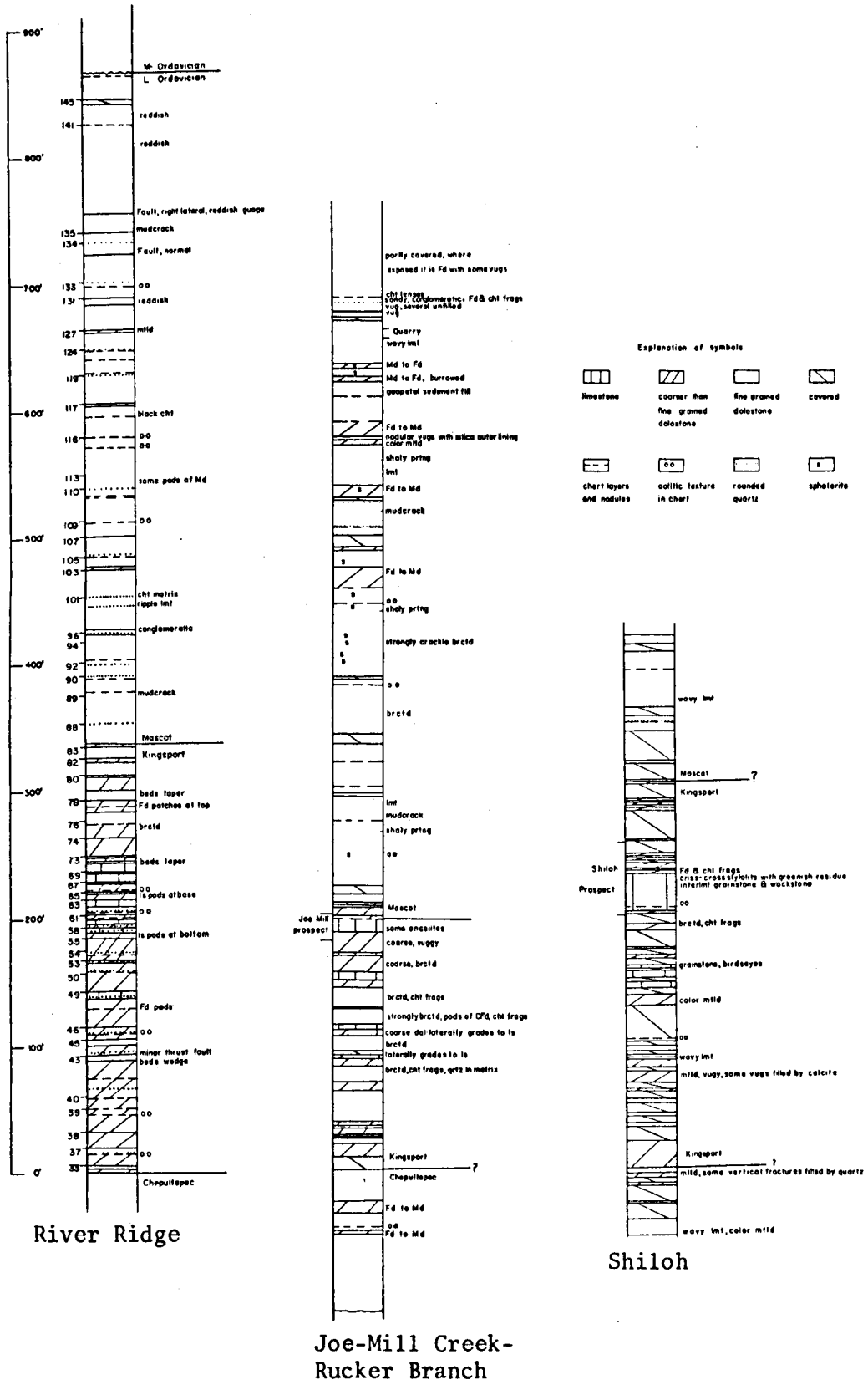

Fig. F-1. Columnar sections of the Upper Knox, Copper Ridge District.

APPENDIX G

PETROGRAPHIC DESCRIPTIONS OF CARBONATES

Table G-1. Petrographic description of carbonates from River Ridge*

Sample Number	
RR-22	Chert. Peloidal, intraclastic, oolitic (0.65 mm) relicts.
RR-23	Fd. Xenotopic, 0.05 mm. Towards top numerous coarse-grained quartz, also an intraclastic oolitic chert fragment. Fractures in chert and allochem boundaries sometimes cemented by length slow chalcedony and quartz. Dolomite grains in the top part are coarser, 0.1 mm. Faint laminations. Dispersed pyrite.
RR-25	CFd. Size mottled, poikilotopic. Generally hypidiotopic; grain size 0.2 mm (but in chert matrix it is idiotopic). Fd: xenotopic, 0.05 mm. Fd patches mostly at center of slide. Numerous subhorizontal microstylolites. Two sizes of quartz: one sub rnd. 0.05 mm, another rounded 0.5 mm. Quartz is about 20% of specimen. Fine-grained quartz less abundant in Fd patches. Para The occurrence of a lot of inclusions in CFd makes it unlikely that they formed by grain boundary migration, as also augmented by the occurrence of idiotopic CFd in chert matrix. The rarity of pyrite and absence of intergranular insoluble material in the Fd patches makes it unlikely that they were formed by grain diminution of the CFd due to stylolitization. Fd + Chert → CFd
RR-31	Fd to CFd. Perfectly size graded, coarsening upward relationship where the grain size increases from 0.04 mm at bottom to 0.14 mm at top. Numerous fine laminations also at the top part, along with color lamination due to oxidized pyrite are horizontally disposed. CFd are poikilotopic with inclusions of minerals of high interference color (calcite?). Both grain sizes of dolomite crystals have xenotopic habit, with porphyrotopes 0.21 mm in the CFd portion. Some laminae in the Fd are marked by slightly coarser 0.06 mm domites.
RR-32	CFd. Xenotopic, porphyrotopic, poikilotopic. Several grain sizes of dolomite; 0.05 mm-sized grains as inclusions, 0.09 mm generally occurring in groups. Eighty percent of slide consists of 0.12 to 0.2 mm crystals. Porphyrotopes up to 0.8 mm. Inclusions in porphyrotopes are not pushed to grain boundaries so that the porphyrotopes were not formed by boundary migration. At top left corner of slide ghost fossil (trilobite?) and pelletal material. At bottom part of slide cherty horizons are pseudomorphous after dolomite. Vugs occur in all orientations and are infilled by poikilotopic, ferroan

Table G-1 (continued)

Sample Number	
	baroque dol. Some cleavage traces in the vug-fills are oxidized to brownish material. Para Fossiliferous, pelletal Ls → Fd + chert → CFd + chert → Vf
RR-33	Fd. Xenotopic. Mostly 0.04 mm or less. Some parallel laminae. Laminae also marked by discontinuous and lensoid pods consisting of quartz and dolomite (≃ 0.06 mm).
RR-34A	CFd. Xenotopic, porphyrotopic, poikilotopic. Cherty horizons more prevalent in horizontal bands, although adjacent dolomites have chert matrix. In chert matrix dispersed dolomite grains range from euhedral rhombs of 0.05 mm to subhedral 0.25 mm with silica and dolomite inclusions. Slide has a patchy appearance with aggregates of dolomites (0.06 mm) grouped together. Such groups do not have a recognizable rhombic dolomite shape around them and have faint and uneven extinction. Anhedral porphyrotopes 0.7 mm of even extinction are loaded with silica and Fd inclusions. Para Ls → Fd + chert → CFd.
RR-34B	CFd to Fd. Porphyrotopic, poikilotopic. Color mottled, vugular. Most 0.09 to 0.1 mm. Fd 0.05 mm, and sub rnd. quartz 0.09 mm as inclusions, smaller crystals occur in groups or as inclusions in porphyrotopes, 1.0 mm; fossil and pelletal relict (under condensed light). Color mottling of CFd probably due to earlier bioturbation. Some vugs are infilled by chert with central poikilotopic CFd. Other vugs by poikilotopic baroque Vf some cleavage traces brownish. Para Fossiliferous, pelletal Ls → Fd + chert → CFd → Vf.
RR-34C	CFd. Same as RR-34B, except for the nonabundance of chert, the presence of subvertical stylolites and subhorizontal fractures infilled by more ferroan Vf. As in most cases stylolites are horizontal and fractures subvertical; this slab was probably rotated.
RR-35	CFd. Fifth percent bimodally distributed quartz. Sub rnd. quartz 0.06 mm, rounded quartz 0.5 mm. Dolomite grains 0.4 mm full of quartz inclusions, others are of variable diameter up to 0.8 mm. Subhedral and repetitively zoned. Chertified peloids, and ooids (0.2 mm). Some of them with CFd at center. Para Oolitic intrapelsparite + quartz → chert → CFd.

Table G-1 (continued)

Sample Number	
RR-36	Fd. Xenotopic, color mottled with birdseyes infilled by more ferroan Cd, some cleavage traces oxidized to brownish coloration. Generally 0.03 mm-sized Fd.
RR-38A	CFd. Xenotopic, poikilotopic, porphyrotopic, color mottled; 0.3 to 0.6 mm. Zoned with clearer rims. Pelletal ghost in porphyrotopes, 1.0 mm in the lighter colored portions. Elsewhere some fossil ghost. Fractures infilled by more ferroan CFd. Para Fossiliferous, pelletal Ls → Fd → CFd → Vf.
RR-38B	CFd. Xenotopic, poikilotopic, porphyrotopic. Size mottled between those generally 0.2 mm portions at bottom and top left, and others 0.5 mm elsewhere. Both portions have porphyrotopes up to 1.0 mm. Some crystals zoned with clearer rims. Pelletal and fossil relicts, some of them with micritic envelops? Chert near vug-fills. Vug-fill is more ferroan repetitively zoned baroque Vf. Para Fossiliferous, pelletal Ls → CFd → Vf.
RR-39A	CFd. Xenotopic porphyrotopic, poikilotopic. Mostly 0.12 to .24 mm; .05 mm crystals as inclusions. More ferroan porphyrotopes 0.4 mm. CFd zoned with clearer rims. Relict fossils. Vugs and fractures infilled by more ferroan baroque Cd. Para Fossiliferous Ls → Fd → CFd → Vf.
RR-39B	Chert. Preserved primary allochems: ooids with radial fabrics, 0.2 mm; peloids, intraclasts, few fossils with micritic envelops. Repetitively zoned vug-fill. Para Biointrapelsparite → chert → Vf.
RR-40	CFd. Hypidiotopic, porphyrotopic, poikilotopic. Portions with chert matrix. CFd: 0.16 to 0.45. Elsewhere 0.5 mm. Inclusions are corroded and of high interference color (calcite?). Relict fossils and pelletal material. Vugs infilled by baroque dol. Para Fossiliferous, pelletal Ls → CFd → Vf.
RR-41A	CFd. Xenotopic, porphyrotopic, poikilotopic. Size and color mottled. About 50% of grains 0.6 mm, about 50% 1.0 mm, some reaching up to 2.5 mm. Few areas of small grains 0.07 to 0.2 mm near stylolites. Inclusions of dolomite, quartz, calcite?

Table G-1 (continued)

Sample Number	
	Two grain sizes of quartz. Faint indication of pelletal and fossil relicts. Para Fossiliferous Ls → CFd + stylolitization → CFd.
RR-41B	CFd. Hypidiotopic, porphyrotopic, poikilotopic, zoned. Numerous sineous subhorizontal stylolites. 0.2 mm at stylolites, 0.4 mm in a shaly matrix. Such crystals have ferroan rims. Seventy percent of slide 0.8 mm. Porphyrotopes up to 2.0 mm. Aggregates of small crystals forming a bigger crystal indicated by uneven extinction at top left corner. Several pelletal and fossil relicts. Fracture infilled by more ferroan Vf. Para Fossiliferous, pelletal Ls → chert + CFd + stylolitization → Vf.
RR-41C	CFd. Xenotopic, porphyrotopic, poikilotopic, zoned. Numerous subhorizontal stylolites. Most grains 0.3 mm, porphyrotopes up to 0.8 mm. Two generations of relict fractures, and a third vertical fracture infilled by more ferroan baroque Vf. Several relict fossils. Para Fossiliferous Ls → 1st generation fracture → stylolitization 2nd generation fracture → chert → CFd → Vf.
RR-42	Fd. Xenotopic, 0.05 mm. Birdseyes infilled by po9kilotopic Vf (straight-extinction) and sometimes by quartz.
RR-43	Fd. Xenotopic, 0.02 mm. Birdseyes filled by sparry dolomite and some fractures by quartz. Rock shattered.
RR-44A	Chert. Preserved allochems: peloids, ooids 0.3 to 0.5 mm. Several rounded beads of brownish material in certain pockets. Except for their small size they resemble ooids. They are interpreted to be silica gel of caliche origin.
RR-44B	CFd. Xenotopic, mostly 0.6 mm. Inclusions of dolomite (0.13 mm) and quartz. Bimodally distributed quartz: sub rnd. 0.12 mm, rounded 0.6 mm, chert fragment.
RR-45	Fd. Xenotopic, 0.05 mm. Horizontal fracture fill. Poikilotopic baroque Vf. Faint subhorizontal laminae and few birdseyes.

Table G-1 (continued)

Sample Number	
(RR-45)	Fd. Brecciated, Fd = 0.05 mm. Vug-fill baroque. Fine-grained sphalerite. Para Fd → Vf + sphalerite.
RR-46	CFd. Xenotopic, variable grain size. Horizontally disposed quartz zones at bottom and at top. Quartz lenses near stylolites in the middle of slide. Bimodially distributed quartz: sub rnd. 0.14 mm, rounded 0.4 mm. Chert fragments with peloidal and oolitic relicts top left. Porphyrotopic, poikilotopic dolomite 1.0 to 2.2 mm, some of them appearing granulated to Fd. 0.1 mm at their grain boundaries. Some porphyrotopes are baroque, others have uneven extinction with discernible subcrystallites, yet others have sharp extinction.
RR-48	CFd. Xenotopic, porphyrotopic, poikilotopic. Mostly 0.7 mm. Inclusions of 0.03 to 0.2 mm dolomite. A few pockets of 0.2 mm dolomites. More ferroan baroque dolomite has relict fossils. Para Fossiliferous Ls → CFd → Vf.
RR-49A	Ls. Three distinct layers. Bottom layer consists of ooids, 0.5 mm with preserved radial fabrics, peloids 0.4 by 0.3 mm, intraclasts, rounded quartz 0.5 by 0.35 mm, and sub rnd. quartz 0.15 mm. Allochems cemented by drusy calcite. This grainstone zone has thin (.2 mm) laminae of micrite. At middle of slide is a layer of biopelsparite, of pellets less than 0.15 mm. Interlaminar birdseyes. Fossils: sponge, gastropod, unrecognized fragments, microboring organisms. Doubly terminated authigenic quartz occur dispersed. Top 2/3 of slide consists of biomicrite (trilobite and other fossil fragments), horizontal stylolites, pockets of pelletal lenses some of which have trilobite fragments. Some authegenic quartz. Vertical fractures infilled by calcite appear to be synstylolitization as they truncate and/or displace each other.
RR-49A$_2$	Ls. Except for a bioturbated biomicrite (few trilobites) at top, 90% slide consists of ooids 0.5 mm; a few intraclasts, peloids, and unrecognized fossil fragments, all cemented by drusy calcite. Lots of micritic envelops. Quartz at center of

Table G-1 (continued)

Sample Number	
	ooids have overgrown some of the ooids authigenically becoming euhedrally hexagonal. Subhorizontal fractures infilled by calcite.
$RR\text{-}49B_1$	Ls. Bottom 2/3 of slide consists of biointrapelsparite, birdseyes mostly at bottom of intraclasts infilled by blocky calcite. Some of the intraclasts are about 3 cm long. Most of the intraclasts consist of pellets, 0.6 mm; very few are of micrite; fossils: trilobite, other fragments, microboring organisms. Top of slide is micrite with stylolites.
$RR\text{-}49C_1$	Ls. Micrite with branching subhorizontal stylolites. Numerous dispersed pyrite.
$RR\text{-}49C_2$	Ls. An assortment of bioturbated micrite and biopelsparite (trilobite). Rounded quartz 0.45 mm with inclusions, sub rnd. quartz 0.1 mm. Moldic porsity infilled by clacite some of it in sharp contrast with poikilotopic CFd. At the same time some dolomite edges on micrite are serrated. CFd appears clear on pore spaces and cloudy over adjacent micrite. Amount of CFd, 1%.
$RR\text{-}49D_1$	Ls + CFd. Interlaminated biopelsparite (trilobite, brachiopod, other fragments) and biomicrite 50% dolomitized. Some subhorizontal stylolites. Dolomite varies from 0.3 to 2.5 mm. Mostly zoned with cloudy centers and clearer ferroan rims. Poikilotopic, some of the inclusions stained like calcite; although other inclusions do not. In unstained portions inclusions have high interference colors and are regarded to be calcite, but unstained because they are too small, or because they are embedded in dolomite. The cloudy centers therefore appear to be calcitic patches. In fact where dolomite grows across a pelsparite, pelletal ghosts are discernible. Where it grows across fillils, fossil form is retained. Where dolomite grows across pore spaces it appears learer, and cloudy on adjacent walls. At some pore spaces it grows in sharp contact with calcite cement. Even when calcite veinlets appear to cut dolomite crystals, a sharp contact between dolomite cleavages and the vein fill calcite is observed, suggesting equilibrium formation of the calcite fill and dolomite. On the other hand, some edges of dolomite on micrite are serrated, indicating that dolomite was in disequilibrium with micritic material which it was replacing.

Table G-1 (continued)

Sample Number	
	An alternative hypothesis would be that the serrated edges of dolomite on micrite, as well as the calcitic inclusions in dolomite are due to micritization of dolomite (dedolomitization). This suggestion may be countered totally, or regarded to be of insignificant consequence because of the primary allochems preserved in the limestones. Some blocky calcite has dolomite along cleavages. The shape of dolomite is rhombic in some cases, rectangular, triangular in others. Some of the edges are zig-zag. Under crossed-nicols some show wavy extinction, others have sharp extinction, still others have uneven extinction and are suggestive of aggregated crystallities of dolomite inside a bigger crystal. Where several dolomite crystals are in fitted fabric they are xenotopic and porphyrotopic. Para Ls → calcite cement + CFd → dedolomitization?
RR-49D$_2$	CFd. Xenotopic, porphyrotopic, poikilotopic. Centimicron to mm sized grains. Relict fossils and pelletal material. Some chert matrix in areas adjacent to subhorizontal microstylolites. Few rounded quartz grains 0.35 mm vertical relict fractures. Para Fossiliferous, pelletal Ls → CFd.
RR-49D$_3$	CFd. No microstylolites, better preserved relict pelletal material and fossils, few "granulated" zones of Fd 0.05 mm, otherwise same characteristics of Md as in 49D$_2$.
RR-50	Fd to CFd. Size mottled and size graded. Pockets of CFd. 0.17 mm-sized in Fd (0.05 mm). Sixty percent of slide is Fd—shows faint lamination marked by crystals 0.03 mm. Towards top left it is mostly porphyrotopic, poikilotopic CFd. Subhorizontal ferroan calcite veins.
RR-51	CFd. Xenotopic, porphyrotopic, zoned. Subhorizontal vug-fills of poikilotopic baroque Vf, latest Vf are more ferroan. Subhorizontal sinuous stylolites. Ninety-five percent of CFd: 0.6 mm except at bottom left of slide where the grain size is 0.25 mm. Relict pelletal material. Para Ls → CFd → Vf.
(RR-53A)	Vf + CFd. Most of slide vug-fill, baroque. A patch of CFd, 0.6 mm. Fine-grained sphalerite associated with Vf. Para CFd → Vf + sphalerite.

Table G-1 (continued)

Sample Number	
RR-53A	CFd. Size mottled. Porphyrotopic, poikilotopic. Patches of chert matrix ferroan CFd, 0.2 mm at middle of slide, otherwise 0.6 mm. Relict peloid. Inclusions of angular quartz crystals. 0.06 mm at top 2/3 of slide. Wavy extinct, poikilotopic ferroan Vf, horizontally disposed near top of slide. Here, patches of unreplaced micrite.
RR-53B	CFd. Xenotopic, poikilotopic. Subhorizontal ferroan baroque vug-fills. Lensoid chert with pelletal ghost. CFd 0.8 mm. Para Ls → CFd → Vf.
$RR-53B_2$	CFd. Hypidiotopic, zoned, poikilotopic. 0.2 mm laminated. Discontinuous lensoid laminae of sub rnd. quartz 0.05 mm.
RR-55A	CFd. Xenotopic, poikilotopic, porphyrotopic. 1.0 mm. Numerous pelletal, fossil relicts. Inclusions of quartz and dolomite 0.12 mm. Para Fossiliferous, pelletal Ls → CFd.
$RR-55B_1$	CFd. Xenotopic, poikilotopic, porphyrotopic, zoned, Fd and angular quartz inclusions. Most grains 1.0 mm, few pockets of 0.22 mm. Pelletal and fossil relicts. Few unreplaced micrite. Para Fossiliferous, pelletal Ls → CFd.
$RR-55B_2$	CFd. Same as above.
RR-56	Ls + CFd. Micrite with biopelsparitic (trilobite, gastropod) pockets 50% dolomitized. Zoned, clearer rimmed dolomite, some 0.45 mm, others 1.0 mm. Pelletal ghost. Subhorizontal microstylolites. Some dolomites on micrite have serrated edges. Para Pelletal Ls → calcite cement + CFd → dedolomitization?
$RR-58A_1$	Ls. Micrite, burrowed, few dispersed dolomite of various grain size, 0.1, 0.2, 0.5 mm. Some crystals at porosity sites have sharp contact with dolomite. But on micrite some dolomite edges are serrated; and some dolomites have rounded shape.
$RR-58A_2$	Ls. Interlaminated micrite and intrapelsparite. Micrite horizontally burrowed.

Table G-1 (continued)

Sample Number	
RR-58B	Ls. Micrite stylolitized. Rounded, poikilotopic quartz 0.3 to 0.8 mm. Clearer rimmed, zoned Md 0.12 to 0.5 mm make up 1% of slide. Some of those dolomites have serrated edges, possibly due to micritization (dedolomitization).
RR-59A	CFd. Senotopic, poikilotopic, some zoned. Subhorizontal stylolites and baroque vug-fills. CFd = 0.8 mm. Pelletal ghost. Few interstitial chert. Para Ls → chert → CFd → Vf.
(RR-59B)	CFd. Hypidiotopic. Zoned, cloudy centered. 0.5 to 0.65 mm. Few rounded quartz: 0.5 to 0.8 mm. Fine-grained sphalerite associated with Vf.
RR-59B	CFd. Xenotopic, poikilotopic, porphyrotopic, zoned. Few rounted quartz 0.3 to 0.7 mm, angular quartz 0.15 mm in subhorizontal laminae. In a shaly matrix rhombs 0.5 mm. Most, however, 0.8 mm, some have ferroan calcitic edges (dedolomitization). Para Impure Ls → CFd → calcitization.
RR-60A	Ls. Pelletal, trilobite biopelsparite, faintly laminated, subhorizontally stylolitized. 3/4 of slide scattered dolomite mostly at stylolites. Top 1/4 of slide trilobite, gastropod biointrapelsparite. Amount of CFd 1%. Some dolomite edges on peloids are serrated.
RR-60B$_1$	Ls. Interlaminated biopelsparite and biomicrite (horizontal burrow). Fossils: trilobite, brachispod, gastorpod, ostracod, pelmatozoa, sponge?, microboring organisms. Rare CFd. Some of it in sharp contact with calcite cement at porosity sites. But on micrite some dolomite edges are serrated. Peloidal ghost. Several doubly terminated quarts. Para Ls → CFd + calcite cement.
RR-60C	Ls. Interlaminated biopelsparite and biomicrite. Fossils: brachiospod, trilobite, pelmatozoa, gastropod, condont? 15% dolomitized to CFd 0.3 mm. Numerous doubly terminated quartz crystals. Dolomite characteristics same as in 49D$_1$. Para Ls → drusy and blocky calcite cement + CFd → dedolomitization?

Table G-1 (continued)

Sample Number	
RR-60D	Ls. Interlaminated biomicrite and biointrapelsparite. Fossils: trilobite, astropod, brachiopod, pelmatozoa, microboring organisms. Rare CFd 0.21 mm on micrite to coarser elsewhere. Some dolomite edges on micrite are serrated. Whispy stylolites on micrite.
$RR\text{-}63A_1$	Ls. Interlaminated, biomicrite, and biointrapelsparite. Fossils: gastropod, trilobite, pelmatozoa, sponge, microboring organisms. Biomicrite burrowed, subhorizontally stylolitized. Circular shaped, poikilotopic dolomite with serrated edges 0.5 mm on biomicrite—0.5% of slide.
$RR\text{-}63A_2$	Ls. Pelsparitic and micritic, 60% dolomitized to CFd. Characteristics same as $49D_1$.
$RR\text{-}63B_1$	Ls. Interlaminated biointrapelsparite and biomicrite. Fossils: trilobite, brachiopod, gastropod, astracod. Biomicrite horizontally burrowed, whispy stylolites. Rare CFd but more developed on intrapelsparite. Characteristics same as $49D_1$.
$RR\text{-}63B_2$	Ls. Micrite with rare fossil fragments of trilobite, other fragments. Few scattered dolomite mostly 0.2 to 0.3 mm, and mostly circular shaped and with serrated edges. Porosities infilled by drusy calcite, vertical veinlets by dolomite. Rare 0.6 mm sized dolomites. Several whispy microstylolites associated with some dolomite.
$RR\text{-}63C_1$	Ls. Micrite with biopelsparite layer towards the bottom. Fossils: trilobite, unrecognized fragments. Burrowed. CFd, 0.3 to 1.3 mm at burrow sites. Subhorizontal microstylolites at very bottom and towards top. Some dolomite edges on micrite are serrated. Para Ls → drusy calcite cement + CFd → dedolomitization?
$RR\text{-}63C_2$	Interlaminated biointrapelsparite and micrite. Fossils: trilobite, brachiopod, pelmatozoa microboring organisms, unrecognized fragments. Round poikilotopic quartz 0.4 to 0.8 mm most at or adjacent to stylolites. Also rounded chert 0.3 mm, 3 ooids. 2% dolomitized. CFd scattered in micrite and micritic intraclasts generally 0.12 to 0.2 mm. Those associated with spary calcite are coarser. Some dolomites on micrite have serrated edges. Also, some have rounded shapes.

Table G-1 (continued)

Sample Number	
RR-64	Ls. Interlaminated biopelsparite and micrite. Stylolites on micrite, and zoned CFd, more abundant at them. CFd 2% of slide. Fossils: trilobite, gastropod, ostracod, pelmatozoa, micriboring organisms. Dolomite over pelsparite shows excellent preservation of interallochem cement. One CFd has hexagonal shape (after quartz?). Some edges of dolomite on micrite are serrated.
RR-65A	Ls. Interlaminated biopelsparite (few intraclasts) and biomicrite. Micrite horizontally burrowed with diffuse burrow boundaries. Fossils: trilobite, brachiopod, pelmatozoa, gastropod, ostracod, sponge?, microboring organisms. 3% dolomitized. CFd 0.2 mm dispersed in micrite up to 2.5 mm on sparite. (CFd description see $49D_1$.) Interallochem porosity infilled by drusy calcite. Moldic porosity by blocky calcite, sometimes in sharp contact with dolomite. At top of section part of pelmatozoa and brachiopod are infilled by length slow chelcedony. Not sure if inclusions in pelmatozoa are micro-dolomite. Few dispersed pyrite. Subhorizontal stylolites. Para Ls → calcite cement → CFd → dedolomitization.
RR-65B	Ls. Fewer fossils, no brachiopod, otherwise same as above.
RR-66	CFd + chert. CFd: porphyrotopic, poikilotopic, pelletal ghost. 0.8 mm with more ferroan baroque. Chert has oolitic and peloidal ghost.
RR-67	CFd. Hypidiotopic, poikilotopic. 0.2 to 0.3 mm with interstitial chert. Quartz laminated; sub rnd. quartz 0.09 mm; ounded, poikilotopic quartz 0.6 to 0.9 mm. Dolomite grain size in quartz laminae 0.1 mm.
RR-68A	Ls. Biointrapelsparite with interlaminar birdseyes. Slightly dolomitized towards top of section. Poikilotopic dolomite up to 3.0 mm in grain size. Few unrecognized fossils with micritic envelops. Allochems primarily peloids, then intraclasts, all cemented by drusy calcite, sometimes in sharp contact with wavy extinct dolomite. Some edges of dolomite on micrite are serrated. Some authgenic quartz, sometimes with slender habit 0.03 by 0.7 mm. Para Ls → drusy calcite cement + CFd → dedolomitization?
(RR-68A)	Ls. Same as above.

Table G-1 (continued)

Sample Number	
RR-68B	Ls. Biointrapelsparite, 1% dolomitized. Few fossils: trilobite, ostracod, gastropod, pelmatozoa. Dolomite crystals concentrated at middle of slide which has bigger micritic, burrowed intraclasts through which runs a stylolite.
RR-68C	Ls. Interlaminated biointrapelsparite and micrite, 10% dolomitized. Dolomite character same as $49D_1$. Slender authgenic quartz. Fossils: gastropod, unrecognized fragments. Stylolite winds through some dolomite crystal. Micritized dolomite outlines on micrite. Para Ls → calcite cement + CFd + stylolitization → dedolomitization.
RR-68D	CFd + Ls. Intrapelsparitic and micritic Ls 70% dolomitized. CFd character same as $49D_1$.
RR-69	CFd. Poikilotopic 0.3 to 0.5 mm. Quartz laminated. Inclusions of Fd. Disseminated pyrite and microstylolites at quartz laminae. Sub rnd. quartz 0.08 mm. Quartz laminae are lensoid. Most edges of dolomite crystals are serrated.
RR-70A	Ls. Biopelsparite. Horizontal stylolites. Severally algally quoted grains. Fossil types unrecognized. 5% dolomitized to CFd. (Same as $49D_1$.)
RR-70B	Ls. Interlaminated (algal) micrite and pelsparite. Horizontal stylolites on micrite. Few rounded dolomite 0.2 mm. Several authgenic quartz.
RR-70C	Ls. Biointrapelsparite 1% dolomitized to CFd (0.2 mm). Bridseyes filled by blocky calcite sometimes in sharp contact with dolomite, but some edges of dolomite on micritic intraclasts are serrated. Interallochem cement drusy calcite. Fossils: gastropod, unrecognized fragments with micritic envelops.
RR-70D	Ls. Interlaminated biointrapelsparite and biomicrite. 40% dolomitized. Fossils: trilobite, sponge?, unrecognized fragments. Isolated CFd on micrite mostly 0.2 to 0.3 mm; on intrapelsparite 0.5 to 2.8 mm. Zoned, mostly clearer rimmed with peloidal ghost. Poikilotopic with calcite and sub rnd. quartz (.09 mm) inclusions. Subhorizontal stylolites mostly associated with CFd. Some edges of dolomite are serrated particularly when on micritic material.

Table G-1 (continued)

Sample Number	
RR-71	Fd. Laminated, horizontally disposed discontinuous and lensoid quartz at laminae. Quartz 0.04 to 1.0 mm-sized, also pyrite disposed parallel to laminae. Fd, mostly 0.02 mm, some .05 mm.
RR-72	Ls + CFd. Interlaminated biopelsparite and biomicrite 50% dolomitized. Fossils: trilobite, gastropod, ostracod, unrecognized fragments, microboring organisms. CFd same as 70C.
(RR-72)	Ls + CFd. Interlaminated biopelsparite and biomicrite. Fossils: trilobite, gastropod, ostracod, unrecognized fragments. CFd, variable sizes mostly 0.8 mm. Some zoned with cloudy centers. A dolomite crystal that crosses trilobite appears micritized yet the trilobite shape is preserved.
RR-73	Ls. Micrite, wavy laminated (algal?), also quartz laminated. Quartz 0.05 mm. Dispersed pyrite. Horizontal stylolites. Horizontally disposed patches of pelletal material at middle. Few rounded grains of Md 0.4 mm.
RR-74B	CFd. Xenotopic porphyrotopic. Most grains 0.25 to 0.5 mm. Porphyrotopes up to 2.0 mm, and have wavy extinction.
RR-76E	Fd. Xenotopic, 0.02 mm. Few porphyrotopes, 0.06 mm. Crackle brecciated, and fractures infilled by ferroan baroque dolomite.
RR-77B	Fd. Xenotopic. Most 0.05 mm. Few porphyrotopes, 0.09 to 0.2 mm subvertical calcite veinlets. Minor calcitization at bottom left. Para Fd → calcitization.
RR-77C	CFd to Fd. Hypidiotopic interstitial brownish material. Most grains 0.09 to 0.14 mm. Few poikilotopic grains 0.17 mm. Faintly laminated (condensed light), also pyrite laminae.
RR-77D	CFd. Xenotopic, porphyrotopic, poikilotopic. Generally baroque dolomite 0.75 mm, except at horizontal stylolites where crystals 0.25 mm. Some grains are zoned, pelletal and fossil relicts. Para Ls → CFd + stylolitization?

Table G-1 (continued)

Sample Number	
RR-78B	Cfd. Xenotopic, porphyrotopic, poikilotopic, baroque dolomite. Variable but centimicron to millimeter sized crystals. Mostly 0.6 mm, some 0.3 mm. Porphyrotopes up to 2.8 mm. Several relict fossils some of them with micritic envelops. Para Fossiliferrous Ls → CFd.
RR-78F	Fd. Xenotopic 0.07 mm. Size laminated. Alternating laminae in addition to 0.07 mm-sized crystals have 0.14 mm-sized crystals. Also birdseyes features filled by dolomite and chert occur on these zones. Few dispersed rounded poikilotopic quartz grains 0.6 mm. Cathodoluminescence shows distinct quartz laminae.
RR-79A	CFd. Chert with variable-sized dolomite rhombs 0.05, 0.2, 0.5 mm overlain by xenotopic CFd 0.12 mm. Autobrecciation fractures are sometimes infilled by radial sheathes of length-fast chalcedony.
RR-79B	Fd. Xenotopic 0.05 to 0.09 mm. Birdseyes features infilled by ferroan poikilotopic Vf and sometimes quartz. Nodule at bottom in mostly infilled by length-slow chalcedony followed by poikilotopic quartz. Note: Chert-matrix part better observed using cathodoluminescence is also seen with the naked eye by holding the slide against light, which would show color mottling.
RR-79C_1	CFd. Xenotopic, poikilotopic, color mottled as above. Most crystals 0.12 mm. Poikilotopes 0.17 mm. Vugs infilled by poikilotopic baroque dolomite.
RR-79C_2	CFd. Color mottled. Xenotopic, highly poikilotopic; some crystals zoned with clearer, ferroan rims. 0.12 to 0.3 mm. Porphyrotopes up to 0.7 mm. Vugs infilled by baroque dolomite. No chert-matrix apparent except (when observed under a luminoscope), or to the naked eye where patches of dolomite appear yellowish. Relict fossils. Para Fossiliferous Ls → CFd → Vf.
RR-79D	FD to CFd. Size mottled. Most grains 0.08 mm, some patches of finer grained 0.05 mm associated with carbonaceous material? Other patches of coarser material 0.3 mm in a shaly zone. Scattered porphyrotopes of 0.15 mm.

Table G-1 (continued)

Sample Number	
RR-79F	CFd. Xenotopic, poikilotopic, porphyrotopic. Generally 0.8 mm. All crystals wavy extinct. Vug-fills have arcuate edges as well (baroque). Some crystals zoned with clearer rims. Relict pelletal material and fossils. Para Fossiliferous Ls → CFd → Vf.
RR-79G	CFd. Xenotopic, poikilotopic, porphyrotopic. Generally 0.8 mm. Vug-fills more ferroan and baroque. Relict, pelletal, peloidal and fossils (condensed light). Para Biointrapelsparite → CFd → Vf.
RR-81A	Fd. Xenotopic, porphyrotopic, color mottled. Mostly 0.07 mm. Faint lamination due to darker material at middle. Brownish staining due to interstitial pyritic material. Porphyrotopes 0.14 to 0.22 mm. Nodular vug-fill of poikilotopic quartz, followed by ferroan baroque.
RR-81B	CFd. Xenotopic, porphyrotopic. Pelletal relict. 0.6 mm. Some porphyrotopes up to 1.0 mm. Subhorizontal microstylolites. Vertical ferroan vug-fills.
RR-81C	Fd to CFd. Wavy, quartz laminae. Intimately intergrown Fd 0.02 to 0.05 mm crystals up to 0.14 mm. Sub rnd. quartz 0.09. Few rounded quartz 0.6 mm. Dispersed opaques.
RR-82A	CFd. Same as 79G, except for presence of small patch of 0.2 mm at middle right edge of slide. Color mottled possibly due to earlier bioturbation.
$RR\text{-}82B_1$	CFd to Fd. Faintly laminated. Brownish laminae. Intimately intergrown Fd 0.02 to 0.05 mm with poikilotopic CFd, 0.14 mm. Towards top of slide CFd more prevalent than at bottom; i.e., coarsening upward relationship.
$RR\text{-}82B_2$	CFd. Xenotopic, porphyrotopic, poikilotopic. Generally 0.3 to 0.7 mm. Repetitively zoned. Porphyrotopes up to 1.0 mm. Vugs infilled by repetitively (ferroan) zoned baroque. Interstitial cherty and shaly material with minute flaky crystals. Minor patch unreplaced Ls.
RR-82D	CFd. Hypidiotopic. Mostly 0.8 mm. Porphyrotopic pelletal ghost. Relict fauna. Abundant chert-matrix. Vugs filled by ferroan baroque dolomite.

Table G-1 (continued)

Sample Number	
(RR-83A)	Cd + CFd. Mostly baroque vug-fill. Few breccia fragments of CFd = 0.14 mm. Dissiminated pyrite in Md. Fine-grained sphalerite associated with Vf.
R-83A	CFd. Poikilotopic, porphyrotopic. Generally 0.6 mm. Some dispersed crystals as low as 0.06 mm in chert-matrix. Relict pelletal and fossil material.
$RR\text{-}83B_1$	Breccia. Chert-matrix breccia. Fragments of CFd (0.15 mm). Fractures in chert filled by quartz and ferroan baroque Vf.
$RR\text{-}83B_2$	Breccia. Coarse, baroque dolomite matrix between breccia. Fragments of CFd (0.15 mm) faintly laminated.
RR-83C	CFd. Hypidiotopic, poikilotopic, 0.4 mm. Interstitial shaly material with some pyrite. Few minute grains of quartz as inclusions.
RR-84A	CFd to Fd. Size mottled and size graded. Bottom 1/6 of slide: hypidiotopic, poikilotopic, porphyrotopic, generally 0.2 mm; porphyrotopes 0.4 mm, zoned; cherty and shaly matrix with quartz and mica flakes. Middle part of slide: xenotopic, porphyrotopic, poikilotopic, generally 0.15 mm; pockets of Fd 0.05 to 0.07 mm; porphyrotopes 0.25 to 0.4 mm; clusters of Fd between porphyrotopes; inclusions in porphyrotopes at edges of crystals. Top 1/4 of slide generally 0.5 mm, corroded edges, some dispersed grains as small as 0.15 mm; about 50% cherty and shaly material with quartz and mica flakes. This part appears to be altered to silica as evidenced by rhombohedrally dispersed mica flakes, corroded edges of dolomites, and early fracture fills that extend beyond dolomite crystals. Subhorizontal baroque Vf towards the top part. Laminated. Para Fd → CFd + chert → silicification.
RR-85A	CFd to Fd. All types of grain sizes from 0.02 to 1.2 mm. Full of silica and shaly matrix and stytocumulates Fd and coarser CFd pockets have less silica. Note: This is a bed parting horizon.
RR-85B	Chert. Preserved alegal laminae. Few dolomite rhombs 0.4 mm, coarser pyrite cubes. Most fracture filled by drusy quartz and some by Vf. Note: This is a bed parting zone.

Table G-1 (continued)

Sample Number	
RR-86A	Fd. Xenotopic, 0.05 mm. Few lensoid quartz laminae; quartz 0.09 to 0.2 mm. Subvertical opaque interstitial zones. Possible algal feature.
RR-86C_2	Fd. Xenotopic, 0.05 mm. Mottled by presence of pockets of 0.02 mm-sized crystals. Fractures infilled by clearer baroque dolomite and sometimes by quartz. Nodule infilled by length-slow chalcedony and poikilotopic quartz.
RR-87B	CFd. Xenotopic. Size mottled. Generally 0.1 mm but with criss-crossing areas of 0.01 mm-sized crystals. Few poikilotopic, porphyrotopes 0.22 mm. Vug-fills at bottom right with granulated fracture infills.
RR-88A	CFd to Fd. Size graded. Fining upward relationship. Bottom 1/2 of slide: xenotopic, shaly (quartz, mica flakes) laminated, generally 0.12 to 0.2 mm; porphyrotopes 0.3 mm. Overlain by Fd: 0.02 to 0.06 mm and CFd: 0.15 mm, with lots of rounded, poikilotopic quartz 0.45 to 1.2 mm. Some quartz are wavy extinct. Some of the inclusions appear to be carbonates. Top 1/6 of slide consists of Fd 0.01 to 0.05 mm.
RR-88B	CFd to Fd. More or less the same as 88A. Some of the rounded quartz are cut by fine dolomite seams.
RR-89D_1	Fd. Xenotopic, 0.02 to 0.05 mm. Crackle brecciated and infilled by more ferroan baroque. Chert nodule with semi-elliptical lamination (caliche), major axis horizontal.
RR-89D_2	CFd. Mostly 0.17 mm, porphyrotopes 0.3 to 0.5 mm. Cherty matrix with drusy quartz crack fills. 15% vugular feature and infilled by more ferroan baroque.
(RR-89D_2)	Vf. Most varoque Vf. Few portions of CFd: 0.14 to 0.17 mm.
RR-89E	Fd. Xenotopic, size graded, 0.01 to 0.05 mm, wavy laminae—few discontinuous lensoid quartz zones. At center. Lensoid chert with an inner zone of Fd. Top 1/5 generally 0.06 to 0.15 mm, becoming mostly 0.15 mm at very top. Numerous poikilotopic rounded quartz, mostly 0.6 mm.

Table G-1 (continued)

Sample Number	
RR-89G	CFd. Xenotopic, mostly 0.14 mm. Abundant shaly matrix. Some chert fragments. Rounded, poikilotopic quartz mostly 0.5 mm. Lots of sub rnd. quartz, 0.06 mm. Subhorizontal calcite veinlets. Pockets of coarser 0.5 mm-sized crystals.
RR-90A	Sandstone + CFd. 50% rounded and sub rnd. quartz, 40% CFd: 0.17 mm. Chert fragments and shaly horizons.
RR-90B	Fd. Xenotopic, wavy laminae. 0.02 to 0.05 mm-sized. 0.02 mm at laminae (algal?) sites. Discontinuous lensoid quartz horizons between laminae. Fd at quartz lenses 0.05 mm. Disseminated interstitial opaques. Possible raindrop casts in the form of round beads 1.5 mm in diameter infilled by Fd.
RR-90C	Fd. Xenotopic, size mottled. Generally 0.01 mm. Few pockets of 0.05 mm with quartz. Fractures infilled by quartz and clearer dolomite. Birdseyes infilled by baroque.
RR-90D	Fd. Xenotopic, size mottled. 0.02 to 0.05 mm. 0.02 mm possibly at algal sites. Some dolomites up to 0.14 mm in angular quartz lenses, the quartz being 0.06 mm. Some vugs infilled by chert, fractures by clearer dolomite.
RR-90E	Chert. Oolitic 0.5 to 0.6 mm in diameter. Fractures infilled by sheathes of chalcedony, some of them length-slow. Fd: 0.05 mm at bottom and at top.
RR-92A	Fd. Xenotopic, size mottled. Mostly 0.02 mm. Few 0.05 mm. Some up to 0.06 mm at quartz zones. Sub rnd. quartz 0.05 mm. Vertical escape burrow, capped by algal? laminae.
RR-92B	Fd. Xenotopic. Laminated. Mostly 0.02 to 0.03 mm. 0.05 to 0.07 mm along horizontal quartz laminae. Quartz-free wavy laminae at bottom. Color mottling (bioturbated?) at middle.
RR-92C	Fd. Xenotopic, 0.02 to 0.05 mm. Dispersed, rounded, poikilotopic quartz 0.6 mm mostly at bottom and top. Needle shaped inclusions in quartz traceable to replacing dolomite. Few rounded chert fragments. Few sub rnd. quartz 0.07 mm. Bridseyes filled by clearer Cd.
RR-92D	Fd. Xenotopic, wavy laminated. Mostly 0.03 mm. 0.05 mm at quartz-bearing lenses and pockets. Few rounded quartz.

Table G-1 (continued)

Sample Number	
RR-94D	Fd. Xenotopic. Size mottled, 0.02 to 0.06 mm. Few rounded quartz. Few fractures and vugs infilled by more ferroan dolomite.
RR-94E	Fd. Xenotopic. Mostly 0.07 mm. Few sub rnd. quartz 0.07 mm.
RR-95A	Fd. Intraclastic dolomite. Generally 0.02 to 0.05 mm. Intraclasts are composed of the finer fraction.
RR-95B	Fd. Xenotopic. Laminated. Mostly 0.05 mm. Cherty horizons with horizontally interlaminated internal structure.
RR-96A	Sandstone. Bimodally distributed; predominantly rounded quartz mostly 0.6 mm; sub rnd. quartz .05 to .07 mm. Some needle-shaped inclusions (rutile?) in rounded quartz, some of the quartz is 3/4 replaced by microdolomite. Few chert fragments. Cementing material is sooty and appears to be replacement of quartz. One rounded feldspar grain.
RR-96B	FD + sandstone. Bottom layer, xenotopic Fd 0.02 mm. Top 2/3 Fd laminated sandstone. Bimodally distributed quartz but mostly rounded, poikilotopic quartz, few chert fragments. At very top, replacement of quartz and chert by dolomite gives rise to coarse crystals 0.7 to 1.2 mm some of which have calcitic rims.
RR-97	Fd. Xenotopic, poikilotopic, 0.01 mm. Faintly laminated. Subvertical veinlets of more ferroan dolomite.
FF-98A	Fd. Intraclastic dolomite. Intraclasts consisting of some fragments of xenotopic, 0.02 mm, other fragments 0.05 mm. Host material is sub rnd. quartz and dolomite 0.05 to 0.11 mm. Some dolomite in chert matrix reaches up to 0.22 mm. Also, more ferroan vug-fill dolomite reaches up to 1 mm.
RR-98B	Fd. Intraclastic dolomite. Intraclasts: some size mottled with 0.02 mm but mostly 0.05 mm, others 0.03 mm. Host: generally variable grain size, some areas 0.05 to 0.07 mm, other areas 0.17 mm some with chert matrix. Abundant vug-fills of more ferroan Vf.—Some of them baroque, others with straight extinction. Rounded quartz on some intraclasts as well as on host.

Table G-1 (continued)

Sample Number	
RR-99A	Fd. Xenotopic, 0.05 mm. Faintly laminated. Microstylolites along quartz laminae. Few pockets of vug-fill and poikilotopic CFd. Several subvertically cracks fills by brownish material and dispersed pyrite—sometimes by calcite.
RR-99B	Fd. Xenotopic. Coarsening upward. Size grading from 0.03 mm at bottom to 0.07 mm at top. Faintly laminated with quartz lenses in between laminae. Scour and fill feature at middle. Microfaults at bottom. Several horizontal stylolites, some of them displaced by microfaults. Birdseyes infilled by more ferroan Vf.
RR-99D$_1$	Fd. Xenotopic, porphyrotopic, size graded, wavy laminae. Most of slide 0.02 to 0.06 mm. At bottom mostly 0.09 mm, with some porphyrotopes reaching 1.2 mm. Numerous angular quartz.
RR-99D$_2$	Fd. Color and size mottled. Patches of 0.02 mm in a generally 0.05 to 0.07 mm-sized crystals. Numerous birdseyes infilled by Vf.
RR-102	Sandstone. Mostly coarse grained, rounded 0.6 mm; cemented by a sooty, brownish material and silica.
RR-103A	Chert. Patchy internal structure. Fractures infilled by chalcedony and quartz.
RR-103B	Fd. Xenotopic, mostly 0.05 mm. Few sub rnd. quartz adjacent to microstylolites.
RR-105A	Fd. Xenotopic, 0.05 mm. Faintly laminated, pockets of CFd: poikilotopic, porphyrotopic, 0.1 to 0.4 mm.
RR-105B	Fd + chert. Fd: size mottled, generally 0.03 mm, with patches of areas of crystals up to 0.07 mm. Chert: as matrix, also peloidal and oolitic (0.6 mm), not sure if of caliche origin. Dispersed sub rnd. quartz. (Unit 106 of Harris?)
RR-107	Fd. Xenotopic, 0.05 mm. Patches of CFd in a shaly matrix—zoned CFd—up to 0.8 mm in size.
RR-109A	Fd. Hypidiotopic, porphyrotopic, poikilotopic. Faintly laminated. Mostly 0.09 mm. Some porphyrotopes 0.15 mm.

Table G-1 (continued)

Sample Number	
RR-109B	Fd. Xenotopic; faintly laminated; disseminated pyrite cubes along laminae imparting brownish coloration. Mostly 0.02 mm, porphyrotopes up to 0.05 mm. Rounded and sub rnd. quartz laminae towards top. Subhorizontal fracture filled by Vf.
RR-109C	Chert. Oolitic textures: 0.2 to 0.4 mm sized. Few elongate fragments. Towards bottom left, possible "geotropic" lengthening, and interference of growth of two or more oolitic textures. Fractures infilled by chalcedony and quartz. At very bottom Fd: 0.05 mm-sized crystals. Probably oolitic texture of caliche origin, not involving replacement of oolitic limestone.
(RR-113)	CFd. Size mottled. Variable grain sizes from 0.14 to 3.0 mm, mostly 0.4 mm slightly poikilotopic. Patches of Fd = 0.5 mm. Patches of shaly material, and chert. Few rounded quartz grains. Baroque vug-fills. The uneven boundary of the Fd patches suggests that they are not reminiscent ob bioturbation, nor are they breccia fragments.
(RR-131)	Fd. Xenotopic, 0.05 mm, few porphyrotopes up to 0.1 mm. Numerous dispersed pyrite.
RR-136	Fd to CFd. Size mottled and full of relict features. Intraclasts, some of them containing oolitic material. Numerous algally? quoted grains including some oncolites, peloids, some fossil? fragments. 0.02 mm-sized crystals on algal? sites and throughout some intraclasts and peloids; 0.05 mm on some intraclasts and peloids. 0.12 to 0.3 mm, and chert as interallochem cement. Vug-fills: in some places surrounded by chert, some of them with straight extinctions, others baroque. Note: This slide is from the bed immediately above a greenish shale (bentonite?) itself overlying the most conspicuous "mudcracks" observed in the field.

*Note: Ls = limestone; Fd = fine-grained dolostone; CFd = coarser than fine-grained dolomite but not occurring as vug-fill; Vf = coarse-grained dolomite occurring as vug-fill; Para = paragenesis.

Table G-2. Petrographic description of carbonates from Joe Mill-Rucker Branch Creeks*

Sample Number	
J-1	Fd. Size mottled; mostly 0.025 mm, and some with 0.05 mm. Shows wavy laminae with disseminated pyrite. Laminae at bottom show scour and fill feature. Nodular vug-fills at bottom and top. Bottom nodule grow after length-slow chalcedony. Vug-fill is highly poikilotopic, wavy extinct, and with arcuate cleavages (baroque).
J-3	CFd. Size mottled. Majority 0.12 mm with patches of 0.05 mm. The 0.12 mm-sized, tend to be in a chert matrix and are hypidiotopic, zoned with ferroan rims. Some appear to be related to stylolites as they taper away from the several sinuous but horizontal stylolites. Bottom part of the section is mostly 0.12 mm, i.e., an indistinct fining upward grain size relationship. Some pyrite. Subvertical veinlets of ferroan dolomite. Para Fd → chert + stylolitization → CFd.
J-4	Fd. Size mottled. Most with 0.05 mm. Few rhombs 0.12 mm and occur in a chert-matrix. Some are pseudomorphous after a crystal of slender habit. Chert appears related to stylolite and has numerous pyrite inclusions. Fractures are infilled by ferroan dolomite (baroque). Para Fd → stylolitization + chert → CFd.
J-5	CFd to Fd. Size and color mottled. Possibly bioturbated (burrowed). One group consists mostly of euhedral crystals 0.04 mm dispersed in a chert matrix. Another variable, between 0.07 to 0.12 mm. This shows more fitted hypidiotopic fabric. This group is interpreted to represent burrow sites. A third group is clearer and ferroan, some of it pseudomorphous after a crystal of slender habit 0.05 by 0.25 mm. Here general crystal size is 0.2 mm. Para Ls → chert + Fd → ferroan CFd.
J-6	Fd. Xenotopic, mostly 0.05 mm. Color mottled, with pyrite and insoluble residue at microstylolites. Vugs infilled by Cd over a geopetal sediment fill mostly of ferroan dol 0.05-0.07 mm with hypidiotopic fabric. Vf are baroque. Some are pseudomorphous after a slender crystal (gypsum?). Mostly Vf are ferroan and are brecciated by calcite. Vf are poikilotopic sometimes with quartz inclusions. Often lining of walls is marked by silica. Para Fd → silica → ferroan Vf → calcite.

Table G-2 (continued)

Sample Number	
J-7	Fd. Xenotopic, mostly 0.05 mm. Some size mottling at bottom with patches of crystals 0.08 mm-sized in the vicinity of sub-horizontal microstylolites. Poikilotopic, wavy extinct ferroan vug fills, after a lining of chalcedony, some of which has crystallized to quartz. Para Fd → silica → Vf.
J-8	Fd. Xenotopic, mostly 0.05 mm; some pockets of ferroan CFd, 0.14 mm. Some lensoid vug-fills of silica, mostly quartz (birdseyes). Para Fd → silica.
J-10	Fd. Xenotopic. Brecciated, mostly 0.08 mm porphyrotopes 0.14 mm dispersed pyrite and sub rnd. quartz. Fractures infilled by poikilotopic baroque Vf. Inclusions in Vf are dol. and quartz although near sphalerite Vf do not have quartz or dolomite inclusions. Para Fd → crackling → Vf + sphalerite.
J-11	Fd. Brecciated. Well laminated with corresponding size difference; i.e., a band of xenotopic Fd (0.03 mm) alternating with that of another (= 0.05 mm-sized crystals). The 0.05 mm size are associated with angular quartz. Microstylolites with associated pyrite parallel to the lamination. Some laminae are broken by scour and fill feature. Some have laminae-aligned birdseyes infilled by Vf. Porphyrotopes up to 0.14 mm occur in the quartz zones. Fracture is infilled by baroque Vf, and in one corner by sphalerite. Some fractures infilled by quartz. Pyrite more abundant adjacent to breccia fills. Para Fd + quartz → quartz + Vf + sphalerite.
J-12	Chert. Well preserved primary allochems—ooids of variable diameters but mostly 0.4 mm, peloids of various sizes, intra-clasts; all cemented by chalcedony and drusy quartz. Judging from the arrow on the specimen and the orientation of elongate fragments the original rock must have been rotated by 90°. The ooids do not interfere with each other, neither was a geotropic lengthening indicative of caliche origin (Dunham, 1969) observed.
J-13	Fd. Algal stromatolitic head at least 6 cm tall. Most of the dolomite crystals here are 0.01 mm sized. Laminae marked by color mottling. Some dispersed porphyrotopes = 0.1 mm. Inter-laminar birdseyes are variously shaped: those with sharp

Table G-2 (continued)

Sample Number	
	bottoms and uneven tops (stromatactid type) and vice versa, as well as perfectly rounded shapes. All infilled by clearer but ferroan dolomite (0.14 to 0.4 mm) with some cleavage traces of brownish staining due to oxidation.
J-14	Fd. Crackle brecciated and mineralized. Most grains consist of xenotopic crystals 0.05 mm. Some porphyrotopes = 0.1 mm. Fractures are infilled by baroque Vf and sphalerite; chert occurs as breccia fragment. Dispersed angular quartz grains 0.05 mm sized. Para Fd + silica → Vf + sphalerites.
J-15A	Fd. Faint wavy laminae, also marked by size mottling of generally 0.05 mm-sized crystals by 0.09 mm parallel to lamination. Fractures infilled by poikilotopic baroque Vf, but sometimes by quartz. Sphalerite occurs associated with Vf. Pyrite disseminated throughout, also occurs as inclusions in Vf. Para Fd + quartz + pyrite → quartz + Vf + sphalerite.
J-15B	Chert. Preserved ooids and pseudo-ooids 0.4 to 0.8 mm-sized; some intraclasts. Adjacently: a silicified shale with mica, quartz. Some pyrite.
J-17	CFd. Hypidiotopic, poikilotopic, 0.4 to 0.5 mm. Zoning due to occurrence of cloudy patches towards the center. Sometimes such patches are off center. Two or more patches occur in some rhombs. Such patches appear to be due to calcite as few of the included crystallites stain red by Alizarins Red S. Vugs infilled by dolomite. Inclusions in Vf are crystals of low interference color. Vf are ferroan but with varying iron amount in the growth zones. At least six growth zones with alternating more ferroan bands are discernible. Subhorizontal stylolites are cut by vug fills. Para Barring dedolomitization to be the case of calcite patches because they occur inside dolomite rhombs. Peloidal Ls → CFd → Vf.
J-18	Fd. Xenotopic, porphyrotopic. Mostly 0.07 to 0.09 mm, few 0.14 mm. Poikilotopic crystals have inclusions of crystals of high interference color, some of which stain like calcite. Poikilotopic baroque dolomite fills vugs with sphalerite in

Table G-2 (continued)

Sample Number	
	one corner. Some cleavage traces in Vf stain brownish due to oxidation. Para Fd → Vf + sphalerite.
J-20	CFd. Size mottled, hypidiotopic, most 0.3 to 0.4 mm. Some patches of zoned clearer rimmed, poikilotopic with quartz and calcite? inclusions. Peloidal ghost. Porphyrotopes 0.6 mm. Adjacent to microstylolites crystals generally 0.19 mm. More sub rnd. quartz and few mica flakes occur at stylolites. Para Ls → CFd → stylolitization.
J-21B	CFd. Hypidiotopic, zoned with ferroan rims—peloidal ghost. Most crystals 0.6 mm, few porphyrotopes 1.0 mm, chert-matrix. Inclusion of quartz and Fd (0.02 mm). Subvertical stylolites. Para Peloidal Ls → Fd + silica → CFd.
J-22	CFd. Hypidiotopic, porphyrotopic, poikilotopic, color mottled rhombic crystals 0.6 mm, porphyrotopes up to 0.8 mm. Zoned with ferroan rims. Inclusions of quartz and calcite. Peloidal ghost. Quartz generally is interstitial to the major less ferroan dolomite crystal, and occur as inclusions mostly at the edges of dolomites. Quartz is authgenic, singly or doubly terminated 0.09 mm, although some are more slender 0.2 mm long. Sub parallel stylolites with micron-sized pyrite cubes truncate some dolomite crystals. Fracture infilled by clearer dolomite. An intraclast ghost feature at middle of slide. Para Ls → less ferroan dolomite cores → authgenic quartz + ferroan rim of dolomites + stylolitization → fracturing.
J-23	Fd to CFd. Xenotopic 0.09 mm. Some porphyrotopes 0.15 mm. Faintly laminated. Subvertically fractured and infilled by ferroan dolomite with some cleavage traces oxidized to brownish coloration. Sphalerite occurs in fractures bounded on two sides by Fd and on the other two sides by ferroan fractures fill dolomite. Para Fd → Vf + sphalerite.
J-24	Ls. Biomicrite. Burrowed and infilled by peloids (0.1 mm or more). Moldic porosity infilled by blocky calcite cement. Fossils: trilolite, gastropod, sponge?, unrecognized fragments. Discernible algal borings. Dolomite is rare, and occurs associated with calcite cement. But such dolomites have uneven edges. Small, unhedral dolomite crystals occur. Separated, probably broken up by calcitization of coarser dolomites.

Table G-2 (continued)

Sample Number	
J-25A	Fd to CFd. Xenotopic, 0.07 to 0.12 mm. Porphyrotopes 0.16 mm. Horizontal crack fill of ferroan dolomite. Pyrite disseminated.
J-25B	Fd to CFd. Xenotopic, 0.09 mm. Some zoned with clearer rims. Inclusions of calcite?; porphyrotopes 0.2 mm. Faint laminations. Rhombs 0.05 mm in porphyrotopes. Porphyrotopes appear like interstitial cement with anhedral sides.
J-25C	Ls. Trilobite biointrapelsparite, 5% dolomitized. Fossils: trilobite, ostracod, microboring organism, unrecognized fragments. Fd: 0.06 mm-sized patches top right corner; elsewhere ferroan CFd. Some perfectly zoned and rhombic (0.5 mm); others unhedral baroque (0.8 mm). Birdseyes infilled by blocky calcite some of them in sharp contact with CFd. Others have corroded edges (dedolomitized?). Subhorizontal stylolites.
J-25D	Ls. Biointrapelsparite with interlaminar birdseyes and some lithic fragments rotated about 90°, as evidenced from the orientation of fossils and intraclasts. This suggests penecontemporaneous brecciation. 5% of slide consists of zoned CFd, ferroan rims, some calcitized, same as above.
J-26A	Biointrapelsparite with bottom 1/4 biomicrite. Middle part silicified to chert with well-preserved relict allochems. Drusy quartz infills porosities. Fossils: ostracod, trilobite, gastropod, numerous micritic envelops. The limestone appears to be a dedolomite, due to the occurrence of numerous corroded dolomite crystals of various sizes. Also dolomitic selvages occur around fossil fragments. It is interesting to note that primary allochems such as fossils and peloidal material are preserved despite the fact that the limestone was dolomitized and then dedolomitized.
J-26B	CFd. Hypidiotopic, porphyrotopic. 0.6 to 0.8 mm generally. Porphyrotopes up to 1.5 mm. Interstitial shaly material. CFd are zoned with more ferroan rims. Minor calcitization. There is a patch of Fd to CFd 0.09 to 0.14 mm.

Table G-2 (continued)

Sample Number	
J-26C	Ls. Interlaminated intrapelsparite and micrite. Few dolomite crystals adjacent to horizontal stylolites have serrated edges possibly doe to calcitization. The dolomites are ferroan and zoned, some growth zones being more ferroan. Up to five growth zones recognized.

*Note: Ls = limestone; Fd = fine-grained dolostone; CFd = coarser than fine-grained dolomite but not occurring as vug-fill; Vf = coarse-grained dolomite occurring as vug-fill; Para = paragenesis.

Table G-3. Petrographic description of carbonate rocks from Shiloh*

Sample Number	
(SS-2)	Ls. Biointrapelsparite with birdseyes. Intraclasts mostly of pelletal material, few of micrite. Fossils: trilobite, algae?, unrecognized fragments. Few micritized dolomite crystals.
(SS-4)	Ls. Wavy laminated, horizontally stylolitized micrite with 5% dolomite. CFd zoned with clearer rims and of variable diameter mostly 0.3 mm.
(SS-7)	Ls. Interlaminated micrite and biointrapelsparite with birdseyes infilled by blocky calcite. Few fragments of trilobite. An oxidized band at corner.
(SS-8)	CFd + Ls. Limestone with 60% dolomite crystals. Dolomite is poikilotopic with calcite inclusions. The calcite inclusions sometimes occur as patches in the center or surrounding a central non-poikilotopic zone. Elsewhere, they occur in the fringes of dolomite crystals. Some edges of dolomites are corroded. Grain size of dolomite is variable but mostly 0.8 to 1.5 mm.
(SS-9)	Ls. Micrite, few poikilotopic dolomite crystals of variable size but mostly 0.25 mm, some 0.8 mm.
(SS-11)	Ls. Burrowed biomicrite with a layer of biointrapelsparite towards bottom. Fossils: trilobite, brachiopod, gastropod, ostracod, pelmatozoa. Few dolomite crystals 0.4 to 0.8 mm.
(S-2)	Fd + CFd. Xenotopic, poikilotopic. 0.05 to 0.17 mm. Generally smaller grains occur in patch es between CFd grains or as inclusions in CFd.
(S-4)	Ls. Interlaminated biointrapelsparite and biomicrite with birdseyes. Fossils: trilobite, gastropod, brachiopod, ostracod, sponge?, unrecognized fragments, microboring organisms. Dolomite: 1% of slide, decimicron to millimicron sized, poikilotopic with calcite inclusions, ferroan and baroque dolomite. Some dolomite crystals are micritized, and some blocky calcite cement has dolomite inclusions. Many of the dolomite crystals have sharp edges. Towards bottom of slide, in a moldic porosity with a lining of drusy calcite followed by crystal silt cement, the center of the porosity is infilled by calcite in sharp contact with

Table G-3 (continued)

Sample Number	
	baroque ferroan dolomite, than it was mudcracked and crack infilled by micrite.
(S-9)	Breccia. Breccia fragments consist predominantly of size mottled Fd and Cfd. Fd: 0.02 mm and faintly laminated; CFd = 0.12 to 0.2 mm with much pyrite in places. One breccia fragment consists of chert with peloidal and intraclastic relicts. Matrix consists of baroque Vf and sphalerite. In some places sphalerite grows directly from breccia fragment without any "gangue" dolomite rind. The side of the breccia fragment from which sphalerite grows in some cases is Fd, in others CFd.
(S-10)	Breccia. Breccia fragment mostly size mottled Fd (0.02 mm to 0.05 mm). Much interstitial pyrite. Some poikilotopic CFd (up to 0.17 mm) occurs as breccia matrix, although most of the matrix is baroque CFd and some chert. Sphalerite occurs predominantly in chert matrix. Some quartz fracture fills are replaced by sphalerite.
(S-12)	Breccia. Breccia fragment, wavy laminated, size graded from 0.02 to 0.09 mm. Fd with several interstitial pyrite. Much pyrite at the boundary of breccia fragment and breccia matrix baroque Vf. Some coarser pyrite in the baroque Vf itself. Rare sphalerite in association with chert in the breccia matrix.
(S-13)	Breccia. Breccia fragment of CFd (0.13 mm) with several interstitial pyrite. Some pyrite occurs in patches. Coarser pyrite occurs at breccia boundary and interstitial to baroque Vf matrix. Sphalerite occurs in a matrix with a rind of quartz and/or baroque Vf separating it from breccia fragment. In some parts, though, sphalerite is directly in contact with breccia fragment.

*Note: Ls = limestone; Fd = fine-grained dolostone; CFd = coarser than fine-grained dolomite but not occurring as vug-fill; Vf = coarse-grained dolomite occurring as vug-fill; Para = paragenesis.

Table G-4. Petrographic description of carbonates from Lee Valley*

Sample Number	
L-1 (208)	Hypidiotopic, poikilotopic, 0.4 mm, chert matrix.
L-2 (210)	CFd. Xenotopic, poikilotopic, vugular. Most grains 0.4 to 0.6 mm with inclusions of 0.05 mm, interstitial dolomite = 0.12 mm. Vugs mostly have a lining of baroque Vf, followed by banded chalcedony (some of it length-slow) followed by quartz, and in some cases by baroque Vf.
L-3 (212)	CFd. Xenotopic, poikilotopic, porphyrotopic. Some zoned. Chert and shaly material are matrix. Inclusions of calcite patches, some crystals are actually corroded and calcitized. Relict fossils. CFd = variable grains size less than 0.09 mm as inclusions, 0.13 to 0.2 mm between coarser grains of 0.4 mm, porphyrotopes reach up to 1.5 mm.
L-4 (214)	Ls. Interlaminated biomicrite (burrowed, grumulosed) and biopelsparite with few intraclasts. Fossils: trilobite, unrecognized fragments. Few dolomite crystals partially to completely micritized.
L-5 (220)	Ls. Biointrapelsparite with interlaminar birdseyes—a layer of micrite towards the bottom. Fossils: trilobite (abundant), pelmatozoa, gastropod, brachiopod?, unrecognized fragments, microboring organisms. Intraclasts largely of pelletal material, some of micrite, sometimes with pyrite cubes. Few poikilotopic and wavy extinct dolomite that sometimes maintain sharp contact with blocky calcite cement, but have serrated edges in allochems, some of them are obviously micritized. Dolomite crystals on interallochem porosity sites are coarser, up to 1.7 mm, on micrite. They have serrated edges, and sometimes are rounded and measure 0.6 mm.
L-6 (225)	Ls. Micrite, faintly laminated. Very few partially to completely micritized dolomites (0.2 to 0.4 mm). Dispersed pyrite.
L-7 (230)	Chert + Ls. Laminated micrite and chert that preserves some laminae. Fractures in chert infilled by dolomite.
L-8 (234)	Ls. Biointrapelsparite with micrite layer at top. Fossils: trilobite, pelmatozoa some of them with microdolomite

Table G-4 (continued)

Sample Number	
	inclusions, other fragments. Some intraclasts are up to 3.5 cm long and are composed of compound grains—pelletal material and fossils, others are of micrite with numerous dolomites of serrated edges, generally 0.25 mm—some of which are zoned with clearer centers. Poikilotopic dolomite of variable size but generally 0.7 mm grows between intraclasts. Some dolomites are calcitized. Para Ls → CFd (0.25 mm on micrite, 0.7 on interallochem cement) → calcitization.
L-9 (235)	Fd. Xenotopic. Mostly 0.02 mm, few 0.05 mm. Vertical fracture infilled by more ferroan dolomite and calcite.
L-10 (239A)	CFd. Hypidiotopic, porphyrotopic, with chert-matrix particularly towards bottom. Grain sizes vary from 0.05 to 0.12 mm occur as inclusions, 0.12 to 0.3 mm as interstitial to the bulk of the dolomite that are generally 0.7 to 1.2 mm. Some relict peloidal material (condensed light).
L-11 (239B)	Fd to CFd. Xenotopic, mostly 0.02 to 0.05 mm with numerous porphyrotopes up to 0.15 mm. Fractures infilled by dolomite and calcite.
L-12 (241A)	Ls. Biomicrite, grumulosed, silicified, dolomitized and calcitized. Fossils: gastropod, ostracod, trilobite. Pore spaces appear to have had an early lining of silica (quartz), some of which still persists; then they were infilled by ferroan baroque Vs. Calcitization appears to have altered both dolomite and quartz.
L-13 (241B)	Ls. Biointrapelsparite—strongly fractured and filled by calcite and some dolomite (baroque).
L-14 (253)	Fd. Xenotopic, mostly 0.02 mm few 0.05 mm. Few discontinuous and whispy stylolites.
L-15 (280)	Fd. Xenotopic, 0.02 mm. Faintly laminated. Some discontinuous lenses of fine-grained dolomite.

Table G-4 (continued)

Sample Number	
L-16 (309)	Fd. Xenotopic, 0.02 mm, birdseyes infilled by more ferroan wavy extinct dolomite.

*Note: Ls = limestone; Fd = fine-grained dolostone; CFd = coarser than fine-grained dolomite but not occurring as vug-fill; Vf = coarse-grained dolomite occurring as vug-fill; Para = paragenesis.

VITA

Habte Giorgis Churnet was born in Menz ena Gishe Aweraja, Shewa Province, Ethiopia, on May 9, 1946. He attended public schools in Addis Abeba, Ethiopia, and graduated from the Haile Sellassie I University in 1969 with a BSc degree in Geology. Between 1969 and 1970 he was employed as a graduate assistant in the Geology Department, Haile Sellassie I University. Between 1970 and 1971 he studied at the University of Leeds, United Kingdom, and graduated with an MSc degree in Geophysics by 1972 (in absentia). Between 1971 and 1974 he was employed as a lecturer at the Haile Sellassie I University. Between 1974-1975 he was elected chairman of the Department of Geology at the Haile Sellassie I University and served, during the later part of the period, as a "Zemecha" administrator at the Mojo district when educated people were dispatched to the countryside due to a change in the system of government of Ethiopia. Between 1975-1979 he attended The University of Tennessee at Knoxville, USA, and received the Doctor of Philosophy degree with a major in Geology in December, 1979.